MUTANT CARDIAC SODIUM CHANNEL DYSFUNCTION ASSOCIATED WITH CARDIOMYOPATHY

By

Thomas Martin Beckermann

Dissertation

Submitted to the Faculty of the

Graduate School of Vanderbilt University

in partial fulfillment of the requirements

for the degree of

DOCTOR OF PHILOSOPHY

in

Pharmacology

August, 2014

Nashville, Tennessee

Approved:	Date:
Bjorn Knollmann	May 15, 2014
Dan Roden	May 15, 2014
Kathy Murray	May 15, 2014
Franz Baudenbacher	May 15, 2014
Al George	May 15, 2014

This work is dedicated to my family. Thank you for always asking what I want to be when I grow up instead of insisting that I merely grow up.

Thomas E. Beckermann (1951-2008)

ACKNOWLEDGEMENTS

The breadth of my graduate research presented here was not possible without the guidance and support of many. First, I need to thank my mentor, Al George. Al took me into his lab knowing that I had various scientific interests and he allowed me to carry a multi-faceted research project that merged novel techniques with the electrophysiological standards of the lab. He gave me the opportunity to work on projects directly related to the public, which helped to motivate me and gave me purpose. Al taught me how to think, speak, and succeed as a scientist and held me to a high standard in all aspects; for this, I am forever grateful.

Next, I would like to thank my thesis committee, Bjorn Knollmann, Dan Roden, Kathy Murray, and Franz Baudenbacher. Your knowledge and insights into cardiac physiology helped guide my project and your personalities created an outstanding atmosphere of learning and communication during committee meetings.

I have seen many people come and go from the George lab and most have had some sort of impact on my research goals. Kris Kahlig first introduced me to patch clamping and taught me the ropes. His attention to detail was greatly appreciated as I was just starting out learning a new field of concepts. Carlos Vanoye and Dao Wang were also instrumental in my growth as an electrophysiologist. Of all people to be stuck in a 6' x 6' patch room with, I couldn't have asked for a better roomie than Rick Welch. He was a welcome distraction that broke the monotony of a long day of patching. Chris Thompson served as a sounding board for quite a few of my thoughts and ideas and he was an outstanding mentor that helped fine tune my patching abilities. Finally, the lab

wouldn't have functioned without our lab manager, Jennifer Kunic. She graciously taught me the basics of lab life and imparted on me her cloning knowledge, all while maintaining a cheery smile that was probably more patient than I deserved.

My graduate career has extended over a long span and it is important to acknowledge that a lot of life has happened during those years. Through good times and bad, many of my lab mates have been there to share in my experiences. Chris, Jennifer, Rick, Lyndsey, and Franck have helped me keep my sanity on a daily basis, expanding far past experimental design. Their friendship extended outside of lab boundaries and will continue as we all move on to new endeavors.

I need to thank Webster University professors Stephanie Schroeder and Joyce Bork for facilitating my interest in science and encouraging me to attend graduate school. Their influence and support went beyond the classroom and I am glad to call them friends. I also need to acknowledge those friends who have nothing to do with science. This group exists mostly in the form of past and current teammates from various softball and ultimate frisbee leagues and are too numerous to individually list. You offered a much needed respite from the scientific process a couple hours a week that helped me to maintain my sanity.

Finally, I need to thank those most important to me, my family. You let me forge my own path and were completely supportive of me becoming a 'professional student.' I need to thank my parents, Gerrie Bader and Thomas E. Beckermann, for my upbringing and creating the person that I am today. My siblings, Ben, Dan, Brian, Eddie, and Mary Rushing, were responsible for fostering my inquisitive nature while growing up and assisting in whatever mischief found me. I wouldn't be where I am now without my

cousins, Mike and Peggy Wolff. Thank you for your support, encouragement, and a home-away-from-home over the past 15 years.

Because she always gets the last word, I need to thank my amazing wife, Katy Beckermann. I can't begin to thank you enough for the encouragement and support you have given me since we met 6 years ago. On both good days and bad, you are the first person I want to see. Your smile is everything that is right in the world.

This work was supported by grants from the National Institutes of Health and the American Heart Association.

TABLE OF CONTENTS

Page

LIST OF TABLES

LIST OF FIGURES

LIST OF ABBREVIATIONS

ATP = Adenosine triphosphate

AV = atrioventricular

bpm = beats per minute

BrS = Brugada syndrome

BSA = bovine serum albumin

Ca^{2+} = calcium ion

CCD = cardiac conduction disease

CD8 = cell surface glycoprotein found on T lymphocytes; encoded by the gene *Leu2*

CICR = calcium-induced calcium release

CMV = human cytomegalovirus promoter

CNS = central nervous system

CPEs = cytopathic effects

DMEM = Dulbecco's Modified Eagles Medium

DMSO = dimethyl sulfoxide

DRG = dorsal root ganglia

dsRed = red fluorescent protein cloned from *Discosoma sp.* coral

EC coupling = excitation – contraction coupling

ECG = electrocardiogram

eGFP = enhanced green fluorescent protein

EtOH = ethanol

FBS = fetal bovine serum

GTVC = University of Iowa Gene Transfer Vector Core

H^+ = hydrogen ion / proton

HBSS = Hank's balanced salt solution

HEK = human embryonic kidney

hUBC = human ubiquitin C promoter

I_{Ca} = calcium current

I_{Kr} = rapidly activating component of delayed rectifier K^+ current

I_{Ks} = slowly activating component of delayed rectifier K+ current

I_{Na} = sodium current

iPSC-CM = induced pluripotent stem cell-derived cardiomyocytes

IRES = internal ribosomal entry site

I_{TO} = transient outward K^+ current

K^+ = potassium ion

KB solution = Krebs-Henseleit Buffer

LQTS = long QT syndrome

MEM = minimum essential medium

Na^+ = sodium ion

NBC = Na^+-HCO^{-3} cotransporter

NCLX = mitochondrial NCX

NCX = sodium – calcium exchanger

NHE = Na^+/H^+ exchanger

NRVMs = neonatal rat ventricular myocytes

PCR = polymerase chain reaction

PNS = peripheral nervous system

PVCs = premature ventricular contractions

QTc = corrected QT interval

RVOT = right ventricular outflow tract

S.E.M. = standard error of the mean

SA node = sinoatrial node

Sarc. = sarcomere

SERCA = sarco/endoplasmic reticulum Ca^{2+}-ATPase

SR = sarcoplasmic reticulum

TS = tyrode's solution

tsA201 = HEK cell line expressing SV40 large T antigen

TTX = tetrodotoxin

$V_{½}$ = voltage midpoint

VGSCs = voltage-gated sodium channels

VSV-G = 'G' glycoprotein of the vesicular stomatitis virus

WT = wild-type; in reference to a native gene

CHAPTER I

INTRODUCTION

Voltage-gated sodium channels

Voltage-gated sodium channels (VGSCs) are a diverse family of proteins that are expressed mostly in excitable tissues and are responsible for the initiation and propagation of action potentials in muscle, nerve, and neuroendocrine cells. Upon activation, Na^+ ions flow through the channel and into the cell, resulting in a rapid depolarization and the initial upstroke of the action potential. The family of VGSCs consists of nine genes encoding distinct pore-forming α subunits and four genes encoding accessory β subunits (Table 1) [1]. Though there are multiple subtypes of the α subunit, all are closely related with greater than 50% amino acid identity (Figure 1) [2]. The tissue specific expression of the various sodium channel isoforms and accessory proteins allows for regulation of channel activity and action potential morphology in various cell types.

Table 1. Summary of the different types of VGSCs and associated subunits. Adapted from Savio-Galimberti *et al*, 2012 [3]

Gene	Channel	Expression	TTX sensitivity
SCN1A	$Na_V1.1$	CNS, PNS	S
SCN2A	$Na_V1.2$	CNS, PNS	S
SCN3A	$Na_V1.3$	CNS, PNS	S
SCN4A	$Na_V1.4$	Skeletal muscle	S
SCN5A	$Na_V1.5$	Cardiac muscle	R
SCN8A	$Na_V1.6$	CNS, PNS	S
SCN9A	$Na_V1.7$	PNS, DRG	S
SCN10A	$Na_V1.8$	PNS, DRG	R
SCN11A	$Na_V1.9$	PNS, DRG	R
SCN6A / SCN7A	Na_X	DRG / Heart / Uterus	Unknown

CNS, central nervous system; PNS, peripheral nervous system;
DRG, dorsal root ganglia; S, sensitive; R, resistant

Gene	β subunit	α subunit
SCN1B	β1	$Na_V1.1$ - $Na_V1.7$
SCN2B	β2	$Na_V1.1$ - $Na_V1.2$, $Na_V1.5$ - $Na_V1.7$
SCN3B	β3	$Na_V1.1$ - $Na_V1.3$ $Na_V1.5$
SCN4B	β4	$Na_V1.1$, $Na_V1.2$, $Na_V1.5$

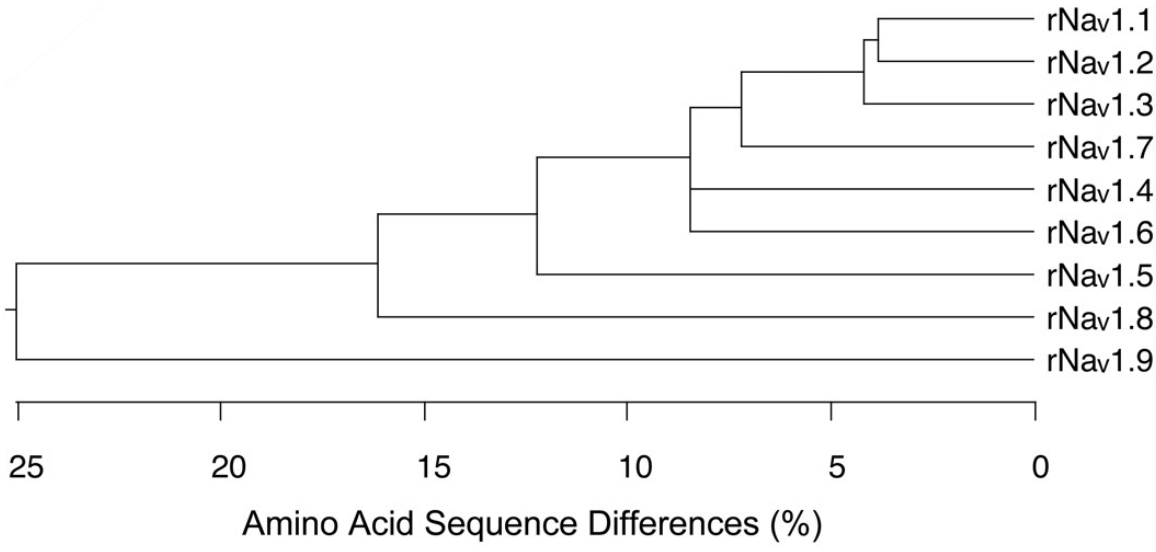

Figure 1. Amino acid sequence similarity of the α subunits of voltage-gated sodium channels NaV1.1-NaV1.9. Adapted from Catterall *et al*, 2005 [2].

Structure and function of VGSCs

The pore-forming α subunit of the VGSC consists of four homologous transmembrane domains, DI – DIV, linked by intracellular loops (Figure 2A). Each domain consists of six transmembrane spanning segments (S1-S6), with the positively charged S4 serving as the voltage-sensor for the channel. The S4 region is critically involved in voltage-dependent activation while channel inactivation is controlled by the inactivation gate, formed by the intracellular loop connecting DIII-DIV, and the C-terminal domain [4]. Ion selectivity and permeation are regulated by the extracellular pore loop between S5 and S6 [1].

VGSCs exist in three main functional states when expressed at the cellular membrane, depending upon the membrane potential (Figure 2B) [1]. A sudden membrane depolarization causes the S4 segments to move in an outward direction, causing a conformational change in the pore region that results in opening of the Na^+ selective channel. Sodium ions entering an excitable cell cause rapid membrane depolarization and initiation of an action potential (Figure 2C). The process of sodium ions moving through open channels is transient, as the channel rapidly inactivates through gating processes involving the DIII-DIV linker, which quenches ion movement through the channel. Upon membrane repolarization, the channel recovers from the inactivated state and returns to a closed state where it is again ready to be activated by a subsequent depolarization.

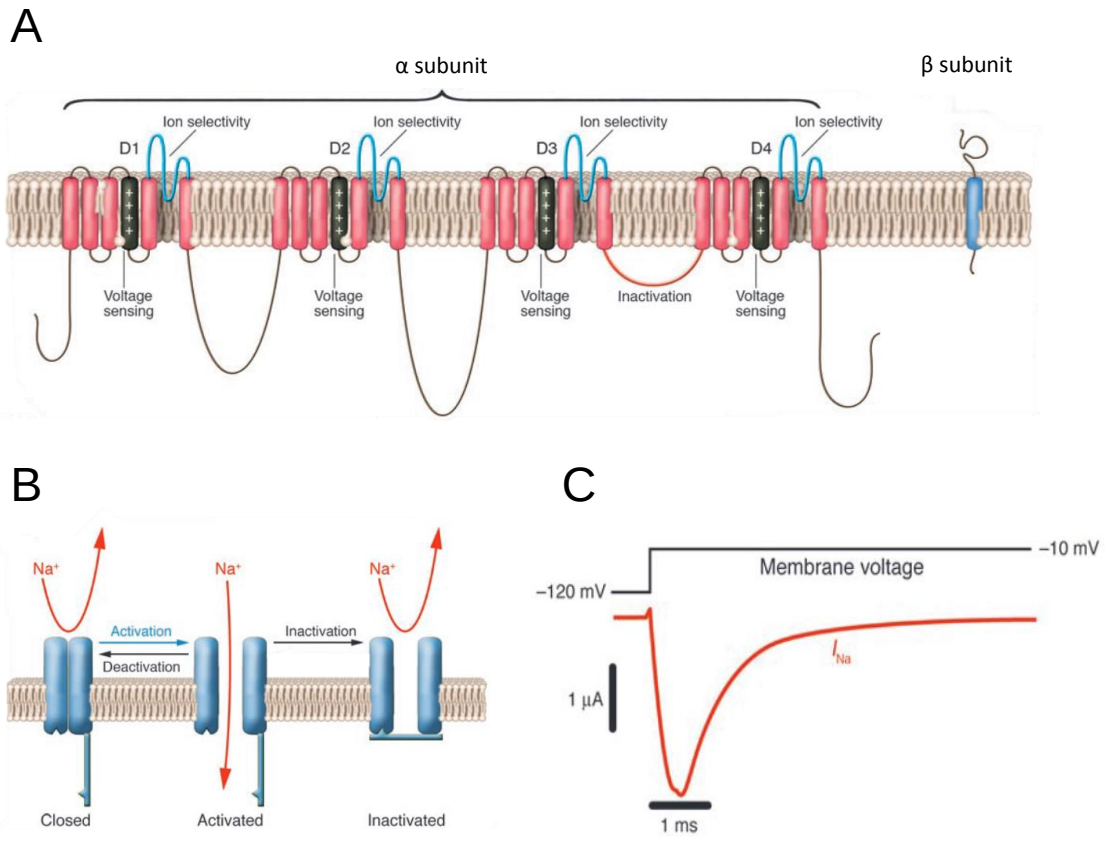

Figure 2. Structure and function of VGSCs. (A) Graphical representation of the pore-forming α subunit and an accessory β subunit. (B) Functional channels exist in a closed, activated, or inactivated state. (C) Activation of VGSCs by a rapid depolarization opens the channel pore allowing Na^+ to flow into the cell, further depolarizing the cell, before inactivating and eventually closing. Modified from George, 2005 {Formatting Citation}.

The role of VGSCs in cardiomyocyte physiology

The cardiac action potential

The cardiac action potential is the result of multiple processes within cardiomyocytes (Figure 3). The cardiac sodium channel, $Na_V1.5$, is responsible for the initial upstroke during Phase 0 of the human cardiac action potential. The Phase 1 notch is the result of the inactivation of the sodium channel and concurrent activity of I_{TO} to remove K^+ from the intracellular space. As a result of the rapid depolarization initiated by $Na_V1.5$, L-type voltage-gated calcium channels activate and open, allowing Ca^{2+} to enter the myocyte, a step critical for excitation-contraction coupling. The plateau, or Phase 2, results from the balance of Ca^{2+} influx through calcium channels and K^+ efflux through inward rectifying channels. Phase 3 occurs as calcium channels close and the inward rectifier K^+ channels repolarize the cell and restores the membrane potential to resting values during Phase 4 [5].

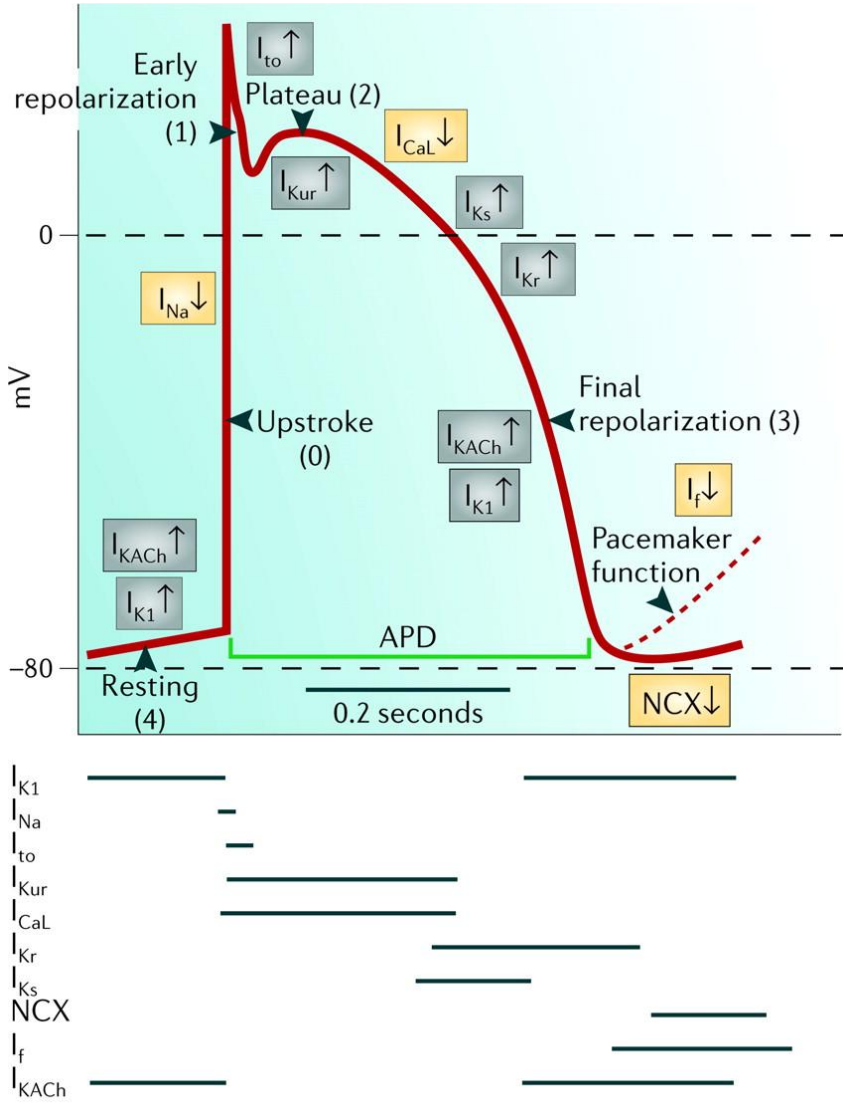

Figure 3. The cardiac action potential. A representative visualization of the cardiac action potential and the respective currents that control the morphology. Adapted from Grant, 2009 [5].

Excitation – contraction coupling

Proper function of the cardiac sodium channel is also critical for the cardiomyocyte to initiate contraction, as membrane depolarization is the first step in the process of excitation – contraction (EC) coupling. EC coupling is the process by which the electrical excitation of the myocyte is directly paired with the myocyte's ability to contract through a mechanism triggered by the second messenger Ca^{2+} (Figure 4) [6]. The initial depolarization of the cardiomyocyte membrane by activation of $Na_V1.5$ causes voltage-regulated L-type calcium channels to open and allows calcium to flow into the myocyte. Ca^{2+} entry is sensed by ryanodine receptors on the sarcoplasmic reticulum (SR) and, as a result, Ca^{2+} stored within the SR is released into the cytosol through calcium-induced calcium release (CICR). Released calcium serves two main functions. One is inactivation of L-type I_{Ca} through direct feedback of localized $[Ca^{2+}]$ that helps to limit calcium influx during periods of high Ca^{2+} influx or SR release. The second function of CICR is to increase the levels of cytosolic Ca^{2+} in order to stimulate contraction of the myofilaments. Free cytosolic Ca^{2+} will bind to the myofilament protein Troponin C and initiate the contraction machinery. Myocytes will relax as cytosolic Ca^{2+} begins to dissipate. This is achieved by reuptake of Ca^{2+} into the SR through SERCA (sarco/endoplasmic reticulum Ca^{2+}-ATPase) or removal through the sodium – calcium exchanger (NCX).

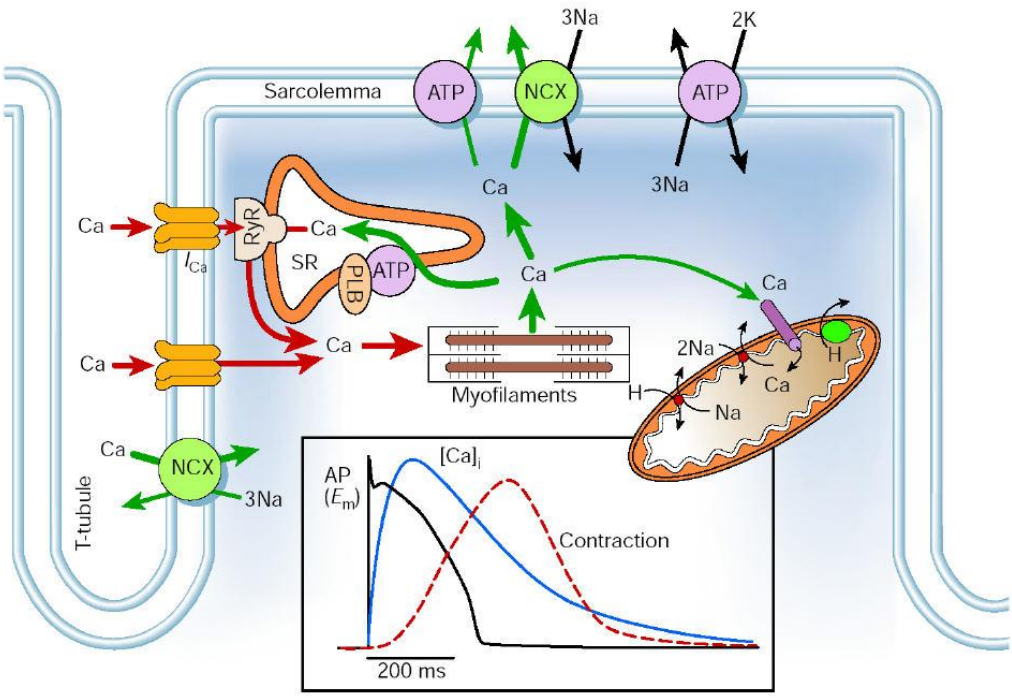

Figure 4. The role of calcium in the process of excitation – contraction coupling. Rapid depolarization of the ventricular myocyte activates voltage-gated L-type calcium channels and initiates EC coupling through the second messenger, Ca^{2+}. Inset demonstrates the timing of the action potential, calcium transient, and resultant myocyte contraction. Adapted from Bers, 2002 [6].

Regulation of intracellular sodium

In a human cardiomyocyte, intracellular sodium concentration is believed to be in the range of 4 – 10 mM while extracellular [Na^+] is roughly 140 mM. The cardiomyocyte uses this Na^+ gradient to drive multiple processes within the cell including proper calcium signaling, pH regulation, and cardiac metabolism (Figure 5) [7], [8].

Sodium – calcium exchanger (NCX)

As previously mentioned, the NCX is partially responsible for calcium regulation in the myocyte. NCX is capable of operating in both forward (Ca^{2+} extrusion) and reverse (Ca^{2+} influx) modes, depending on ion concentration gradients and membrane potential. Depolarization of the membrane by $Na_V1.5$ hinders Ca^{2+} efflux at the start of the action potential, helping to stimulate CICR from the SR by limiting Ca^{2+} extrusion [9]. As the membrane potential begins to repolarize during systole, the forward mode of the NCX exchanges 3 extracellular Na^+ ions for 1 intracellular Ca^{2+}, producing an inward current that extends the plateau phase of the action potential. Removal of cytosolic Ca^{2+} through the forward mode of NCX contributes to relaxation of the contracted myocyte. During diastole, abnormal calcium release within a myocyte can activate the NCX and produce delayed afterdepolarizations (DADs) and is capable of triggering arrhythmias.

Modest increases in $[Na^+]_i$ (a few mM) causes the NCX to extrude less Ca^{2+}, effectively increasing $[Ca^{2+}]_i$, which is recovered by the SR. This loads the SR and can increase Ca^{2+} transients that intensify myocyte contraction. This is the mechanism of cardiac glycoside treatment (Digoxin, Ouabain, etc.) of congestive heart failure. By limiting extrusion of Na^+_i through inhibition of the Na^+/K^+-ATPase, $[Na^+]_i$ is increased

and the resultant increase in $[Ca^{2+}]_i$ loads the SR and increases inotropy. Excessive $[Na^+]_i$ can result in the exchanger to operate in reverse, extruding sodium and driving Ca^{2+} into cells. Reverse mode of NCX is initiated by membrane depolarization and elevated levels of cytosolic Na^+. This influx of Ca^{2+} can also load the SR and increase inotropy and, inadvertently, be arrhythmogenic [7].

pH regulation

The Na^+ gradient is also coupled to regulation of intracellular pH through the Na^+/H^+ exchanger (NHE) and the Na^+-HCO^-_3 cotransporter (NBC), which transport protons out and bicarbonate into the cell, respectively [7], [10], [11]. Both mechanisms are equally functional at an intracellular pH close to basal levels (pH 7.2). A decrease in pH_i results in increased activity of both pathways and a resultant influx of Na^+ into the cell. Activation of NHE is mainly through a drop in pH that promotes a rapid extrusion of acid. NBC is also regulated by pH_i, however, its ability to buffer the cytosol is not as expansive as NHE. Increased levels of $[Na^+]_i$ can have an impact on function of these transporters, but not near the physiological Na^+ levels. It is important to note, that during ischemia/reperfusion injury, the activity of NHE, and to a lesser extent, NBC, can increase $[Na^+]_i$ to a point of forcing the NCX into reverse mode. The drug cariporide has been successfully used as a protective agent with respect to reperfusion injury [10] as well as instances of induced heart failure in a rabbit model [12].

Cardiac metabolism

Intracellular Na^+ is an important regulator of cardiac metabolism. Proper function of mitochondria rely upon activity of the mitochondrial NCX (NCLX) where $[Na]_i$ directly controls mitochondrial $[Ca^{2+}]$. The NCLX is similar to the sarcolemmal NCX in which it exchanges 3 Na^+ for 1 Ca^{2+} and is very sensitive to changes in $[Na]_i$. Calcium enters the mitochondria through the calcium uniporter. At high workloads, Ca^{2+} uniporter activity is upregulated and increased $[Ca^{2+}]_m$ stimulates further ATP production and enhances the maintenance of redox homeostasis. In conditions of high $[Na^+]_i$, such as reperfusion injury and heart failure, the NCLX increases activity with a concurrent removal of $Ca^{2+}{}_m$, increasing oxidative stress within the myocyte [7].

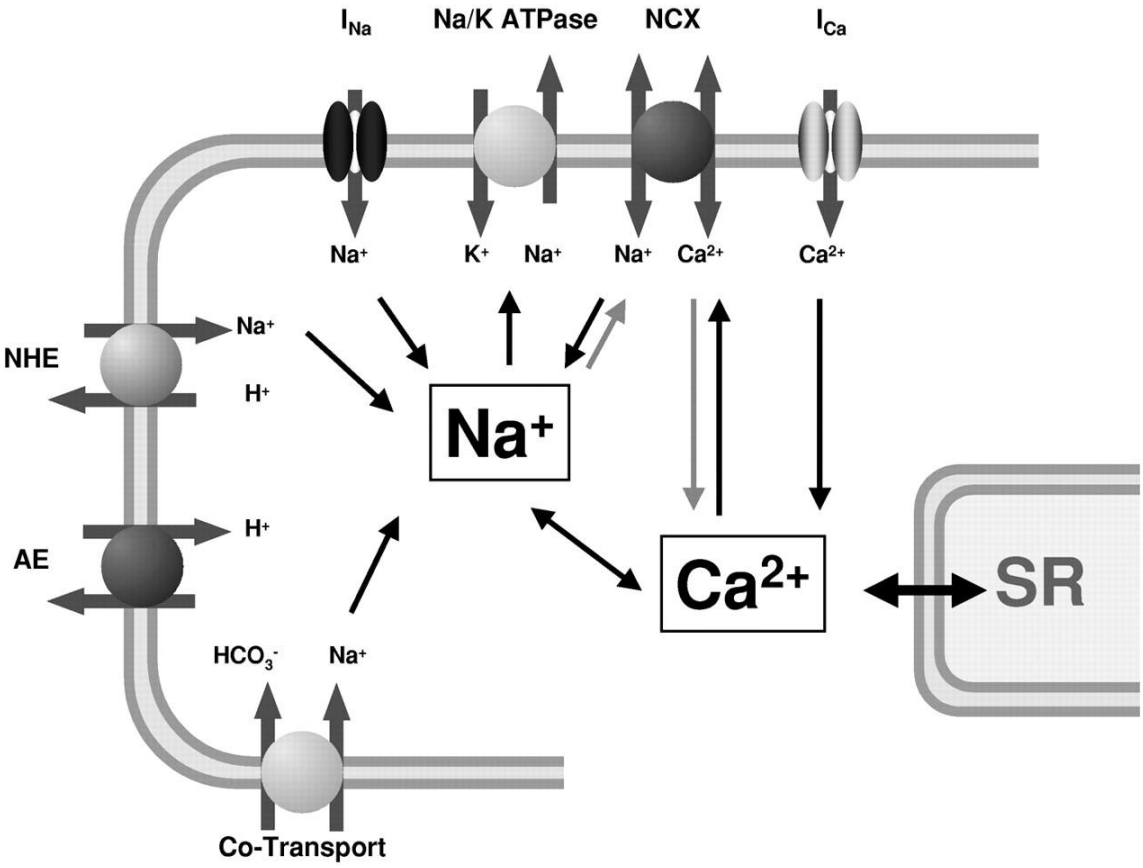

Figure 5. Sodium handling in the human heart. $[Na^+]_i$ is influenced by many processes in the ventricular myocyte including action potential firing, pH regulation, and generation and recovery of Ca^{2+} transients. $[Na^+]_i$ is maintained at proper levels in a healthy myocyte by extrusion through the Na^+/K^+ ATPase. Modified from Pieske *et al*, 2003 [8].

Conduction of the cardiac impulse

Examining the fine details of the ventricular cardiomyocyte is extremely valuable and it affords a greater understanding of the intricacies associated with proper myocyte function. The delicate balance of ion concentrations and the processes that control them are impressive; however, it is important to examine the larger picture and understand how the contraction of one cardiomyocyte factors into the physiology of the heart.

The electrical impulse to initiate a contraction in a healthy heart originates in the sinoatrial (SA) node located in the wall of the right atrium (Figure 6) [13]. Cells within the SA node generate regular, spontaneous action potentials using calcium currents to produce the electrical activity. The action potential generated by the SA node is spread through the atria by cell-to-cell conduction. The wave of action potentials spreading across the atria depolarizes the atrial muscle and induces contraction through EC coupling. The depolarization of the atria is responsible for the P wave on an electrocardiogram (ECG) while repolarization occurs simultaneously with the QRS complex.

The electrical impulse quickly reaches the atrioventricular (AV) node located at the interatrial septum. The AV node also conducts action potentials by using Ca^{2+} currents and is responsible for slightly slowing the electrical signal before the impulse is transmitted from the atria to the ventricles. The slight delay allows the atria to fully contract and push blood into the ventricles before the ventricles begin to contract. This is noted as the PR interval on the ECG.

The impulse then reaches the bundle of His and follows the left and right bundle branches along the intraventricular septum. The signal is spread very rapidly along the

bundle branches, which eventually divide into a network of Purkinje fibers running throughout the ventricles. As the action potential passes through the Purkinje fibers, the electrical impulse is conducted to ventricular myocytes, initiating a concerted contraction through the ventricular walls which pumps blood into the aorta and pulmonary artery. The QRS complex seen on a typical ECG represents depolarization of the left and right ventricles while the T wave represents repolarization. Abnormalities in any part of the ECG can indicate a potential disease state, including those caused by mutations in $Na_V1.5$, such as long QT and Brugada syndromes.

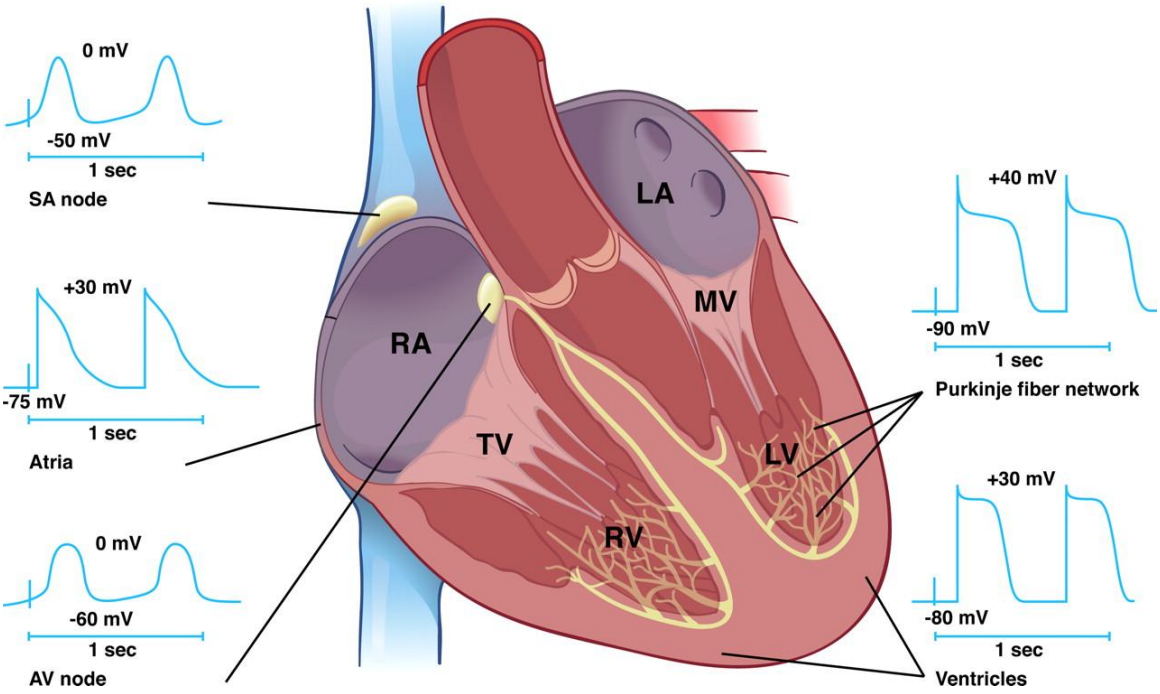

Figure 6. The cardiac conduction system. The electrical signal that initiates conduction begins in the SA node and rapidly spreads through the right (RA) and left (LA) atria. The impulse passes through the AV node, along the left and right bundle branches, and stimulates firing of purkinje fibers. The action potential is then propagated throughout the ventricles. Shown are action potential characteristics associated with different parts of the conduction system. The differing firing properties allow for specific control and timing of the impulse over the heart. Modified from Munshi 2012 [13].

Diseases associated with $Na_V1.5$ mutations

The cardiac sodium channel $Na_V1.5$ is responsible for the influx of Na^+ that drives initiation of the action potential. Regulation of the sodium current, I_{Na}, is critical as changes in current density or activation and inactivation patterns can have detrimental consequences. Most cardiac channelopathies, including those caused by $Na_V1.5$ mutations, are arrhythmogenic as they alter the balance of currents shaping the action potential or they affect how the action potential conducts across the heart.

Inherited arrhythmia syndromes such as long QT syndrome (LQTS) may have altered action potential morphology. Most cases of LQTS associated with $Na_V1.5$ mutations are a result of defective inactivation that allows Na^+ to continually pass through $Na_V1.5$ channels without fully inactivating (Figure 7A). This causes an elongation of the plateau phase of the cardiac action potential and delays repolarization (Figure 7B). This lengthens the action potential duration and the QT interval measured on the ECG. Ventricular arrhythmias can manifest through early afterdepolarizations as a result of calcium channel reactivation during the prolonged plateau of the action potential, creating a depolarized region that is capable of stimulating regions of the heart that have already repolarized. Early afterdepolarizations can result in reentrant arrhythmias and may trigger torsades de pointes, a form of polymorphic ventricular tachycardia in which the electrical axis rotates and the amplitude of the QRS complex oscillates in a sinusoidal pattern [14]. Torsades occurs when ventricular depolarization (signified by the QRS complex) is triggered late in diastole during the repolarization phase (T wave) [15]. It is important to note that milder forms of LQTS can be

exacerbated by medications that prolong the action potential, such as drugs that block I_{Kr} (hERG channel).

Brugada syndrome (BrS) has been associated with almost 100 mutations in the cardiac sodium channel gene, *SCN5A* [16]. Most *SCN5A* mutations in BrS result in a loss-of-function, predicting reduced myocardial I_{Na} density. Two mechanisms have been proposed to explain the cellular basis of BrS [17]. One mechanism suggests that reduced I_{Na} results in unopposed I_{TO}, disproportionate shortening of epicardial action potentials and an exaggerated transmural voltage gradient resulting in a substrate susceptible to potentially lethal reentrant arrhythmias (Figure 8) [1], [17]. The second mechanism proposes that reduced I_{Na} causes slowing of impulse conduction in the right ventricle and a delayed activation of the right ventricular outflow tract (RVOT) [18]. This causes the membrane potential of the RVOT to become more positive compared to the right ventricle and can trigger reentry arrhythmias as the RVOT now acts as a source of current instead of a sink.

Cardiac conduction disease (CCD) has also been attributed to *SCN5A* mutations. CCD is a potentially life threatening disorder of the heart where the function of the conduction system is impaired. This can result in a slowing or complete blockage of impulse conduction and may cause life-threatening rhythm disturbances [19]. The role that mutations in $Na_V1.5$ have are complex; however, mutations causing isolated conduction defects have generally been observed to cause reduced channel availability as a consequence of mixed gating disturbances [1]. Treatment for CCD is implantation of a mechanical pacing device in order to stimulate the appropriate regions of the heart in a time-dependent cycle.

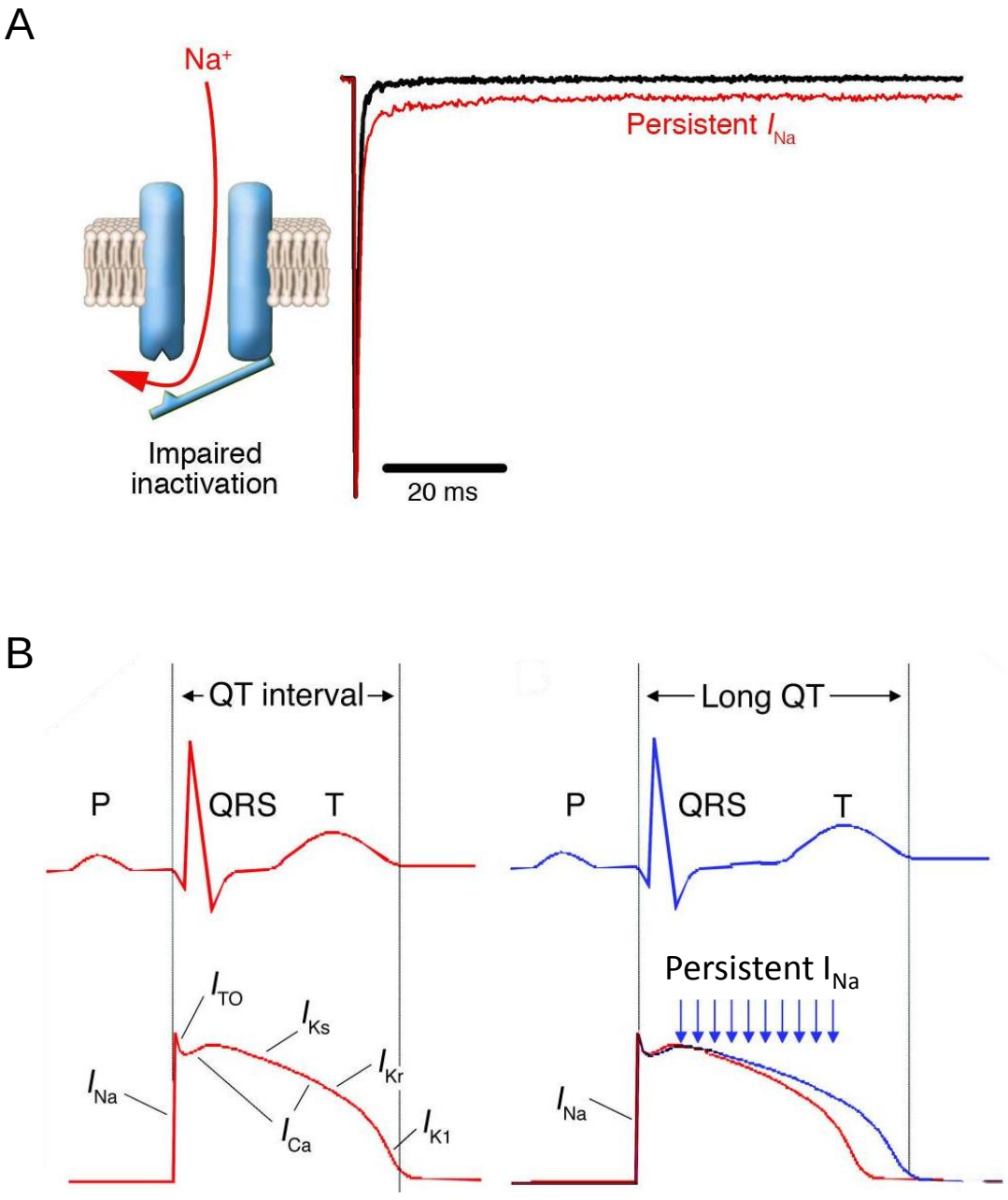

Figure 7. Persistent I_{Na} contributes to LQTS. (A) Mutations in $Na_V1.5$ that impair inactivation, such as delKPQ, can result in persistent current that can elongate the cardiac action potential. (B) The extended time course of the action potential lengthens the depolarization and repolarization cycle of the ventricles and causes a concurrent lengthening of the QT interval. Adapted from George, 2005 [1].

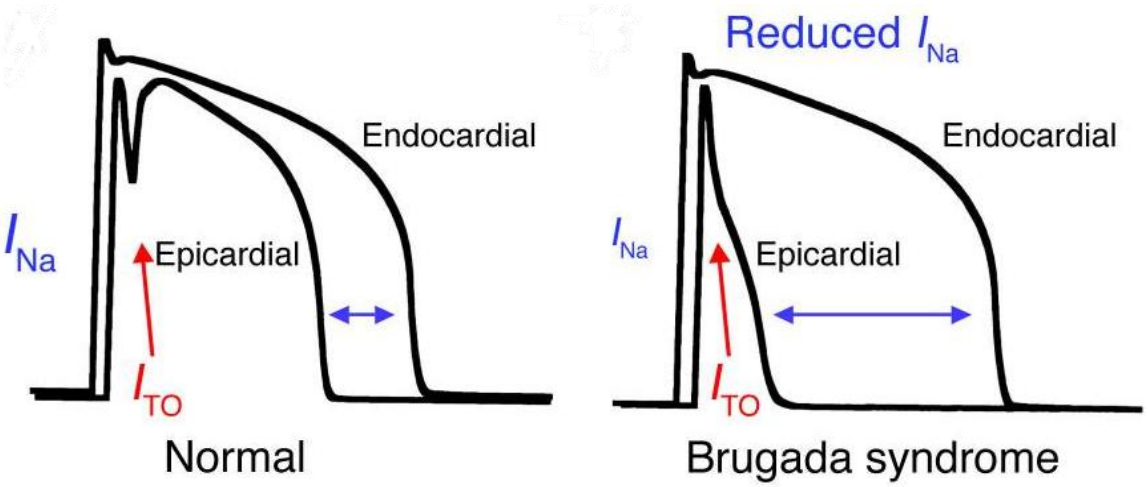

Figure 8. Brugada syndrome as a result of reduced I_{Na}. Modified from George, 2005 [1].

Heart failure and the cardiac sodium channel

A new subset of mutations has been identified that expand the clinical spectrum of sodium channelopathies to disease states resulting in a cardiomyopathic phenotype. In 2004, McNair *et al* provided the first glimpse into $Na_V1.5$-associated heart failure, describing the mutation D1275N segregated in a large family with conduction disorder and dilated cardiomyopathy [20]. Shortly thereafter, Olson *et al* analyzed a cohort of patients diagnosed with idiopathic dilated cardiomyopathy and identified a small number of $Na_V1.5$ mutations, including the already mentioned D1275N and the novel voltage sensor mutation R814W [21]. Multiple cardiomyopathy mutations have since been identified that cluster within voltage sensing regions of $Na_V1.5$ [22]. Critical analysis has revealed that mutations of arginine residues in the S4 regions of DI and DII of $Na_V1.5$ (R219H, R222Q, and R814W) have resulted in a similar form of heart failure, typically diagnosed as dilated cardiomyopathy.

Mutations in voltage sensing region of DI and DII have been identified to alter gating charges and can shift the channel's inherent sensitivity to changes in membrane potential. In 2006, our lab characterized R814W and noted significant changes to window-currents and ramp-currents that indicate this mutant channel activates at hyperpolarized potentials compared with wild-type channel, signifying possible channel openings during diastole [23]. Biophysical analysis of R222Q revealed a similar pattern of hyperpolarized window- and ramp-currents, however, the complexity of the clinical outcome is extensive and those individuals with this mutation present with multiple arrhythmias linked to Purkinje system dysfunction and heart failure often in the form of dilated cardiomyopathy [24], [25]. Many of these patients were successfully treated with

quinidine, which often resulted in a decrease in PVCs and a recovery of heart function, consistent with previous publications indicating treatment of PVCs improves left ventricular function (Figure 9).

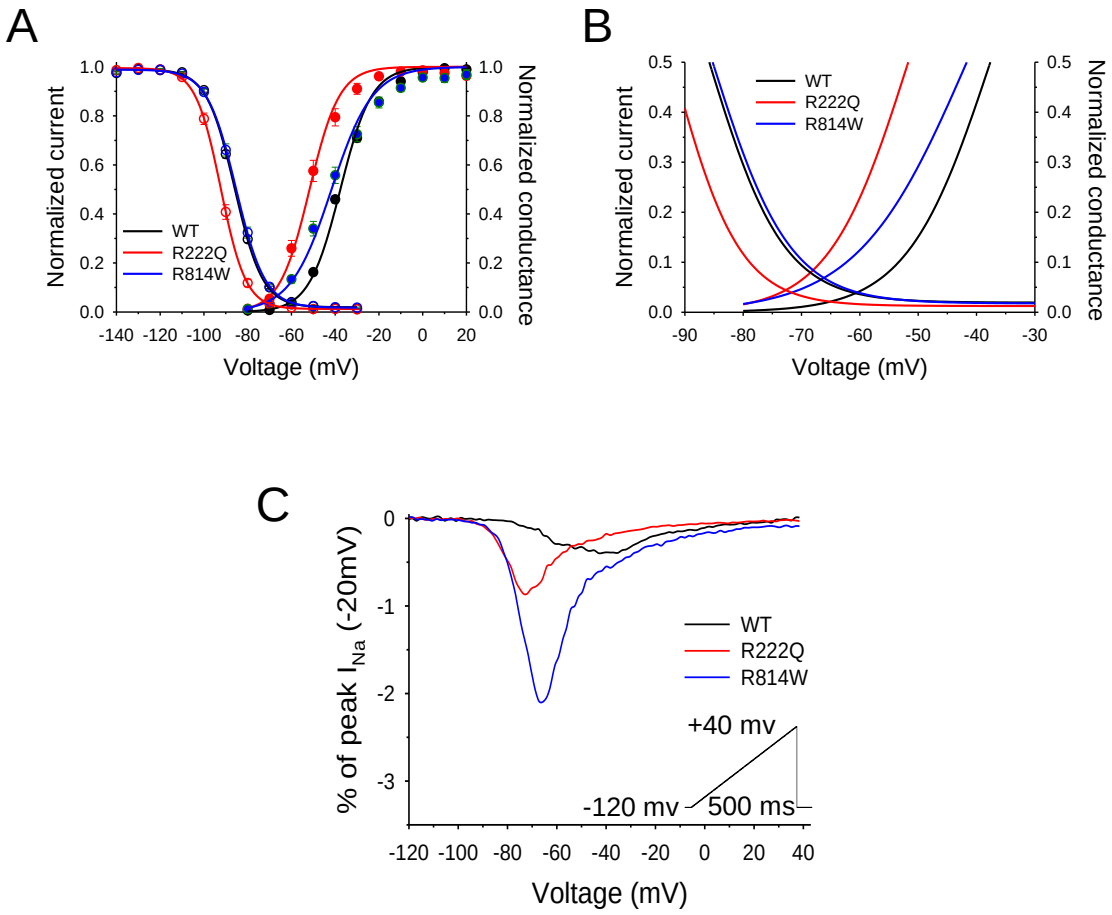

Figure 9. Cardiac sodium channel mutations associated with heart failure. The mutations R222Q and R814W are located in the voltage-sensing regions of domains I and II, respectively. Activation properties are shifted to a hyperpolarized state, thus increasing the window current seen in panels A and B. Panel C shows a larger hyperpolarized peak during a slow ramp current compared with WT channels.

Project summary and specific aims

The aim of this thesis is to identify and characterize cardiac sodium channel ($Na_V1.5$) mutations associated with heart failure phenotypes. We present biophysical analysis of multiple mutations, including the novel mutation, R225P, with similarly hyperpolarized window- and ramp-currents in order to identify a potential indicator for the progression of heart failure.

Part I: Characterization of cardiac sodium channel mutation $Na_V1.5$-R225P

Previous research on cardiac sodium channel mutations have revealed specific channel properties that correlate directly to disease states, such as persistent current leading to LQT syndrome. Here, we identify a hyperpolarized ramp current as a shared functional consequence of mutations that result in a heart failure phenotype. Two mutations resulting in similar cardiomyopathies, $Na_V1.5$-R814W and $Na_V1.5$-R222Q, have been previously identified and characterized [21], [23]–[28]. We corroborated the biophysical findings with our own data on these mutations and compared them to a novel missense mutation, $Na_V1.5$-R225P, found in a patient with amiodarone-responsive ventricular ectopy and impaired contractility. Interestingly, biophysical characterization of these 3 mutations showed similarly altered channel activation with a larger, hyperpolarized ramp current compared to wild type channels. We propose that this ramp current defect could be a biophysical fingerprint for those mutations with a propensity for cardiomyopathies.

Part II: Analysis of $Na_V1.5$ mutations in an isolated, virally-transduced ventricular cardiomyocyte

Mutations in the human heart sodium channel most often cause disorders affecting cardiac rhythm. However, recent research has identified multiple mutations in $Na_V1.5$ associated with a heart failure phenotype. This unexpected association creates an expanded clinical spectrum of conditions associated with cardiac sodium channelopathies and establishes a need to elucidate the link between cardiac Na channel dysfunction and cardiomyopathies.

Intracellular ion homeostasis in cardiomyocytes is tightly regulated by multiple exchangers and transporters that directly couple Na^+ to important cellular processes such as calcium removal via the Na^+/Ca^{2+} exchanger (NCX) and regulation of intracellular pH through the Na^+/H^+ exchanger (NHE). Previous data predicts that the mutations $Na_V1.5$-R814W and $Na_V1.5$-R222Q allow for an inappropriate influx of Na^+ during diastole which has the potential of disturbing intracellular Ca^{2+} and H^+ dynamics leading to myocardial failure. The objective of this section is to establish a relationship between sodium channel dysfunction and impaired contraction as a consequence of altered Ca^{2+} and/or pH homeostasis in cardiac myocytes.

Specific aims

Specific aim 1. To characterize the novel cardiac sodium channel mutation $Na_V1.5$-R225P in comparison to wild type channel and previously identified mutations associated with cardiomyopathy. Mutations to critical arginine residues in the voltage sensing region of $Na_V1.5$ (R814W and R222Q) have been previously identified and

exhibit similar heart failure phenotypes and comparable biophysical characteristics. Because the novel mutation R225P has a similar clinical phenotype and mutates a critical arginine in the S4 region, **I hypothesized that biophysical characterization of the mutation $Na_V1.5$-R225P would reveal a hyperpolarized window-current with a large, hyperpolarized ramp-current** similar to that seen in R814W and R222Q**.**

Specific Aim 2. To determine if mutant Na^+ channel expression in myocytes alters intracellular Ca^{2+} handling. I hypothesized that human mutant Na^+ channel expression alters Ca^{2+} handling within isolated ventricular cardiomyocytes. I predicted that excess intracellular Na^+ would limit the ability of the NCX to extrude cytosolic calcium which will result in aberrant calcium levels during systole and diastole. To test this, I expressed the mutant Na^+ channel in rabbit cardiomyocytes and examined calcium levels during pacing using fluorescent dyes. I expected to see altered calcium kinetics and an increase in basal and peak Ca^{2+} levels.

CHAPTER II

NOVEL *SCN5A* MUTATION IN AMIODARONE-RESPONSIVE MULTIFOCAL VENTRICULAR ECTOPY-ASSOCIATED CARDIOMYOPATHY

Introduction

The voltage-gated cardiac sodium channel $Na_V1.5$ encoded by *SCN5A* is responsible for the initial upstroke of the cardiac action potential [17]. Mutations in *SCN5A* typically manifest as cardiac arrhythmias such as the congenital long-QT or Brugada syndromes, or by variable degrees of impaired cardiac conduction. Importantly, some *SCN5A* mutations are associated with clinical features that overlap more than one disorder [29]. Additionally, a new genotype-phenotype correlation has emerged recently that has expanded the clinical spectrum of sodium channelopathies to include disorders which feature impaired cardiac contractility.

In 2004, McNair *et al*. described a multigenerational family segregating *SCN5A*-D1275N with a complex disorder featuring variable combinations of supraventricular arrhythmias, impaired atrioventricular conduction and dilated cardiomyopathy [20]. Shortly thereafter, Olson *et al.* screened a cohort of patients diagnosed with idiopathic dilated cardiomyopathy and identified five *SCN5A* mutations including a novel voltage sensor mutation (R814W) [21]. Subsequent functional studies of R814W revealed a novel pattern of sodium channel dysfunction featuring a prominent defect in the voltage-dependence of activation [23]. Two other *SCN5A* voltage sensor mutations associated with cardiomyopathy and variable arrhythmias have been identified (R219H, R222Q)

[22], [24]–[26], [28], [30]. The R222Q mutation exhibits many of the same biophysical abnormalities as R814W, whereas R219H appears to have a distinct functional perturbation (gating pore leak current). Importantly, the clinical syndrome associated with some of these mutations, best illustrated for R222Q, exhibits reversibility of contractile dysfunction with antiarrhythmic therapy [24]. However, the pharmacological mechanism responsible for this effect has not been explored.

Here, we present a novel *SCN5A* mutation ($Na_V1.5$-R225P) associated with prenatal arrhythmias, impaired cardiac contractility, and postnatal multifocal ventricular ectopy-associated ventricular dysfunction reversed by amiodarone treatment. We elucidated the functional consequences of the mutation and demonstrated the likely mechanism for amiodarone efficacy. These findings extend the phenotypic spectrum of *SCN5A* mutations and reveal a plausible pharmacological mechanism underlying the reversibility of arrhythmia-associated cardiomyopathy.

Materials and Methods

Subject Ascertainment

The mother of the proband volunteered her son's clinical history and genetic information without solicitation. Subsequently, informed consent was obtained to evaluate medical record information including genetic testing data. The informed consent procedure was approved by the Vanderbilt University Institutional Review Board. Genetic testing for mutations in *KCNQ1*, *KCNH2*, *SCN5A*, *KCNE1*, *KCNE2* and *KCNJ2* was performed by The Scottish Genetics Laboratory, Aberdeen.

Cloning and expression of $Na_V1.5$

A cDNA encoding human $Na_V1.5$ was cloned into the bicistronic vector pRc-CMV_IRES2-CD8 and mutations were created using site-directed mutagenesis. Human-derived tsA201 cells (HEK293 cell line expressing SV40 large T antigen) were transiently transfected with 1.0 μg of WT or mutant $Na_V1.5$ plasmid using FuGeneHD (Roche Diagnostics, Indianapolis, IN) in combination with 0.6 μg of a bicistronic plasmid (pIRES-GFP-hβ1) encoding enhanced green fluorescent protein (GFP) and the human β1 subunit (hβ1) under the control of the CMV immediate early promoter. Positively transfected cells were determined by GFP emission and the binding of beads conjugated with anti-CD8 antibodies.

Electrophysiology

Sodium currents were recorded at room temperature (22-23°C) 48-72 hours after transfection using the whole-cell patch clamp technique as previously described [23]. All data were analyzed using pCLAMP 10.0 or Microsoft Excel 2007 and plotted using SigmaPlot 10.0 (Systat Software, Inc., San Jose, CA). Statistical analysis was performed using Student's t-Test.

Experiments examining persistent I_{Na} and ramp-currents utilized tetrodotoxin (TTX; Tocris Bioscience, Bristol, UK) to allow for the determination of TTX-sensitive sodium current. TTX was added to the bath solution from a stock solution of TTX (3 mM in water) to a final concentration of 30 μM. TTX-sensitive current was determined by offline digital subtraction.

Pharmacology

Amiodarone hydrochloride (Sigma-Aldrich, St. Louis, MO) was dissolved in dimethyl sulfoxide (DMSO; Sigma-Aldrich) to create a stock concentration of 30 mM. For experiments, amiodarone stock was diluted into bath solution for use at 3 μM concentration. Fresh dilutions were made on the day of experiments. Amiodarone or DMSO was continually present in the superfusate during experiments examining the biophysical effects of amiodarone. DMSO concentration never exceeded 0.01% in control or test conditions.

Results

Case Presentation

A Caucasian male was delivered at 37 weeks gestation following an eventful 15 week antenatal course. Fetal tachycardia accompanied by poor ventricular function was noted at 22 weeks. Maternal flecainide administration was initiated at 27 weeks. At 28 weeks, fetal tachycardia with 2:1 atrioventricular (AV) conduction was noted and suggested a supraventricular origin of the arrhythmia. Tachycardia persisted despite escalating the dosage of flecainide. Propranolol was added at 31 weeks and fetal heart rate normalized with concomitant improvement in ventricular function. A maternal flecainide/propranolol regimen was maintained through parturition.

Immediately following birth, a wandering atrial rhythm at 137 bpm with frequent, multifocal ventricular ectopic beats was noted (Figure 10A, Figure 11A). Treatment with amiodarone (5 mg/kg initially three times daily for one week, then twice daily for one week followed by a maintenance dose of amiodarone 5 mg/kg daily) in combination with propranolol (1 mg/kg four times daily; 3 mg four times daily absolute dose) was initiated. Continued atrial and ventricular ectopy was evident at age 1 month, and an ECG obtained at 7 weeks showed atrial tachycardia (atrial rate 260 bpm) with 2:1 AV block (Figure 10B, Figure 11B). The antiarrhythmic regimen was not changed. By 3 months of age, an ECG was reported as showing predominantly sinus rhythm with some ectopy (trace not available). Because of persistent sinus rhythm at age 6 months, amiodarone was discontinued while propranolol was continued (3 mg four times daily). Two weeks after stopping amiodarone, an ECG showed sinus rhythm but with a prolonged QTc interval of

480 msec (Figure 10C, Figure 11C). Propranolol was discontinued at that time. However, he was hospitalized 6 weeks later with supraventricular tachycardia (200 bpm) and multifocal ventricular ectopy (Figure 10D, Figure 11D). Echocardiography demonstrated impaired ventricular function (ejection fraction 43%, fractional shortening 17%; Figure 12). Amiodarone was restarted with an initial loading dose followed by a maintenance dose of 5 mg/kg/day. Propranolol was reinstituted at a dose of 1 mg/kg four times daily and he was started on captopril 0.5 mg/kg three times daily. This regimen suppressed abnormal rhythms (Figure 10E, Figure 11E) and there was improvement in ventricular function albeit with an unexplained change in P wave morphology as compared to age 6.5 months (Figure 10C). Subsequent attempts to replace amiodarone with sotalol were unsuccessful with recurrence of tachycardia, increased frequency of ventricular ectopy and one episode of nonsustained ventricular tachycardia. There were no documented episodes of ventricular arrhythmia that resembled torsades de pointes. At age 6 years, the proband remained on amiodarone but propranolol was substituted with nadolol. There have been rare syncopal events, no occurrences of cardiac arrest, but mild growth retardation was noted. Invasive electrophysiological testing was not performed.

There is no family history of cardiac arrhythmia or sudden unexplained death. Both parents and an older female sibling are healthy with normal heart rhythms and normal ECG indices including normal QTc intervals. Genetic testing of the proband revealed a novel missense mutation in *SCN5A* predicting the substitution of arginine at position 225 with proline (R225P). Neither parent nor the sibling carried this variant, consistent with a *de novo* mutation in the proband.

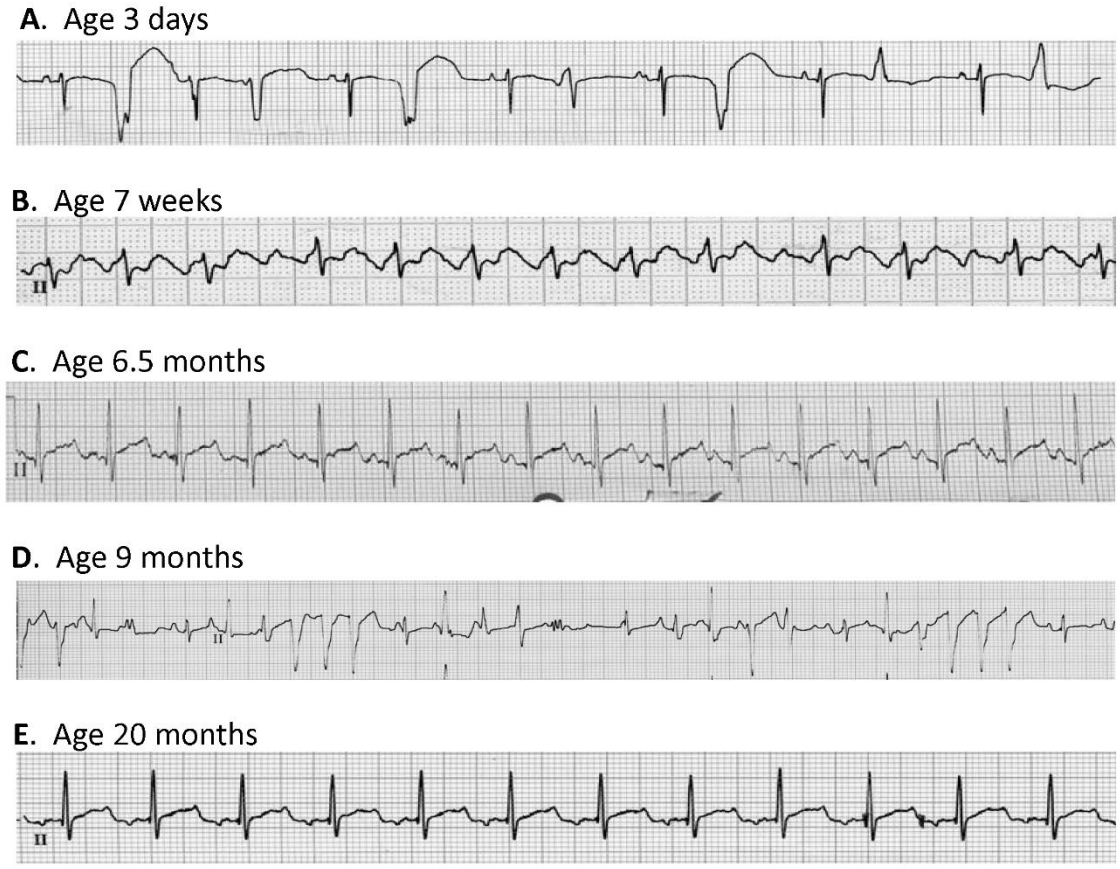

Figure 10. Electrocardiograms from the proband. (A) Representative lead II recording obtained at age 3 days illustrating wandering atrial rhythm with frequent multifocal premature ventricular beats. (B) Representative lead II recording obtained at age 7 weeks illustrating an episode of supraventricular tachycardia with variable 2:1 and 3:1 AV block. (C) Representative lead II recording obtained at age 6.5 months two weeks off amiodarone illustrating sinus rhythm with a prolonged QTc (480 ms). (D) Representative lead II recording obtained at age 9 months while the proband was off antiarrhythmic drugs illustrating multifocal ventricular ectopy and two 3-4 beat runs of nonsustained ventricular tachycardia. (E) Representative lead II recording obtained at age 20 months while treated with amiodarone and propranolol illustrating sinus rhythm. More complete ECG recordings corresponding to each of these events are provided as Figure 11.

A. Age 3 days

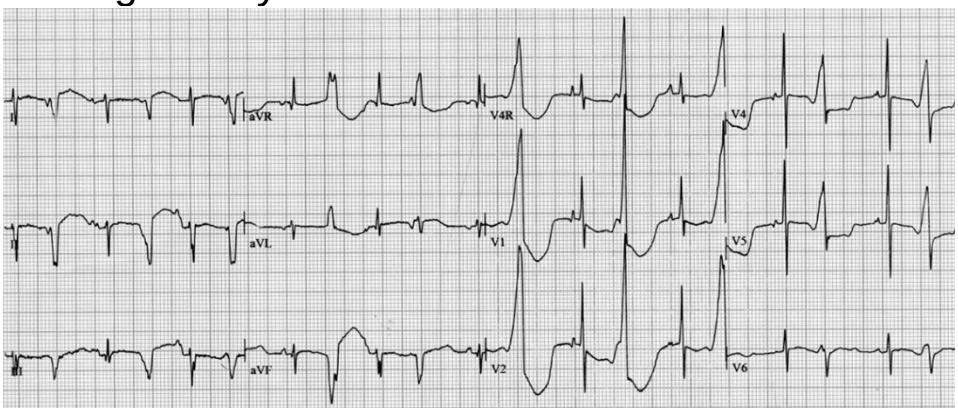

B. Age 7 weeks

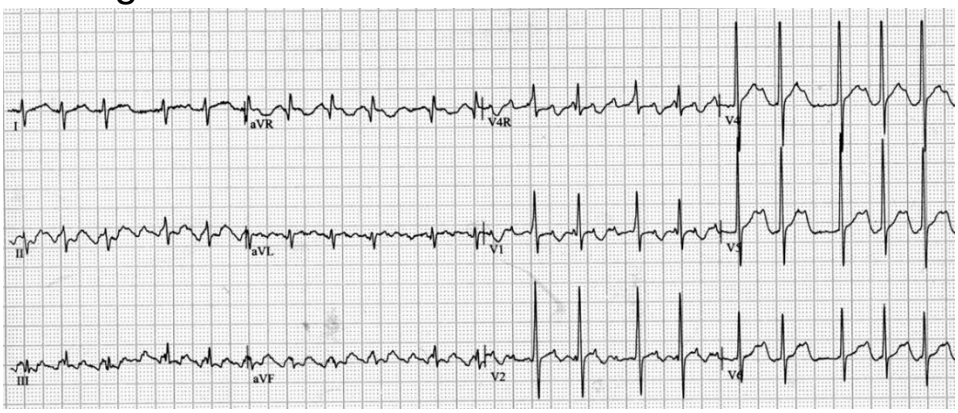

C. Age 6.5 months

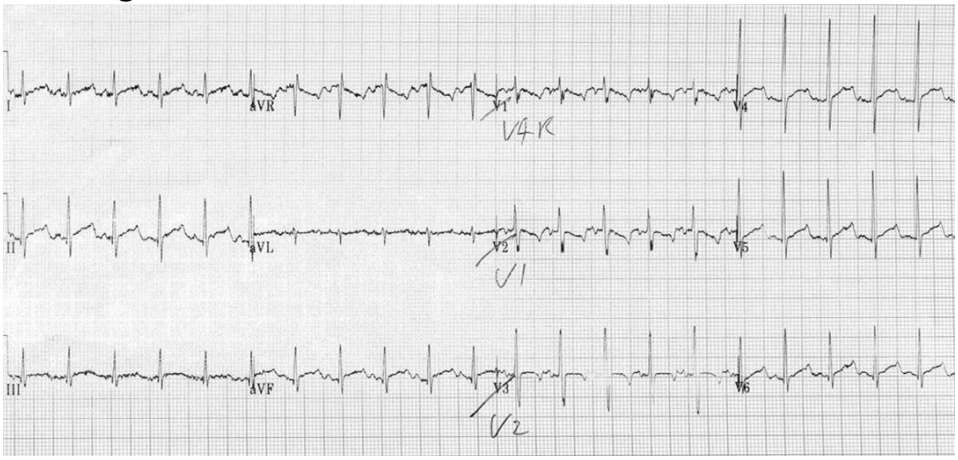

D. Age 9 months

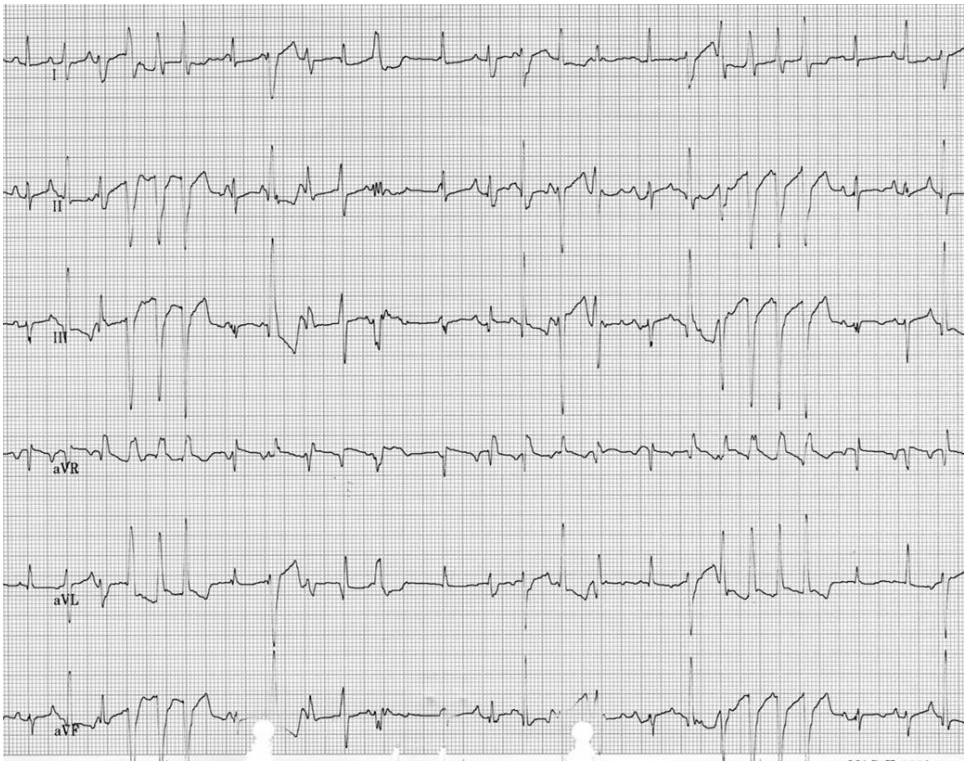

E. Age 20 months

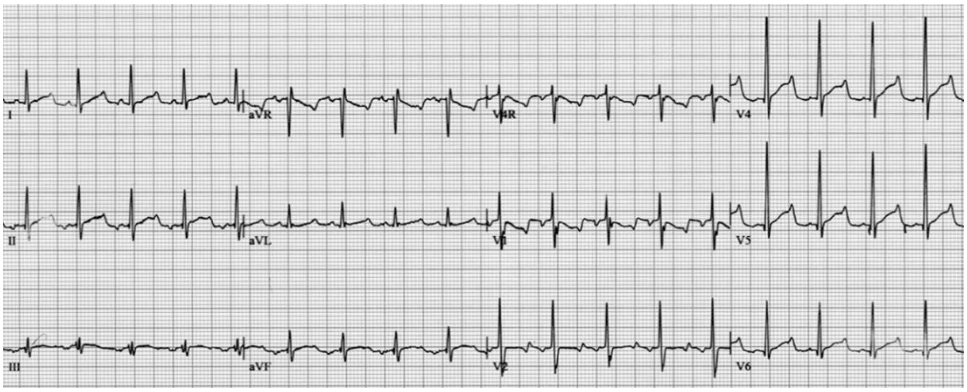

Figure 11. Additional electrocardiographic recordings of the proband.

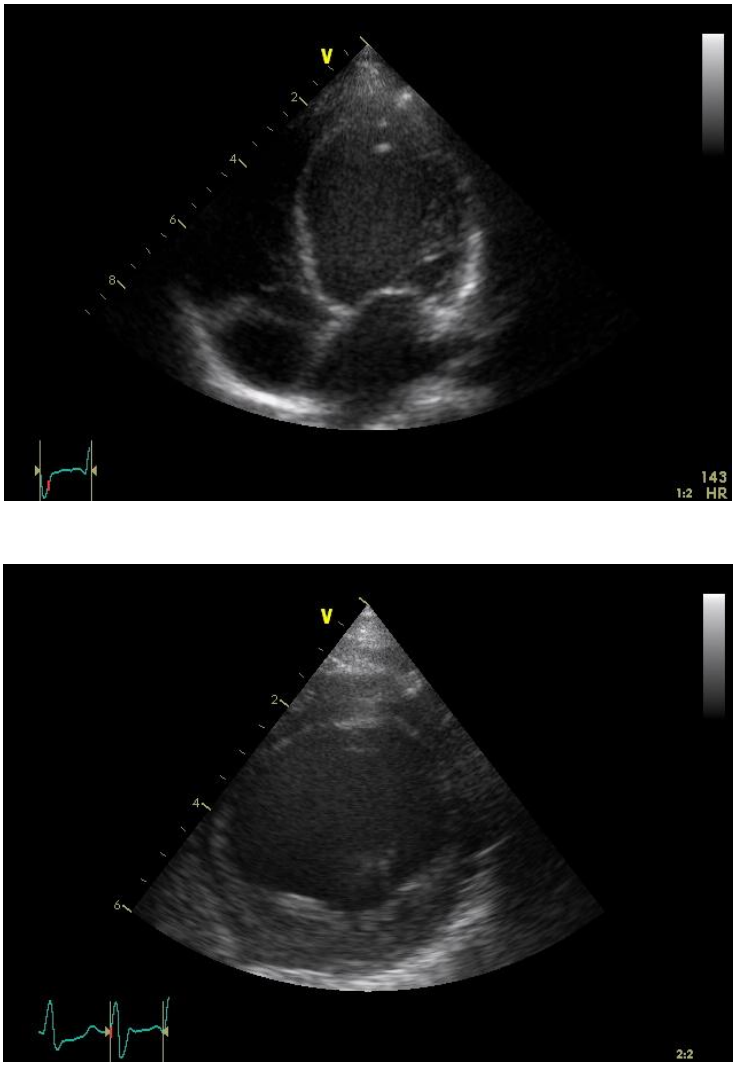

Figure 12. Echocardiographic images of the proband (weight 8.4 kg, height 69 cm) illustrating dilation of all cardiac chambers.

Functional properties of $Na_V1.5$-R225P

We compared the functional properties of WT and R225P mutant cardiac sodium channels ($Na_V1.5$) heterologously expressed in tsA201 cells with the human β_1 subunit (Figure 13). Cells expressing R225P exhibited significantly greater current density and appeared to activate at more hyperpolarized potentials than WT channels (Figure 13A,B). Boltzmann fits of the conductance-voltage plots revealed similar voltage dependence of activation for WT and R225P ($V_{½}$ values: WT, -37.3±0.06 mV; R225P, -37.1±1.0) but R225P exhibited a significantly shallower slope (WT: 8.4±0.2, R225P: 12.3±0.3; $p<0.005$; Figure 13C; Table 2) suggesting a blunted voltage sensitivity. Activation kinetics, as determined by the time-to-peak current at an activating potential of -20mV, were also significantly altered in the mutant channel (R225P: 0.96±0.01 ms; WT: 0.67±0.02 ms; $p<0.005$; Figure 14A; Table 2). These findings were consistent with a structural perturbation of the domain 1 voltage-sensor segment that disrupts channel activation.

In addition to abnormalities in activation, inactivation of R225P channels was also abnormal (Figure 13D). Time constants for inactivation determined by fitting current decay with a double exponential function were significantly larger for R225P channels across a range of voltages compared to WT channels indicating slower inactivation (Figure 13E). Additionally, the mutant channels exhibited a significantly larger fraction of current inactivating with a slow component (time constant τ_2; Figure 14B). Cells expressing R225P also had a significantly larger persistent current measured as a percentage of peak current (0.87±0.06%, n=10) compared to WT channels (0.13±0.02%, n=18; $p<0.005$; Figure 13F; Table 2). This level of increased persistent current was

similar to what we observed in parallel experiments for an LQTS-associated mutant $Na_V1.5$ channel (delKPQ: 0.65±0.04%, n=8; Table 2) [31]. By contrast, the voltage dependence of steady-state inactivation (channel availability) and the time course of recovery from fast inactivation of R225P were not overtly different from WT channels (Figure 14C,D; Table 2). Although the voltage midpoints ($V_{½}$ values) for activation and inactivation were not affected by the mutation, the more shallow activation curve slope caused a significantly expanded 'window current' defined as the extent of overlap between the two curves (Figure 15A). This suggests that the R225P mutation could evoke aberrant sodium current activation at voltages within the window.

The potential for aberrant sodium current activation was further probed by examining channel responses to depolarizing voltage ramps. Comparing R225P ramp-currents to those of WT channels revealed critical differences in magnitude and kinetics. For R225P, averaged ramp currents exhibit activation with a broad, nearly bifid peak at significantly more hyperpolarized potentials than WT channels (Figure 15B; Table 2). Net charge movement during voltage ramps was 8-fold greater for R225P than WT channels (WT: 0.66±0.1 pC/nA, R225P: 5.86±0.6 pC/nA; $p<0.005$) (Figure 16; Table 2). These findings indicate that aberrant sodium current conducted by R225P channels can be evoked by voltages close to the resting membrane potential of cardiomyocytes.

Figure 13. Biophysical properties of $Na_V1.5$-R225P. (A) Representative traces of WT (top) and R225P (bottom) sodium channels. (B) Current-density/voltage plots of WT and R225P. (C) Voltage dependence of activation for WT and R225P from -80 to +20 mV. (D) Representative traces of WT and R225P illustrating altered activation and inactivation kinetics. (E) Voltage-dependence of inactivation time constants (open symbols represent fast component; closed symbols represent slow component) for WT and R225P. (F) Representative TTX-subtracted whole cell current for WT and R225P. Persistent current was measured over the final 10 ms of a 200 ms pulse to -20 mV and normalized to peak current. Inset shows persistent current over the final 50 ms. All data are represented as mean ± S.E.M for n=11-18 cells.

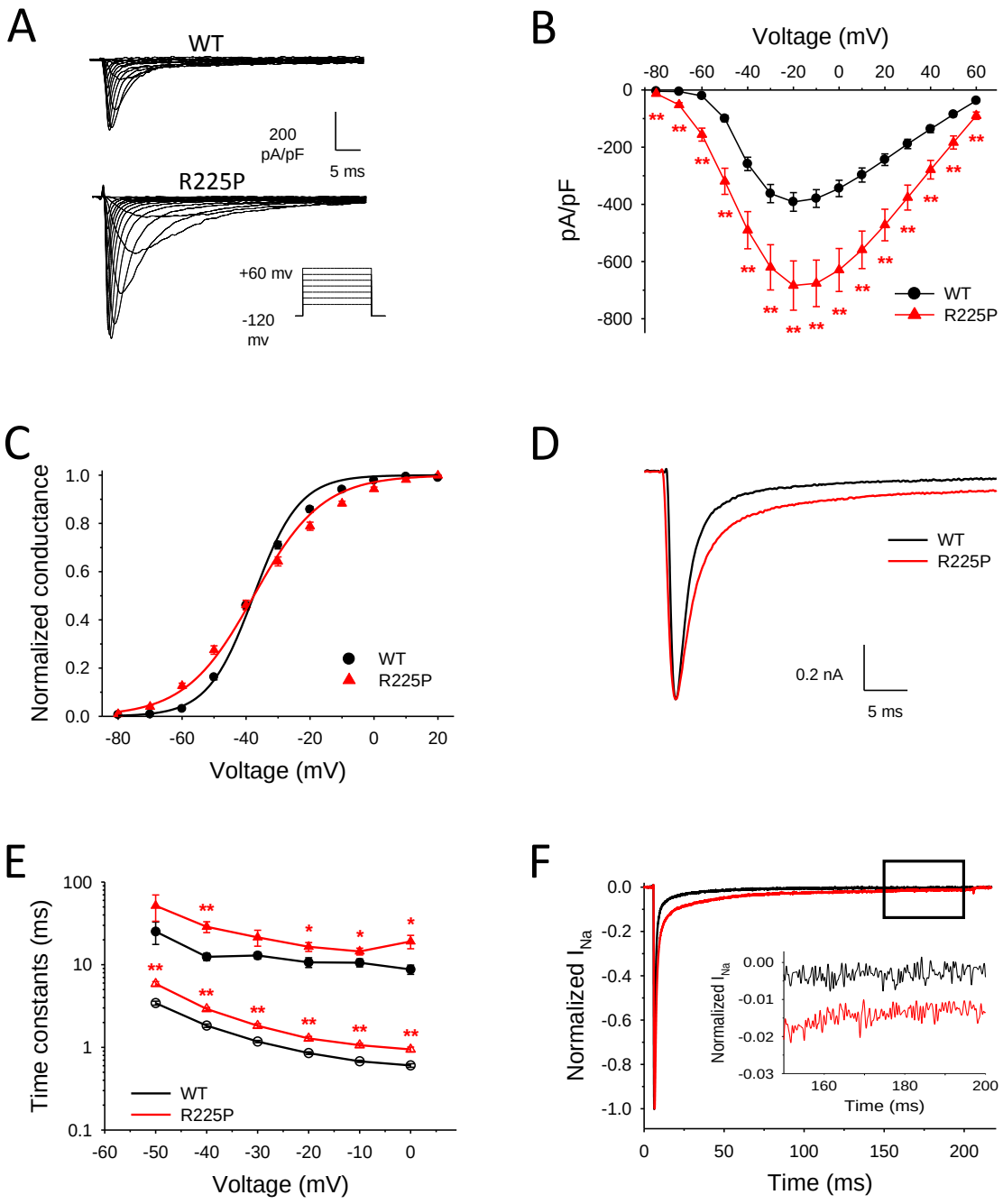
A
WT
200
pA/pF
5 ms
R225P
+60 mv
-120
mv
B
Voltage (mV)
-80 -60 -40 -20 0 20 40 60
0
-200
-400
-600
-800
pA/pF
WT
R225P
C
Normalized conductance
1.0
0.8
0.6
0.4
0.2
0.0
-80 -60 -40 -20 0 20
Voltage (mV)
WT
R225P
D
WT
R225P
0.2 nA
5 ms
E
Time constants (ms)
100
10
1
0.1
-60 -50 -40 -30 -20 -10 0
Voltage (mV)
WT
R225P
F
Normalized I_{Na}
0.0
-0.2
-0.4
-0.6
-0.8
-1.0
0 50 100 150 200
Time (ms)
Normalized I_{Na}
0.00
-0.01
-0.02
-0.03
160 180 200
Time (ms)

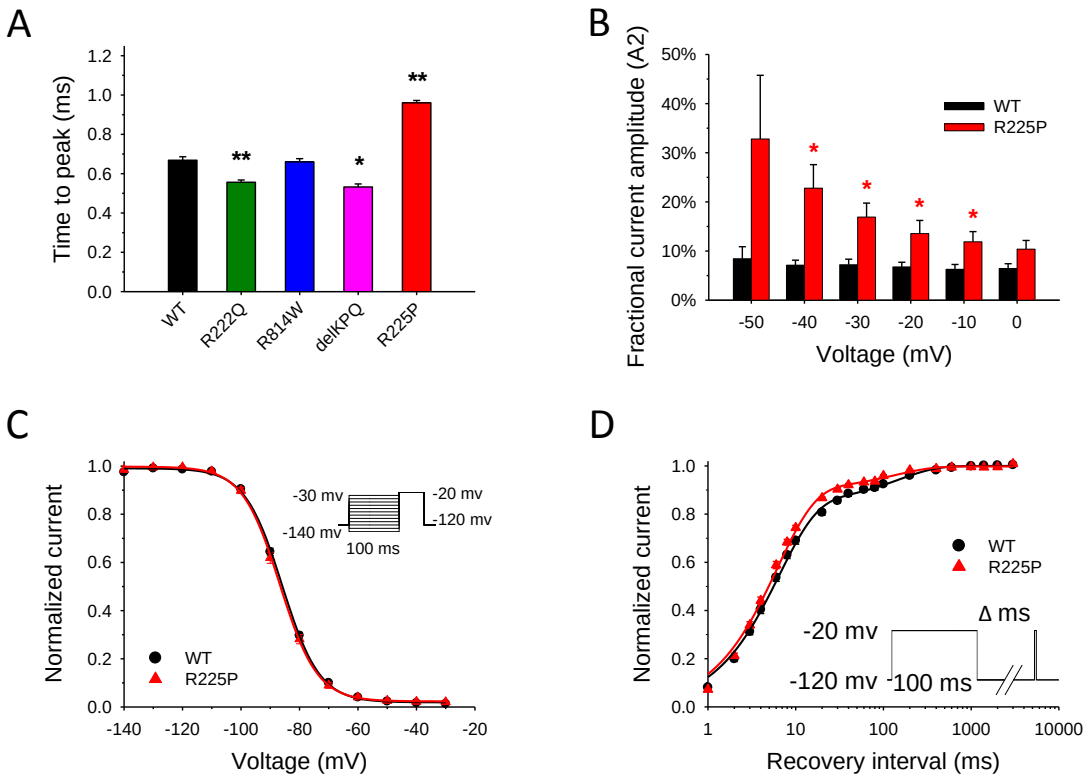

Figure 14. Activation and inactivation of R225P. (A) Activation kinetics measured as time to peak current derived from activating pulses to -20mV (holding potential -120 mV) for WT and mutant channels. (B) Percentage of current inactivation associated with the slow component (time constant, τ2) of current decay for WT and R225P. (C) Channel availability of WT and R225P. (D). Recovery from fast inactivation. All data are represented as mean ± S.E.M. for n= 8 - 9 cells.

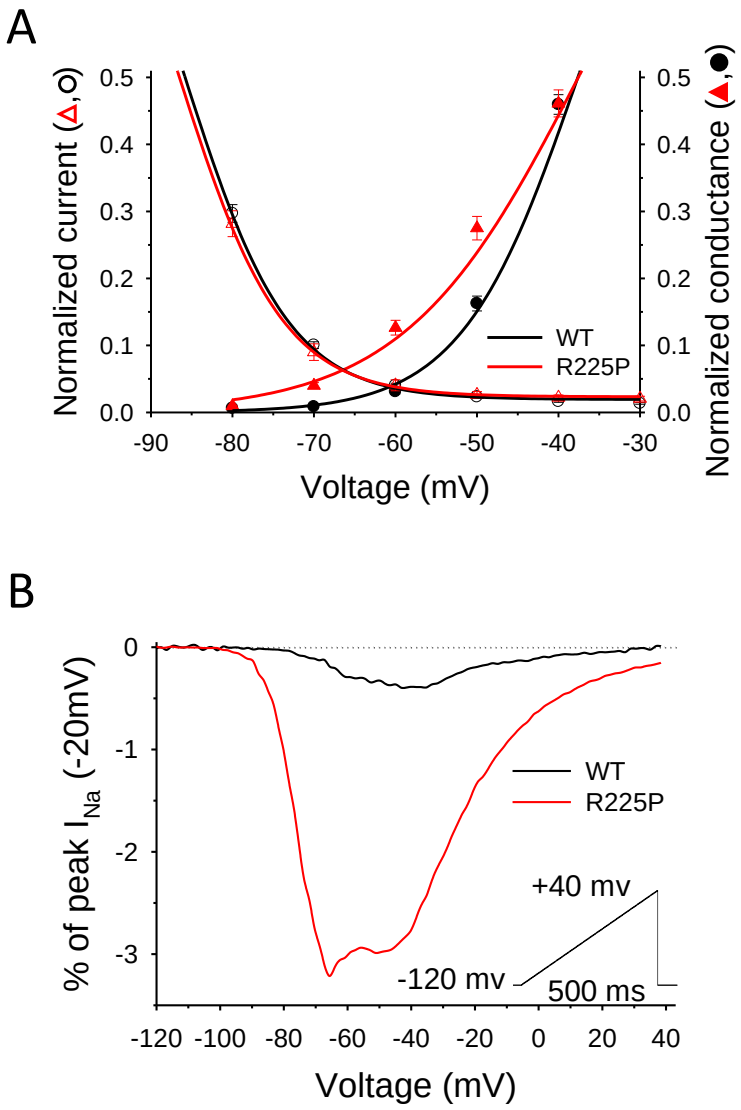

Figure 15. Window and ramp-currents of $Na_V1.5$-R225P reveal aberrant I_{Na} at hyperpolarized potentials. (A) Overlay of Boltzmann-fitted G/V and channel availability curves of WT and R225P emphasizing window-currents. (B) Normalized TTX-subtracted average ramp-currents (0.32 mV/ms) of WT and R225P measured as a percentage of peak I_{Na} (-20mV). All data are represented as mean ± S.E.M for n=7-15 cells.

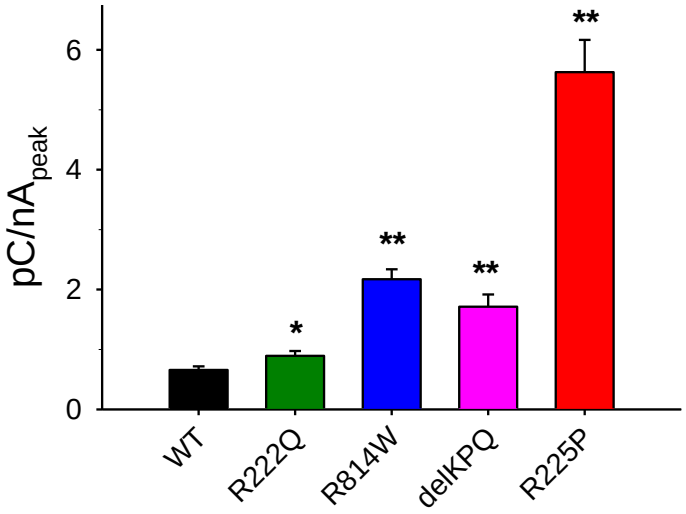

Figure 16. Ramp-current analysis. Net charge movement during slow voltage-ramps of WT and mutant channels.

Table 2. Biophysical properties of WT-$Na_V1.5$ and mutant channels.

		WT	R225P	R222Q
Activation	$V_{½}$	-37.3 ± 0.6	-37.1 ± 1.0	-51.2 ± 1.5**
	k	8.4 ± 0.2	12.3 ± 0.3**	7.6 ± 0.4
	n	14	11	13
Inactivation	$V_{½}$	-86.0 ± 0.4	-86.8 ± 0.6	-92.7 ± 0.8**
	k	-6.4 ± 0.1	-6.3 ± 0.1	-5.6 ± 0.1**
	n	11	10	14
Window-current peak	*Voltage*	-60.4 ± 0.4	-67.0 ± 1.2**	-74.7 ± 0.4**
	Activity	0.037 ± 0.001	0.063 ± 0.002**	0.050 ± 0.002**
	n	10	7	8
Time to peak (-20 mV)	*Peak (ms)*	0.67 ± 0.02	0.96 ± 0.01**	0.56 ± 0.01**
	n	18	10	7
Recovery from fast inactivation	*A1*	0.85 ± 0.01	0.90 ± 0.01*	0.87 ± 0.02
	τ_1	6.5 ± 0.3	6.2 ± 0.3	7.0 ± 0.3
	A2	0.15 ± 0.01	0.10 ± 0.01**	0.14 ± 0.02
	τ_2	178 ± 18	147 ± 14	153 ± 17
	n	18	9	10
500ms Ramps	*Peak (mV)*	45.7 ± 2.7	-57.1 ± 3.0*	-70.9 ± 0.9**
	% peak	-0.60 ± 0.04	-4.9 ± 0.3**	-1.0 ± 0.1**
	Area (pC/nA)	0.66 ± 0.1	5.86 ± 0.6**	0.89 ± 0.1
	n	15	11	8
Ramp-current activation threshold	*Voltage*	-77.2 ± 1.2	-96.5 ± 1.2**	-97.3 ± 1.6**
	n	13	16	8
Persistent I_{Na}	*% peak*	0.13 ± 0.02	0.87 ± 0.06**	0.09 ± 0.03
	n	18	10	7

		R814W	R225Q	delKPQ
Activation	$V_{½}$	-41.1 ± 1.6*	-40.2 ± 0.7*	-28.4 ± 1.2**
	k	10.7 ± 0.4**	9.8 ± 0.2**	10.4 ± 0.1**
	n	15	13	12
Inactivation	$V_{½}$	-84.9 ± 0.8	-90.2 ± 0.6**	-92.5 ± 0.8**
	k	-6.5 ± 0.2	-6.6 ± 0.2	-5.6 ± 0.1**
	n	14	10	14
Window-current peak	***Voltage***	-65.3 ± 0.9**	-65.6 ± 0.7**	-60.7 ± 1.5
	Activity	0.064 ± 0.003**	0.038 ± 0.002	0.025 ± 0.002**
	n	12	11	10
Time to peak (-20 mV)	***Peak (ms)***	0.66 ± 0.02	0.75 ± 0.03*	0.53 ± 0.02**
	n	7	14	8
Recovery from fast inactivation	***A1***	0.88 ± 0.01	0.85 ± 0.02	0.86 ± 0.02
	τ_1	6.8 ± 0.5	7.8 ± 0.7	4.9 ± 0.2**
	A2	0.11 ± 0.01*	0.15 ± 0.02	0.14 ± 0.02
	τ_2	190 ± 29	209 ± 289	265 ± 49
	n	8	8	10
500ms Ramps	***Peak (mV)***	-64.9 ± 1.4**	-56.7 ± 3.4*	-35.0 ± 1.9*
	% peak	-2.4 ± 0.1**	-0.9 ± 0.1**	-1.0 ± 0.1**
	Area (pC/nA)	2.17 ± 0.2**	1.01 ± 0.2	1.71 ± 0.2**
	n	7	12	8
Ramp-current activation threshold	***Voltage***	-95.4 ± 2.3**	-86.42 ± 1.6**	-68.5 ± 1.2**
	n	7	11	7
Persistent I_{Na}	***% peak***	0.17 ± 0.03	0.24 ± 0.03*	0.65 ± 0.04**
	n	7	14	8

Versus WT

* = P < 0.05

** = P < 0.005

Altered slow inactivation of R225P channels

To further investigate the functional consequences of R225P, we examined the sensitivity of the mutant channel to frequency-dependent inhibition. Stimulating at 2 Hz with a 5 ms test pulse, we did not identify a difference in current amplitude between WT and R225P following 100 pulses (Figure 17A, Figure 18A; Table 3). However, at pulse lengths of 100 ms and 300 ms, there was a significant divergence in current amplitude for WT and R225P at pulse 100, with the mutant channel exhibiting a greater sensitivity to the frequency-dependent protocol. This dependence on the pulse duration without an overt difference in recovery from fast inactivation suggested possible involvement of enhanced slow inactivation to explain the greater activity-dependent loss of channel availability observed for R225P.

We compared the slow inactivation properties of WT and R225P channels. As illustrated by Figure 17B and data in Table 3, both WT and R225P channels enter slow inactivation with similar rates during conditioning pulses up to 3000 ms. However, for conditioning pulse durations longer than 3000 ms, the behavior of WT and R225P channels diverge, with R225P showing enhanced entry into a slow inactivated state. Using a 3000 ms test pulse (approximate midpoint for onset of slow inactivation for both WT and R225P), we measured recovery from slow inactivation (Figure 17C, Table 3). The biexponential time course of recovery from slow inactivation observed for R225P was significantly slower than WT channels. Further, we observed that the voltage-dependence of slow inactivation was significantly shifted in the hyperpolarized direction for R225P compared with WT channels (Figure 17D, Table 3). Collectively, these findings indicate that the R225P mutation stabilizes the slow inactivated state and

enhances the tendency for slow inactivation. To determine whether this enhanced slow inactivation might affect the ramp current, we examined channel availability following a series of ramp depolarizations (500 ms ramps; 1.1 Hz). There was a significant decrease in charge movement at pulse 100 for R225P but not WT channels. Despite this effect of repetitive pulsing, charge movement associated with voltage ramps remained greater for R225P than WT channels (Figure 19; Table 3).

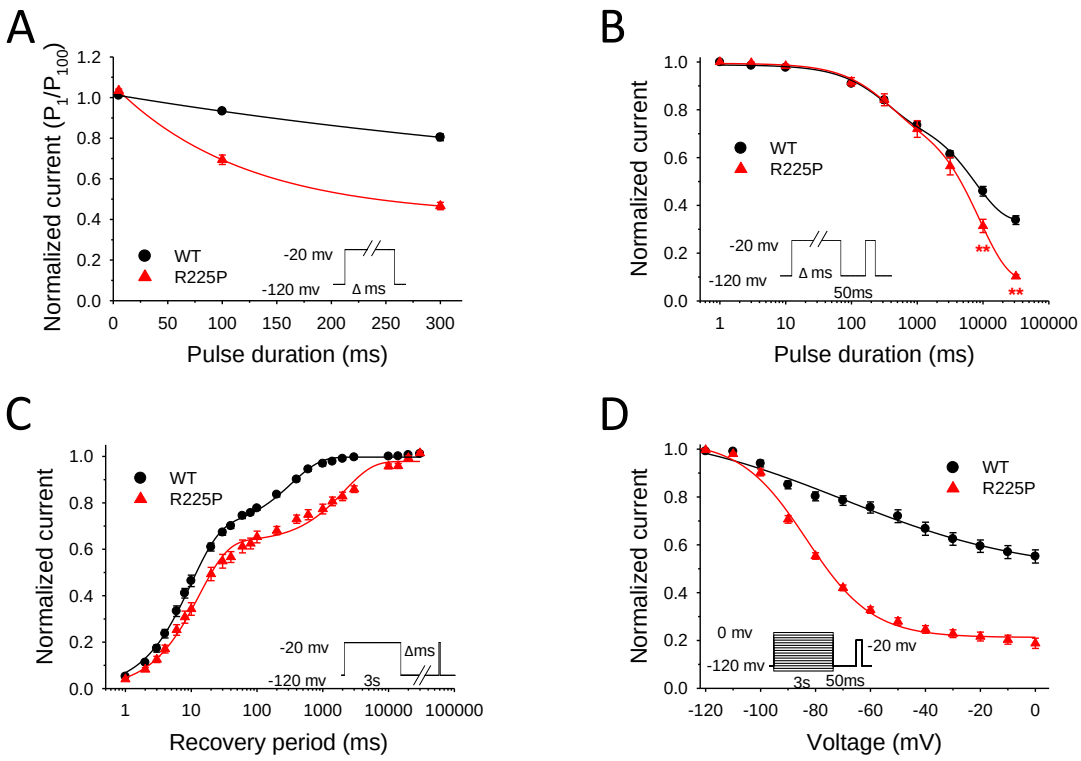

Figure 17. $Na_V1.5$-R225P stabilizes the slow-inactivated state. (A) Frequency-dependent channel inhibition of WT (black) and R225P (red) observed for activating pulse durations of 5, 100, and 300 ms. Curves were fit with exponential decay functions. (B) Onset of slow inactivation for WT and R225P. (C) Recovery from slow inactivation. WT (black line) and R225P (red line) data fit with double-exponential curves. (D) Voltage-dependence of slow-inactivation of WT and R225P. Curves are the result of data fittings with the Boltzmann function. All data are represented as mean ± S.E.M for n=7-15 cells.

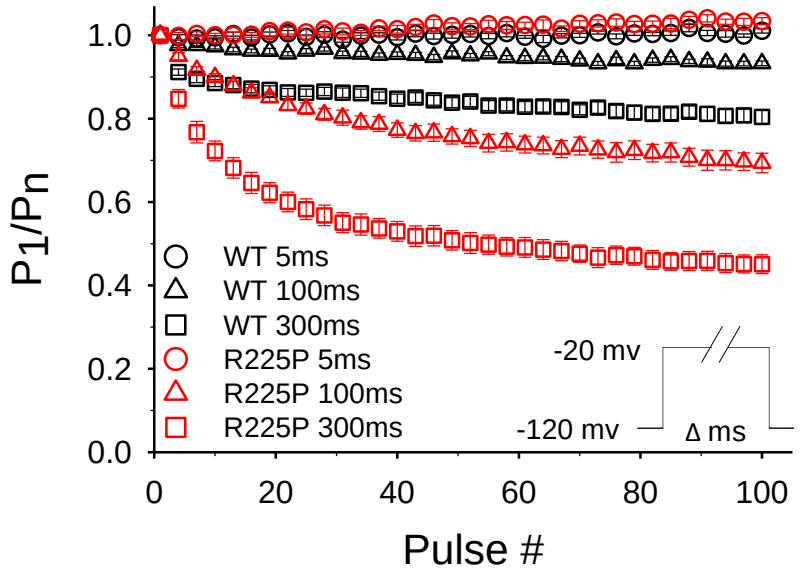

Figure 18. Frequency-dependent inhibition. Pulse trains (2Hz; -20mV) illustrated for WT (black) and R225P (red) channels with activating pulses of 5 ms (open circles), 100 ms (open triangles), or 300 ms (open square). All data are represented as mean ± S.E.M. for n = 11 - 15 cells.

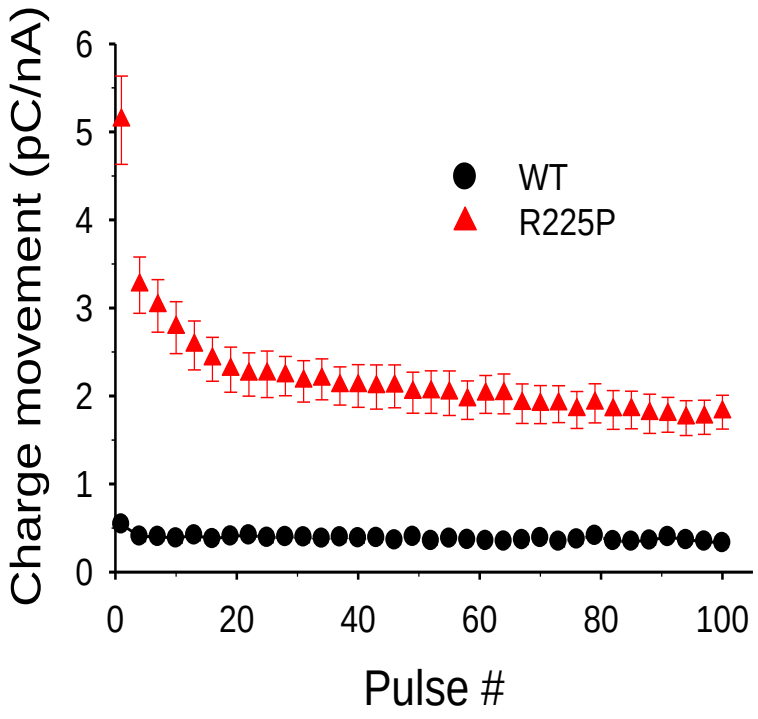

Figure 19. Ramp-current analysis. Charge movement in response to consecutive 500 ms ramp-current protocols (1.1 Hz; 100 pulses). All data are represented as mean ± S.E.M. for n = 7 - 16 cells.

Table 3. Frequency-dependent inhibition and slow inactivation properties of WT-$Na_V1.5$ and R225P.

			WT	R225P
Frequency dependent inhibition 2 Hz	**5 ms pulse length**	P_1/P_{100}	1.01 ± 0.01	1.03 ± 0.01*
		n	11	12
	100 ms pulse length	P_1/P_{100}	0.93 ± 0.01	0.69 ± 0.02**
		n	15	15
	300 ms pulse length	P_1/P_{100}	0.80 ± 0.02	0.47 ± 0.02**
		n	14	12
Onset of slow inactivation		***A1***	0.21 ± 0.03	0.21 ± 0.04
		τ_1	314.1 ± 41.5	373.3 ± 81.5
		A2	0.45 ± 0.04	0.7 ± 0.04**
		τ_2	9973.5 ± 1601.2	10321.1 ± 224.5
		y0	0.32 ± 0.02	0.08 ± 0.003**
		n	8	7
Recovery from slow inactivation (3s pre-pulse)		***A1***	0.69 ± 0.01	0.63 ± 0.02*
		τ_1	10.1 ± 0.9	14.0 ± 1.1*
		A2	0.31 ± 0.01	0.35 ± 0.02
		τ_2	352.3 ± 24.4	2261.9 ±
		n	9	9
Voltage dependence of slow inactivation		$V_{½}$	-68.9 ± 5.2	-83.5 ± 0.8*
		k	-32.9 ± 2.2	-12.0 ± 0.4**
		n	8	8
1.1 Hz ramp train (P_{100})		***Area (pC/nA)***	0.33 ± 0.04	1.82 ± 0.19**
		n	8	13

Versus WT
* = P < 0.05
** = P < 0.005

Comparisons with other *SCN5A* mutations

Two other mutations have been identified previously affecting the same residue as R225P, but the associated clinical phenotypes and functional disturbances are different. Mutation R225Q was identified in a heterozygous subject exhibiting a mild form of LQTS without reported features of cardiomyopathy [32]. We characterized $Na_V1.5$-R225Q. (Figure 20; Table 2) and found rather minor differences in channel activation and channel availability (hyperpolarized shifts) compared with WT channels. We also observed an increased persistent current (Table 2) although ramp currents did not differ with that of WT channels. Mutation R225W was identified in a heterozygous woman without symptoms, but also in her child with severe conduction disturbances who had a second mutation (W156X) inherited from the father [33]. Functional studies of the R225W mutation demonstrated a positively shifted channel availability curve and a significant decrease in current density, distinct from the constellation of findings we observed for R225P.

By contrast, the functional properties of R225P channels resembled features of two other *SCN5A* mutations identified in subjects diagnosed with either dilated cardiomyopathy (R814W) [21], [23] or multifocal ventricular ectopy with reversible contractile dysfunction (R222Q) [24], [25]. Mutation R222Q affects another conserved arginine residue in the D1/S4 voltage sensor segment and is located approximately one helix turn away from position 225. The R814W mutation also alters a conserved voltage sensor arginine residue but in the second domain. We compared biophysical properties of R222Q and R814W and found that both mutations exhibit altered conductance-voltage relationships and predispose channels to activation at more hyperpolarized potentials

during slow voltage ramps similar to R225P (Figure 21; Figure 22). In contrast to R225P, neither R222Q nor R814W exhibited increased persistent sodium current (Table 2).

A comparison of normalized ramp currents for these three mutants with that of a representative LQTS mutation (delKPQ) reveals an interesting segregation of the voltage range in which the currents peak (Figure 21; Table 2). Specifically, those mutations clinically associated with impaired ventricular function peak at more hyperpolarized potentials than the LQTS mutation. Additionally, average ramp currents exhibited by R225P are nearly bifid with one component peaking around -70 mV (similar to R222Q and R814W) while the second component peaks near -40 mV, closer to delKPQ. We suggest that the hyperpolarized activation of R222Q, R814W and the main component of R225P ramp currents correlate with the altered activation voltage dependence, whereas the more depolarized activation observed for delKPQ and the second component of R225P are associated with increased persistent sodium current and a slower time course of fast inactivation. Finally, both R814W [23] and R225P exhibit similar enhanced slow inactivation properties, but R222Q was not previously tested in this manner.

Figure 20. Biophysical properties of $Na_V1.5$-R225Q. (A) Representative traces of WT (top) and R225Q (bottom) sodium channels. (B) Current-density/voltage plots of WT and R225Q. (C) Voltage dependence of activation and channel availability for WT and R225Q. (D) Representative traces of WT and R225Q at -20 mV. (E) Voltage-dependence of inactivation time constants (open symbols represent fast component; closed symbols represent slow component) for WT and R225Q. (F) Normalized TTX-subtracted average ramp-currents (0.32 mV/ms) of WT and R225Q measured as a percentage of peak I_{Na} (-20 mV). All data are represented as mean ± S.E.M for n = 7 - 15 cells.

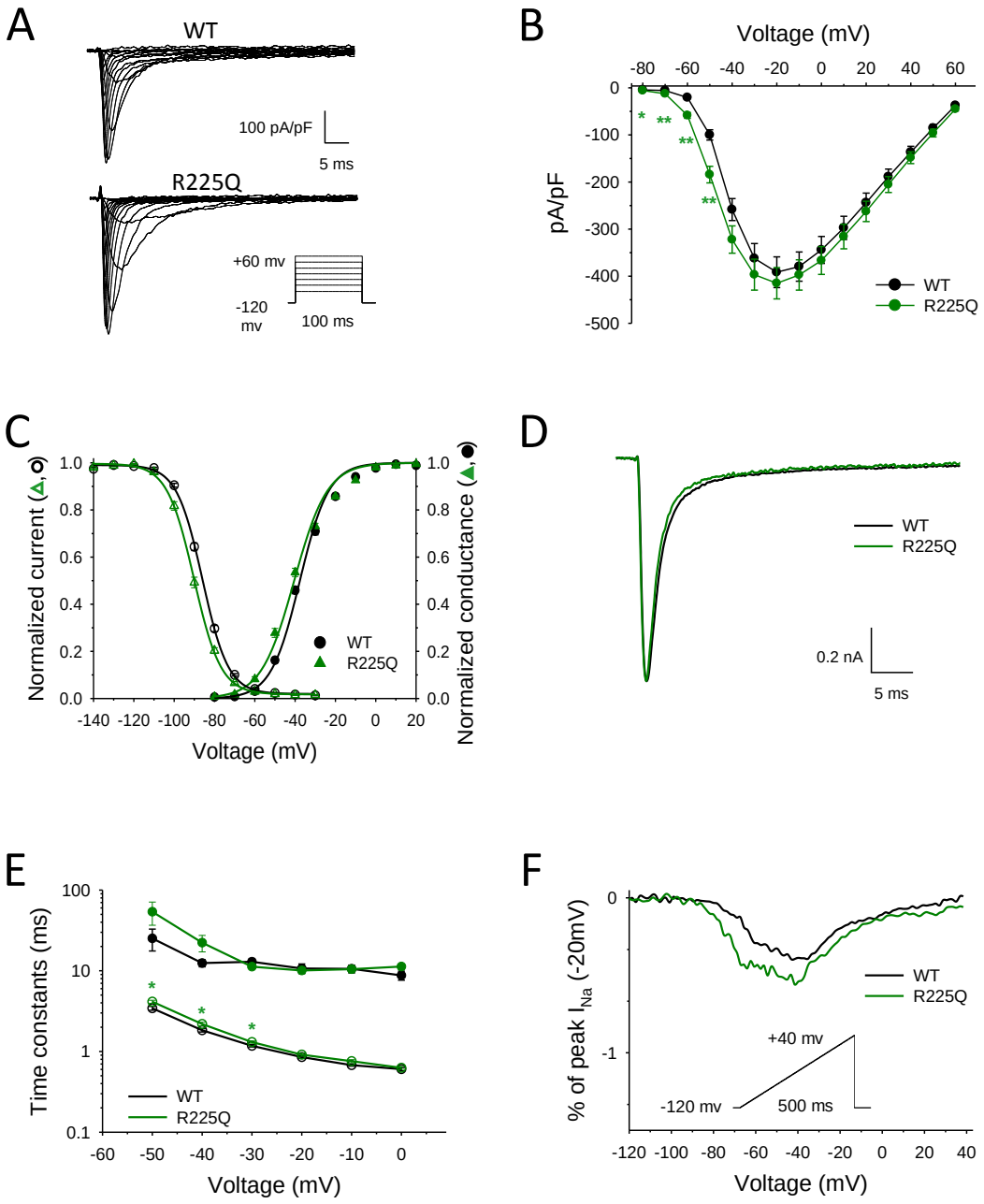
A
WT
100 pA/pF
5 ms
R225Q
+60 mv
-120 mv
100 ms
B
Voltage (mV)
pA/pF
WT
R225Q
C
Normalized current (▲, ○)
Normalized conductance (▲, ●)
Voltage (mV)
WT
R225Q
D
WT
R225Q
0.2 nA
5 ms
E
Time constants (ms)
Voltage (mV)
WT
R225Q
F
% of peak I_{Na} (-20mV)
WT
R225Q
+40 mv
-120 mv
500 ms
Voltage (mV)

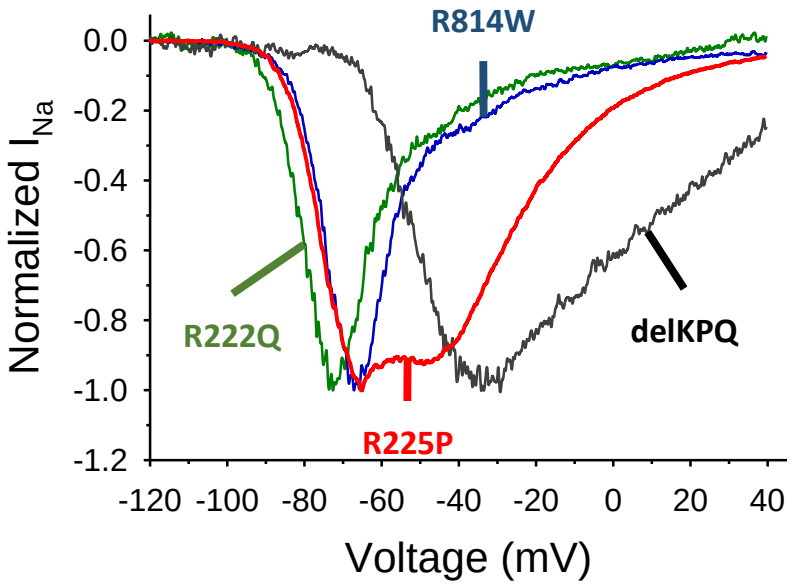

Figure 21. Comparison of normalized ramp-currents. Normalized TTX-subtracted averaged ramp-currents from R225P and other $Na_V1.5$ mutations associated with multifocal ventricular ectopy with impaired cardiac contractility (R222Q), sporadic dilated cardiomyopathy (R814W), and congenital long-QT syndrome (delKPQ). All data are represented as mean for n=7-15 cells.

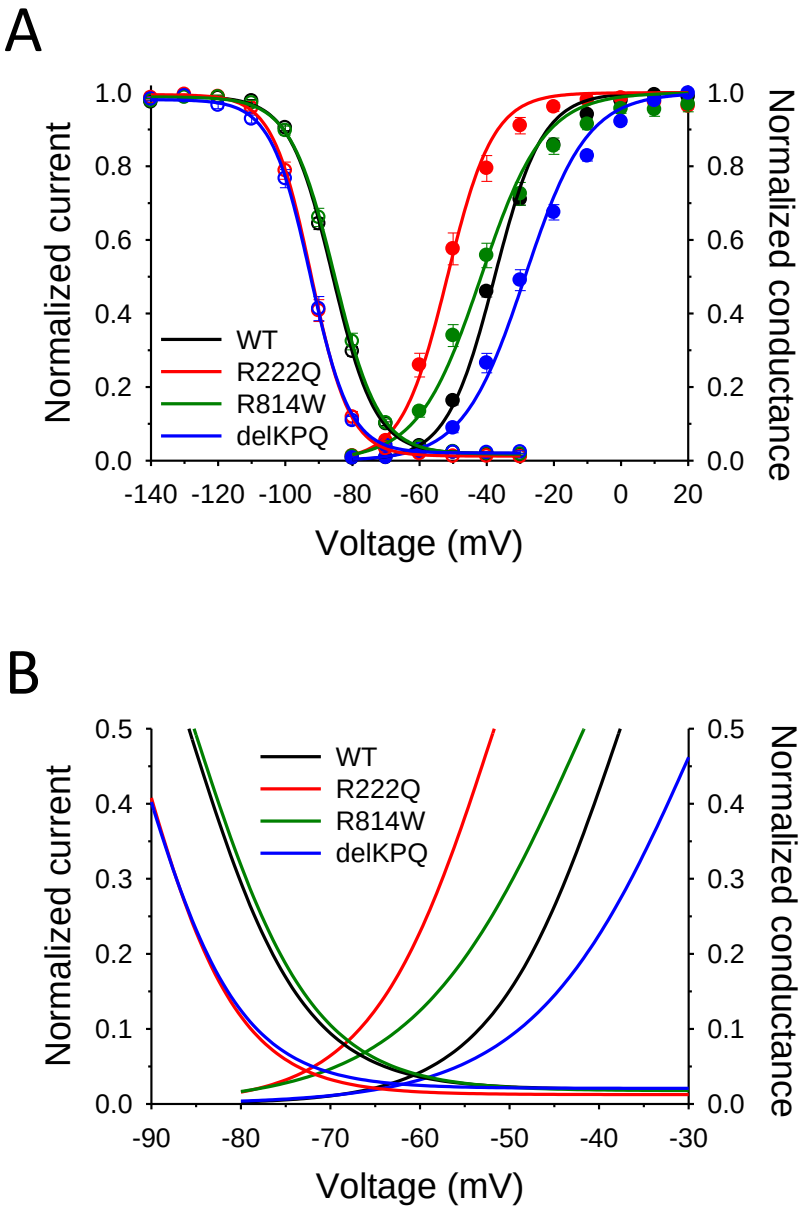

Figure 22. Window-currents. (A) Overlay of Boltzmann-fitted conductance – voltage (filled symbols) and channel availability (open symbols) curves of WT and mutations R222Q, R814W, and delKPQ. (B) Panel A enhanced to emphasize window-currents. All data are represented as mean ± S.E.M. for n = 7 - 12 cells.

Amiodarone effects on R225P

Because the proband responded to treatment with amiodarone, we compared the pharmacological effects of this drug on WT and mutant channels (Figure 23; Figure 24; Table 4). For both WT and R225P, amiodarone (3 μM) slowed activation kinetics (Figure 24B), and significantly altered voltage-dependence of inactivation (Figure 23A) and recovery from inactivation (Figure 23C). Additionally, the drug had mutant-specific effects including suppression of persistent sodium current (Figure 24C; Table 4) and a hyperpolarized shift in the conductance-voltage relationship (Figure 23A) resulting in an accentuated window current. Interestingly, amiodarone did not alter the peak ramp current density, but caused a significant decrease in charge movement determined for R225P channels (Figure 23B). The effect of amiodarone to slow recovery from inactivation for both WT and R225P channels likely explains a profound reduction in channel availability during pulse trains (Figure 23D; Table 4) and a decrease in charge movement observed in repetitive ramp experiments (Figure 24D; Table 4). The suppression of channel availability most likely dominates the effects of amiodarone on $Na_V1.5$ and may account for the suppression of ventricular ectopy in the proband.

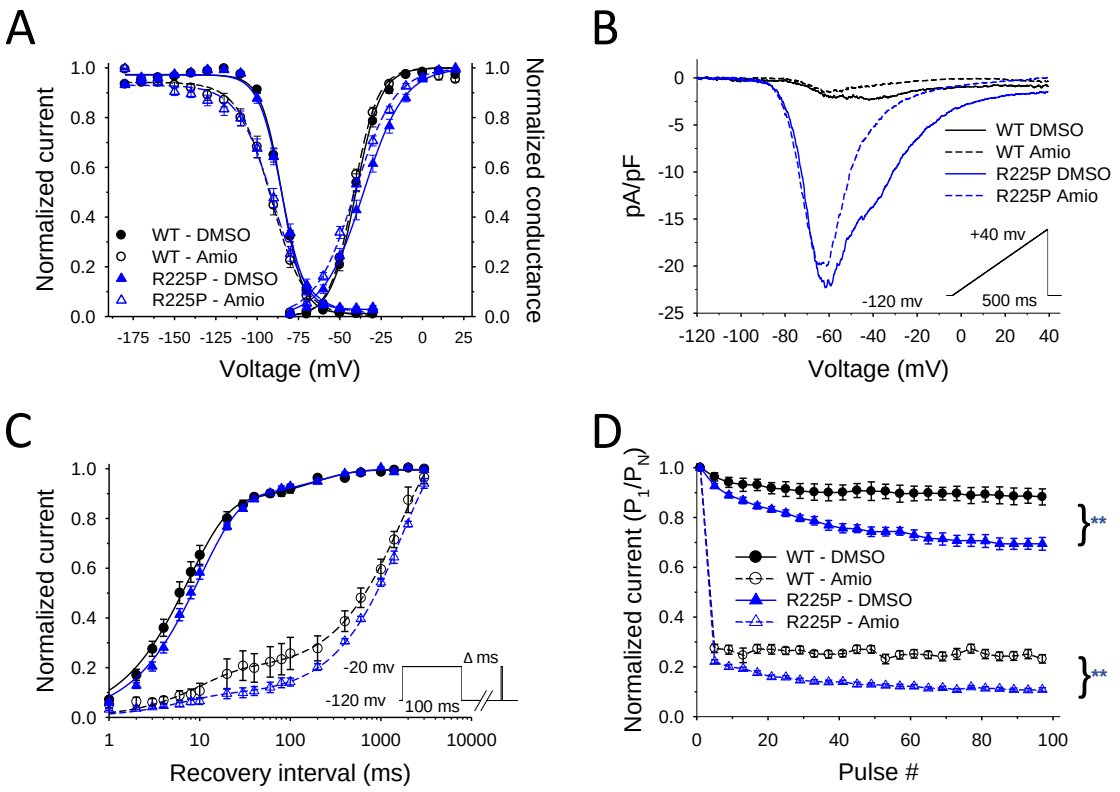

Figure 23. Effects of amiodarone on $Na_V1.5$-R225P. (A) Activation and channel availability properties of WT and R225P in the presence of amiodarone (open symbols, dashed lines) or DMSO (filled circles, solid lines). All data were fit with a Boltzmann function. (B) TTX-subtracted averaged ramp-currents (0.32 mV/ms) of WT and R225P normalized to cell capacitance in the presence of amiodarone (dashed lines) or DMSO (solid lines). (C) Recovery from fast inactivation of WT and R225P in in the presence of amiodarone (open symbols, dashed lines) or DMSO (filled circles, solid lines). The data were fit with a double exponential curve. (D) Pulse trains (2Hz; -20mV) with an activating pulse of 100ms of WT and R225P channels in the presence of amiodarone (open symbols, dashed lines) or DMSO (filled circles, solid lines). All data are represented as mean ± S.E.M for n=5-12 cells.

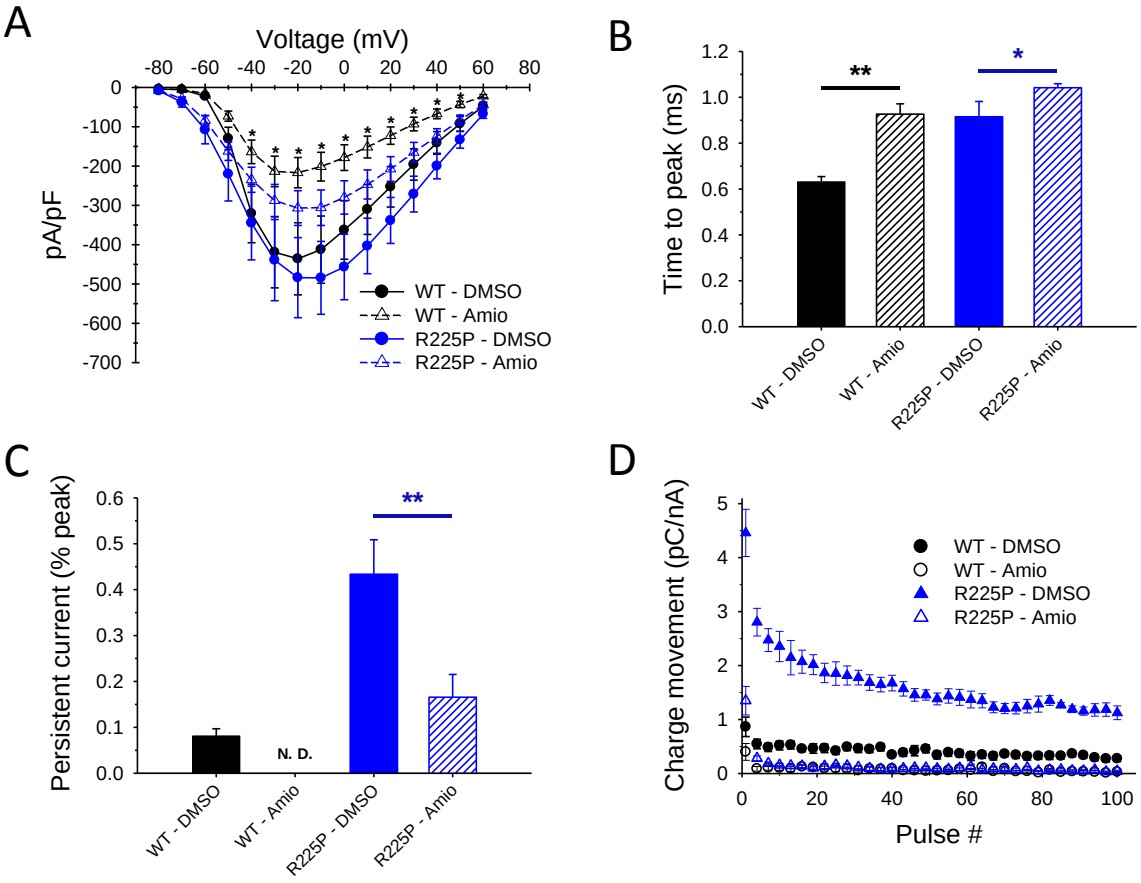

Figure 24. Effects of amiodarone on $Na_V1.5$-R225P. (A) Current-density – voltage plots of WT and R225P channels in the presence of 0.01% DMSO (control, solid symbols) or amiodarone (open symbols). (B) Activation kinetics measured as time to peak current following an activation pulse to -20 mV (holding potential -120 mV). (C) Persistent current as a percentage of peak I_{Na} from WT and R225P in the presence of DMSO or amiodarone. WT persistent current non-determinable (N. D.) in the presence of amiodarone. (D) Charge movement in response to consecutive 500 ms ramp-current protocols (1.1 Hz; 100 pulses) in DMSO (closed symbols) and amiodarone (open symbols) for WT (black circles) and R225P blue (triangles).

Table 4. Effects of amiodarone on WT-$Na_V1.5$ and R225P channels.

Amiodarone (3µM)		WT – DMSO	WT - Amiodarone	R225P - DMSO	R225P - Amiodarone
Activation	$V_{½}$	-40.4 ± 1.1	-41.4 ± 0.7	-34.5 ± 1.5*	***-41.0 ± 1.2***
	k	6.7 ± 0.3	6.8 ± 0.2	11.1 ± 0.5**	10.7 ± 0.4**
	n	7	11	6	10
Inactivation	$V_{½}$	-85.0 ± 0.8	-92.2 ± 1.8**	-85.2 ± 1.1	**-91.6 ± 1.9***
	k	-6.2 ± 0.1	-10.1 ± 0.7**	-6.8 ± 0.2*	***-10.8 ± 0.7****
	n	8	10	8	12
Window-currents	***Voltage***	-61.00 ± 0.03	-61.6 ± 0.7	-63.2 ± 1.8	**-68.0 ± 1.3****
	Activity	0.034 ± 0.001	0.044 ± 0.002**	0.072 ± 0.004**	***0.093 ± 0.003****
	n	5	7	7	9
Recovery from inactivation	***A1***	0.87 ± 0.01	0.19 ± 0.07**	0.88 ± 0.02	***0.13 ± 0.03****
	τ_1	8.0 ± 1.1	6.8 ± 2.7	10.3 ± 1.0	5.6 ± 1.4
	A2	0.13 ± 0.01	1.03 ± 0.06**	0.12 ± 0.02	***1.04 ± 0.05****
	τ_2	217 ± 36	2130 ± 434**	245 ± 39	***1940 ± 293****
	n	7	8	8	8
Persistent I_{Na}	***% peak***	0.08 ± 0.02	-0.15 ± 1.16	0.43 ± 0.08**	**0.17± 0.05**
	n	5	8	8	7

Amiodarone (3µM)			WT – DMSO	WT - Amiodarone	R225P - DMSO	R225P - Amiodarone
Time to peak (-20 mV)	***Peak (ms)***		0.63 ± 0.02	0.93 ± 0.05**	0.92 ± 0.05*	**1.04 ± 0.02***
	n		5	8	9	14
500ms Ramps (Paired)	***mV***		-49.0 ± 3.6	-59.7 ± 1.7**	-57.2 ± 2.5	***-62.4 ± 1.0***
	% peak		-0.9 ± 0.1	-0.5 ± 0.1**	-4.6 ± 0.5**	-3.5 ± 0.5**
	Area (pC/nA)		1.2 ± 0.2	1.1 ± 0.3	5.8 ± 0.9**	**2.8 ± 0.3****
	n		10	10	11	11
Frequency dependent inhibition 100ms	***1 Hz***	P_1/P_{100}	0.96± 0.04	0.30 ± 0.01**	0.86 ± 0.03**	***0.18 ± 0.01****
		n	10	10	10	10
	2 Hz	P_1/P_{100}	0.89 ± 0.03	0.25 ± 0.01**	0.69 ± 0.02**	***0.10 ± 0.01****
		n	7	8	8	12
1.1 Hz ramp train (P_{100})	***Area (pC/nA)***		0.30 ± 0.5	0.02 ± 0.01*	1.12 ± 0.13**	***0.04 ± 0.02****
	n		6	6	6	7

Versus WT (DMSO)

* = P < 0.05

** = P < 0.005

Versus R225P (DMSO)

Bold P < 0.05

Bold, Italices P < 0.005

Discussion

We present functional and pharmacological studies of a novel mutation in the principal cardiac voltage-gated sodium channel associated with multifocal ventricular ectopy with reversible ventricular dysfunction. Our data provide a biophysical profile of the mutant channel and examine pharmacological mechanisms responsible for the favorable clinical response to amiodarone. The novel mutation, R225P, adds to the growing structural and functional diversity of mutations in *SCN5A* responsible for inherited arrhythmia susceptibility and highlights the unique phenotype associated with mutations in first and second domain voltage sensors.

Phenotypes associated with *SCN5A* voltage sensor mutations

The mutation $Na_V1.5$-R225P alters a critical arginine residue located in the voltage sensing S4 segment of the first domain (D1), one of the α-helical structures involved with detecting changes in membrane potential. Insertion of a proline is generally predicted to distort the secondary structure of an α helix. Despite this predicted change in a critical voltage-sensor domain, the R225P channel was functional. A similar surprising tolerance of proline substitution in a voltage-sensor segment was noted in previous studies on a skeletal muscle sodium channel mutation, $Na_V1.4$-R1448P [34].

Three previously identified *SCN5A* mutations associated with cardiomyopathy also affect critical arginine residues within the D1/S4 (R219H, R222Q) or D2/S4 (R814W) segments and are associated with complex clinical phenotypes featuring atrial and ventricular arrhythmias, and cardiomyopathy [22], [24]–[26], [28], [30]. By contrast,

missense mutations replacing S4 segment arginine residues in D4 cause congenital long-QT syndrome without contractile dysfunction [35]–[37]. This intriguing genotype-phenotype divergence may stem from differences in the contributions of the various voltage sensing segments and how mutations within each domain affect sodium channel gating [38]. Importantly, the two other mutations identified at position $Na_V1.5$-R225 (R225W, R225Q) are associated with different clinical phenotypes and, correspondingly, different functional disturbances.

The association of arrhythmia and cardiomyopathy with voltage sensor mutations was originally reported in 2005 by Olson and colleagues. A *de novo* D2/S4 mutation (R814W) was identified in a young woman who had dilated cardiomyopathy combined with atrial flutter and nonsustained ventricular tachycardia [21]. Our laboratory later demonstrated that this mutation causes prominent defects in the kinetics and voltage dependence of activation that promoted aberrant activation during slow voltage ramps [23]. A similar functional defect was subsequently observed for the D1/S4 mutation R222Q, which had been identified independently by four groups. The phenotype associated with R222Q was described variably as peripartum dilated cardiomyopathy [26], [27], arrhythmic dilated cardiomyopathy [22], escape capture bigeminy and cardiomyopathy [28], reversible ventricular ectopy and dilated cardiomyopathy or multifocal ectopic Purkinje-related premature contractions [24]. Most of these reports emphasized the high burden of ectopic premature ventricular beats and impaired cardiac contractility with the variable presence of atrial tachyarrhythmias.

Pathophysiological implications

Given that three of the D1/S4 and D2/S4 mutations have common patterns of dysfunction, most notable for altered activation voltage dependence, a shared pathophysiology would be logical to assume. One demonstrable consequence of altered activation is aberrant sodium conductance at hyperpolarized potentials during voltage ramps. This *in vitro* phenomenon suggests that mutant sodium channels could produce an aberrant inward current at near resting membrane potentials of cardiac myocytes. This would promote enhanced automaticity and may specifically trigger ventricular extrasystoles arising ectopically from Purkinje fibers as suggested by computer modeling studies [24], [25]. A high burden of ectopic beats may lead to heart failure that can be reversed by pharmacological suppression of sodium current as was noted in our case and previous reports of R222Q. However, this same functional defect could possibly induce contractile dysfunction through disordered calcium handling [10], improper pH regulation [8], or disrupted mitochondrial function [39], [40] that might not be reversible. Interestingly, another D1/S4 mutation (R219H) associated with dilated cardiomyopathy and ventricular arrhythmia causes a novel type of sodium channel dysfunction (proton leak current) that could also disrupt intracellular pH regulation in myocytes [30].

Unlike the previously characterized $Na_V1.5$ voltage sensor mutations discussed above, ramp-currents produced by R225P propagate in two distinct sets of peaks. The first peak can be attributed to the large, hyperpolarized window current of the mutant channel, as seen with R814W and R222Q, while the second peak is a result of the persistent current produced by R225P, similar to the LQTS mutation delKPQ [31]. This interesting characteristic has been previously discussed in relation to the neuronal sodium

channel $Na_V1.3$ in which biphasic peaks were attributed to window- and persistent currents respectively [41]. Consistent with observations made with other *SCN5A* mutations associated with LQTS [31], R225P exhibits increased persistent current and this may explain the prolonged QTc observed in the proband.

Mechanism of amiodarone response

Because amiodarone was successful in suppressing ventricular ectopy and restoring normal contractile function, we sought to determine the pharmacological effects of this drug on the mutant sodium channel. We found that amiodarone significantly suppressed persistent current recorded from cells expressing R225P, induced a slightly hyperpolarized increase in window-current, and changed the overall morphology of the ramp-current resulting in a decreased charge movement for the mutant channel. In addition, amiodarone also had a profound impact on recovery from inactivation that suggested a mechanism for dampening the deleterious biophysical dysfunction of R225P. Specifically, by prolonging recovery time from fast inactivation, amiodarone effectively diminished the pool of available mutant channels. Further, frequency-dependent block of channels in the presence of amiodarone was greater for R225P than WT channels. Because R225P is more sensitive to inactivation induced inhibition, we predict that amiodarone administration results in a global decrease in the total number of channels available to be activated, however, the proportion of WT channels in the population is enriched compared to R225P.

Conclusions

We identified a novel *de novo SCN5A* mutation in a child with an amiodarone-responsive multifocal ventricular ectopy-associated cardiomyopathy and elucidated the molecular mechanism responsible for the disorder. The mutation, R225P, affects a voltage sensor domain and causes a hyperpolarized shift in the voltage dependence of activation. Additionally, this mutation evokes increased persistent sodium current, a recognized biophysical defect underlying type 3 LQTS, and other biophysical abnormalities including enhanced slow inactivation. Amiodarone suppresses channel availability to a greater extent for the mutant and attenuates the aberrant ramp current, two plausible explanations for its therapeutic success in this case. The unique functional consequences of *SCN5A* voltage sensor mutations in D1 and D2 help explain the pathogenesis of an arrhythmia-associated cardiomyopathy that can be reversed with certain sodium channel blocking drugs.

CHAPTER III

ELUCIDATING THE IMPACT OF $NA_V1.5$ MUTATIONS ON CA^{2+} HANDLING IN ISOLATED VENTRICULAR CARDIOMYOCYTES

Introduction

Mutations in the human heart Na channel $Na_V1.5$ have been associated with a range of disorders affecting cardiac rhythm. More recently, a subset of $Na_V1.5$ mutations have also been associated with a form of heart failure [23]–[25]. This unexpected association creates an expanded clinical spectrum of conditions associated with cardiac sodium channelopathies and establishes a need to elucidate the relationship between cardiac Na channel dysfunction and cardiomyopathies.

Intracellular ion homeostasis in myocytes is tightly regulated by multiple exchangers and transporters including the Na/Ca exchanger (NCX) and the Na/H exchanger (NHE) [8]. Through the NCX and the NHE, Na^+ is directly coupled to Ca^{2+} and pH levels within the cell such that an abnormally high intracellular [Na^+] might affect Ca^{2+} and H^+ handling. Therefore, any change of intracellular Na^+ levels due to cardiac sodium channel dysfunction might influence homeostasis of other intracellular ions. Some of the $Na_V1.5$ mutations identified in heart failure patients (R222Q, R225P, and R814W) are predicted to cause an inappropriate influx of Na^+ during diastole. Diastolic Na^+ influx has the potential of disturbing Na^+ and Ca^{2+} homeostasis that in turn could lead to myocardial damage. We hypothesized that certain cardiac sodium channel

mutations such as R222Q, R225P, and R814W may disturb intracellular Ca^{2+} and H^{+} dynamics, indirectly leading to myocardial failure.

The objective of this project is to establish a mechanistic relationship between Na channel dysfunction and impaired contraction as a consequence of altered ion and/or pH homeostasis in cardiac myocytes. We tested this by expressing WT or mutant cardiac sodium channels in rabbit cardiomyocytes using lentiviral vector. We then analyzed and compared the effects of these channels on intracellular Ca^{2+} measurements, with future experiments planned to analyze pH regulation. We expected to see alterations in intracellular Ca^{2+} and H^{+} levels compared to myocytes expressing wild-type $Na_V1.5$.

Materials and Methods

Cloning of $Na_V1.5$ and mutant cardiac sodium channels

A cDNA encoding human $Na_V1.5$ was cloned into the first position of the bicistronic vector pRc-CMV_IRES2_ with a marker gene (dsRed; eGFP; CD8) under the control of the IRES2 element. Positively transfected cells were identified by their fluorescent emission or the binding of beads conjugated with anti-CD8 antibodies. Mutations were created in the pRc-CMV-$Na_V1.5$-IRES2-(marker) plasmid using site-directed PCR mutagenesis. Disease-related cardiac sodium channel mutations created for use in this set of experiments were: $Na_V1.5$-R222Q, $Na_V1.5$-R814W, and $Na_V1.5$-delKPQ. In some experiments, the mutation F1760A was designed and introduced into $Na_V1.5$ and mutants to create a lidocaine-resistant mutation. In order to test function of all plasmids, human-derived tsA201 cells (HEK293 cell line expressing SV40 large T antigen) were transiently co-transfected with 1.0 μg of WT or mutant $Na_V1.5$ plasmid and the β1 subunit using FuGeneHD (Roche Diagnostics, Indianapolis, IN). Biophysical characterization was performed as described in Chapter II to validate channel properties.

Adenoviral vector production

Adenovator

Adenovirus was produced using the AdenoVator system (QBiogene; now MP Biomedicals, Santa Ana, California, USA) as instructed within the manual (Figure 25). Briefly, the gene of interest was cloned into the multiple cloning site of the transfer vector supplied in the kit using restriction enzyme digests and ligations. The completed

transfer vector was then linearized with the restriction enzyme PmeI and co-transformed into electrocompetent bacterial cells, BJ5183, using an Ecoli Pulser Transformation Apparatus (Bio-Rad, Hercules, California, USA). Recombinant plasmid DNA was selected for on agar plates containing Kanamycin. AdenoVator (pAd) plasmids containing the adenoviral backbone and gene of interest were identified by screening the recombinants for plasmid size and banding pattern through restriction enzyme analysis. Positive pAd clones were then amplified in DH5α bacteria to produce transfection quality DNA.

The vector plasmid pAd was then linearized with the enzyme PacI and transferred into QBI-293A cells containing complementary adenoviral proteins necessary to create functional adenovirus by electroporation (ECM 830 Square Wave Electroporation System; BTX, Harvard Apparatus, Holliston, Massachusetts, USA) or FuGene6. Transfected cells were then overlaid with agarose for viral plaque production. After 15-20 days, plugs were removed from the agarose above visible plaques and added to fresh media then applied to QBI-293A (Qbiogene) cells in a 10cm dish for small scale virus amplification. This virus was collected after 5-7 days and tested on tsA201 cells for function by fluorescence. Functional adenoviral vectors were then amplified in 15cm plates and collected after 15 days, concentrated using spin columns, and frozen in single use aliquots for future experiments.

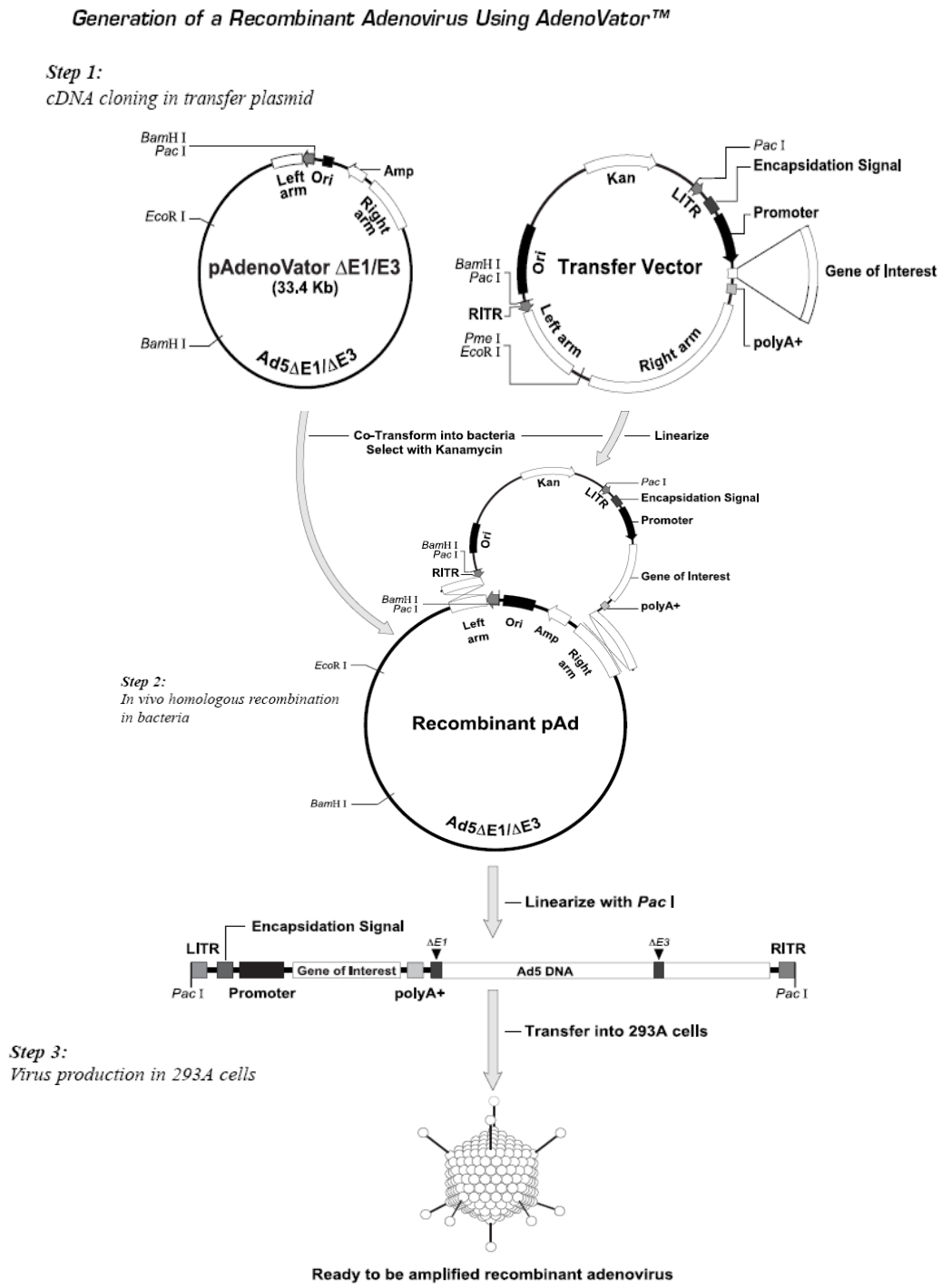

Figure 25. Recombinant adenovirus production by AdenoVator. Flowchart describing the process of adenoviral vector creation and production using the AdenoVator method from QBiogene. Image adapted from the AdenoVator product applications manual (Version 1.1) (QBiogene, Carlsbad, California, USA).

RAPAd

A second method for creating functional adenovirus (RAPAd) was acquired from the Gene Transfer Vector Core of the University of Iowa (Courtesy of Beverly L. Davidson, Ph.D. and Maria L. Scheel) (Figure 26) [42]. In brief, the RAPAd adenoviral system uses a two plasmid method for adenoviral vector creation. The gene of interest is cloned into the multiple cloning site of the pacAD5-K-NpA shuttle vector. Both the shuttle vector and the backbone plasmid, pacAd5 9.2-100, are digested with PacI then transfected together into QBI-293A cells with FuGene6 for viral production. Plaque formation generally occurred 10-14 days after transfection. After plaques began to form, the crude viral lysate was harvested by collecting all the cells and media from the dish and subjecting the lysate to three freeze/thaw cycles in a dry ice/EtOH bath and a 37°C water bath. Cell debris was then pelleted by centrifugation and the lysate was collected and stored at -80°C or used immediately for amplification. Virus was amplified by adding a proportion of viral lysate to 293A cells cultured in T150 cell culture flasks. After cells demonstrated cytopathic effects (CPEs), the cells and media were gently collected and cells were pelleted by centrifugation and cell media was removed. The cells were resuspended in 10mM Tris, pH 8.0, 100 mM NaCl (0.5mL – 1.0mL per flask) and subjected to three freeze/thaw cycles with subsequent centrifugation to pellet the cell debris. The viral supernatant was then collected and frozen at -80°C as the viral stock in single use aliquots.

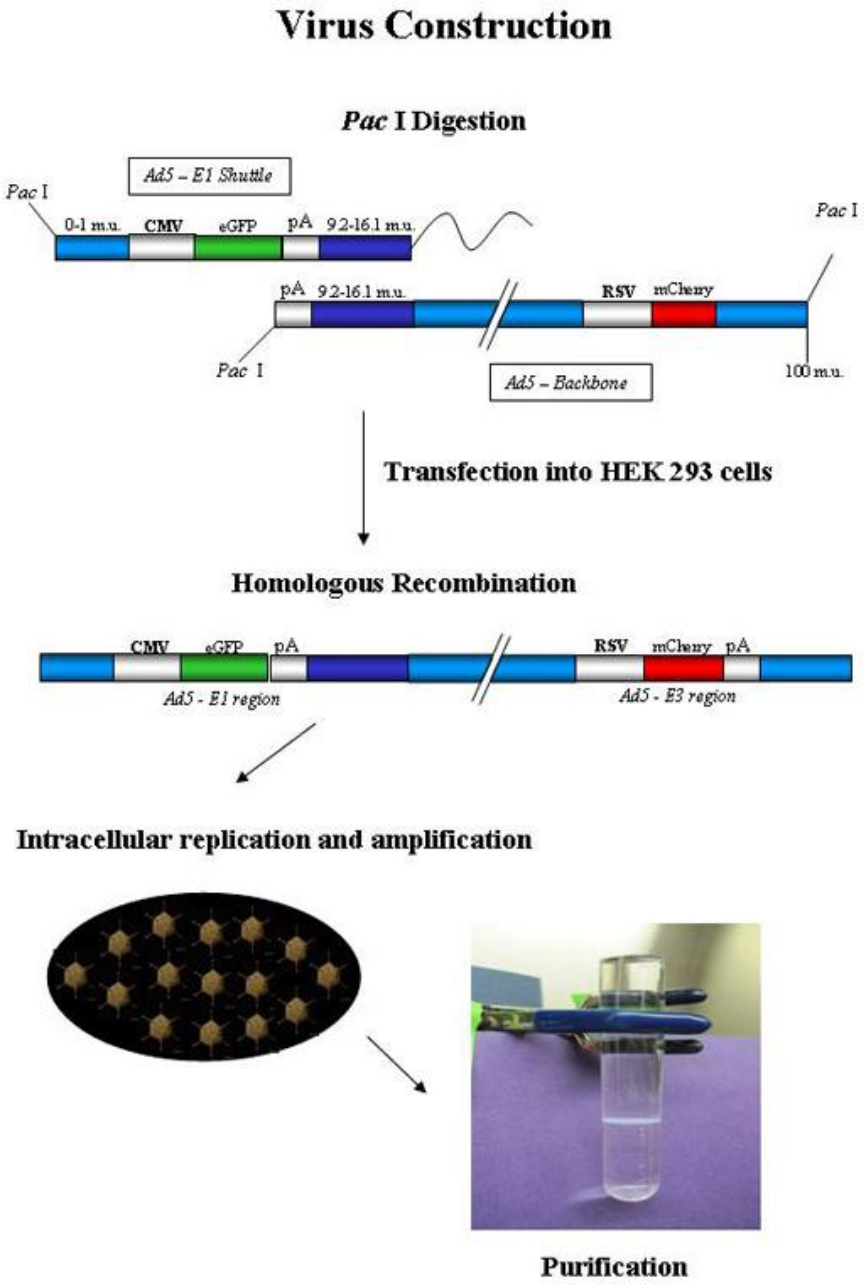

Figure 26. Recombinant adenoviral vector production using the RAPAd adenoviral expression system. Minimal steps are necessary to produce adenoviral vectors using the RAPAd approach. This image used courtesy of the Gene Transfer Vector Core at the University of Iowa.

Production of recombinant lentivirus

Lentivirus carrying the desired gene was produced by transient transfection of three plasmids (gift from Dr. Josh Bauer, Vanderbilt University, Nashville, Tennessee, USA) into a packaging cell line (HEK-293FT). WT or mutant channel cDNA was cloned into the FG12-CMV plasmid containing one of three expression markers, hUBC-GFP, IRES2-dsRed.MST, or IRES2-CD8. FuGeneHD was used to co-transfect the FG12 vector plasmid, packaging plasmid psPax2, and the envelope plasmid pMD2.G containing the 'G' glycoproteins of the vesicular stomatitis virus (VSV-G), important for increased tropism [43], at a ratio of 16:9:5. Over expression of VSV-G is toxic and a larger proportion of pMD2.G resulted in cell death and inefficient viral production.

After 24 hours, media was changed and supplemented with 4mM caffeine and 10mM Na-butyrate. Three days post-transfection, supernatant was collected and filtered through a 45 micron filter then concentrated using Amicon Ultra-15 centrifugal filters (EMD Millipore, Billerica, Massachusetts, USA). Concentrated virus was collected and stored in single-use aliquots at -80°C.

Isolated guinea pig or rabbit ventricular cardiomyocytes were infected with lentivirus containing either WT or mutant channel cDNA. Polybrene (Hexadimethrine bromide; Sigma-Aldrich, St. Louis, Missouri, USA) (8ug/mL) was supplemented at time of infection to increase cell susceptibility to the lentivirus. One day post-infection, the media was changed to avoid polybrene toxicity. Experiments were performed 48 – 72 hours post-infection to allow for adequate expression of transduced gene. Dr. Peter Mohler (Ohio State University, Columbus, Ohio, USA) provided helpful guidance with lentiviral production.

Neonatal rat ventricular myocytes

Neonatal rat ventricular myocytes (NRVMs) were supplied as a gift from the lab of Dr. Chee Lim (Isolations by Manuel Chiusa, Ph.D.; Vanderbilt University) and isolated as previously described [44], [45]. Briefly, hearts were removed and collected from several neonatal rat pups and placed in ice cold HBSS (Hank's Balanced Salt Solution; Life Technologies, Grand Island, New York, USA). Ventricles were removed from whole hearts and transferred to a fresh dish of HBSS where each ventricle was cut into 3 – 4 pieces. Ventricular tissue was then transferred into containers containing trypsin solution (15 mg trypsin (Gibco; Life Technologies), 25 mL HBSS; filtered and kept on ice) and shaken overnight in a cold room (approximately 18 hours). The next day, the trypsin was aspirated and washed with media containing DMEM (Dulbecco's Modified Eagles Medium; Life Technologies), 7% Fetal Bovine Serum (FBS; Gibco). The media was aspirated and replaced with collagenase solution (50mg Worthington collagenase type II (Worthington Biochemical Corporation, Lakewood, New Jersey, USA), 50 mL HBSS) and the tissue and collagenase were shaken at 40°C until myocytes broke free from tissue and the media became cloudy. The supernatant was collected and stored on ice and collagenase solution was added back to the tissue. The collagenase collection was repeated 4 more times. Myocytes were collected from the combined supernatants by centrifugation and washed with 7% FBS/DMEM, spun again, then finally brought up in 7% FBS/DMEM. Cells were initially plated for 45-60 minutes to allow fibroblasts to settle. Supernatant containing an enriched ventricular myocyte population was then collected and plated as needed for experiments and cultured at 37°C and 5% CO_2.

Guinea pig cardiomyocyte isolation

This protocol for isolation of guinea pig cardiomyocytes was modified from the lab of Robert Harvey, Ph.D. [46] (University of Nevada School of Medicine, Reno, Nevada, USA) and approved by the IACUC of Vanderbilt University. All solutions used during the isolation were bubbled with 100% O_2 and warmed in a water bath to maintain 37°C when applied to the heart. Male, adult Hartley guinea pigs (250-350g) were purchased from Charles River (Wilmington, Massachusetts, USA). The guinea pig was given an intraperitoneal injection of heparin (500 units) five minutes prior to administration of pentobarbital (100mg/kg). After the animal no longer responded to stimuli, the chest was shaved and doused with ethanol. The chest cavity was opened and the heart was excised. The aorta was cannulated and the heart was attached to a pump-driven Langendorff apparatus.

The heart was then perfused with a physiological saline solution (PSS) plus calcium (in mM: 140 NaCl, 5.4 KCl, 2.5, $MgCl_2$, 11 glucose, 5.5 HEPES, 1.5 $CaCl_2$; pH 7.4 at 37°C). After five minutes, the perfusion solution was changed to Ca-free PSS to suppress mechanical activity and allowed to flow through the heart for five minutes. Collagenase (Worthington Class II) was added to Ca-free PSS (0.4 mg/ml) and perfused through the heart for ten minutes. After eight minutes of collagenase perfusion, the heart was removed from the Langendorff setup and placed in KB solution (Krebs-Henseleit Buffer; in mM: 110 potassium glutamate, 10 KH_2PO_4, 25 KCl, 2 $MgSO_4$, 20 taurine, 5 creatine, 0.5 EGTA, 20 glucose and 5 HEPES; pH 7.4 at 37°C). Vessels and fat were trimmed away from the heart muscle, then ventricles were collected and separated from

the atria. Ventricular tissue was cut into small pieces and placed in warmed KB solution then finely minced and triturated with a wide-mouth sterile transfer pipette in order to release individual cells from the tissue. The slurry was then filtered through a 300 μm filter and the myocytes were pelleted by centrifugation (20xg for 5 minutes). The supernatant was aspirated and replaced with fresh KB solution and allowed to recover for 30 minutes before plating in culture media. The media contained Mimimum Essential Medium (MEM) containing Hanks salts and L-glutamine (Gibco-Invitrogen 11575-032) supplemented with streptomycin (100 μg/ml), penicillin (100 units/ml), bovine serum albumin 1 mg/ml, Insulin-Transferrin-Selenium-X Supplement (Gibco-Invitrogen 51500-056) (1X). Isolated ventricular myocytes recovered in a 37°C incubator (5% CO_2) for 2 hours before being infected with virus. Cells typically remained viable for 72 – 96 hours.

Rabbit ventricular cardiomycoyte isolation

Isolated rabbit ventricular myocytes were acquired from Courtney Campbell, Ph.D. and Rick Welch (George lab). Cardiomyocytes were isolated as previously described [47]. Briefly, New Zealand White rabbits (6-7 lbs; Charles River Canada) were sedated with intramuscular acepromazine then anesthetized with intravenous pentobarbital sodium. Hearts were quickly excised and arrested on ice for 5 minutes in nominally calcium-free minimum essential medium solution (MEM, Joklik modification). Hearts were hung on a Langendorff apparatus and perfused at 37°C for 10-15 minutes in the same MEM solution gassed with 95% O_2 and 5% CO_2. The perfusion was then switched to MEM solution containing 0.05 mg/ml Liberase TH (Roche Applied Sciences, Indianapolis, Indiana, USA). After 5 minutes, serial tissue samples were

collected in order to determine the progression of tissue digestion. When the majority of ventricular myocytes released were quiescent and rod-shaped (7-20 minutes), the ventricles were removed from the heart and placed in MEM solution containing 1% bovine serum albumin (BSA). The tissue was minced, gently triturated with a wide-mouthed sterile transfer pipette, and filtered through a 100 μm cell strainer (BD Biosciences, San Jose, California, USA) into a 50 ml conical tube. The myocytes were allowed to settle by gravity at room temperature until a soft pellet was formed (30 – 45 minutes). The supernatant was aspirated and ventricular myocytes were resuspended in MEM with BSA. Myocytes were plated and incubated at 37°C with 5% CO_2. The experimental procedure for isolating rabbit cardiac myocytes was approved by Vanderbilt University IACUC.

Calcium imaging of isolated cardiomyocytes

Isolated rabbit or guinea pig ventricular cardiomyocytes were collected from culture conditions by gentle centrifugation (20xg; 5 minutes). The supernatant was removed and cells were resuspended in Tyrode's solution (TS) then loaded with the ratiometric calcium-sensitive dye, Fura-2 AM (2μM), for 20 minutes. The composition of TS for Fura-2 loading was (in mM): 145 NaCl, 5.4 KCl, 1.2 $CaCl_2$, 0.3 NaH_2PO_4, 0.5 $MgCl_2$, 5.5 glucose, and 5 HEPES, pH adjusted to 7.4 with NaOH. After dye loading, the cardiomyocytes were centrifuged, washed with TS to remove excess extracellular Fura-2, and then suspended in TS with 2 mM Ca^{2+} for 30 min to ensure complete hydrolysis of the intracellular ester.

Fura-2 signals were recorded on an IonOptix calcium-imaging station (Ionoptix, Milton, Massachusetts, USA). Briefly, Fura-2 loaded myocytes were placed in the recording chamber and field-stimulated (5ms; 15V) to induce cardiomyocyte contractions at 0.5 Hz or 1 Hz. Calcium transients were recorded by alternating excitation of the Fura-2 dye from 340nm to 380nm (250 Hz) and recording the fluorescent emission at 510nm. Background fluorescence was subtracted from all recordings. The ratio of emission (F_{340}/F_{380}) is indicative of the calcium transient in the individual myocyte. Data acquisition and offline analysis were performed using IonWizard 6.2 software (IonOptix).

Electrophysiology

Biophysical characterization of sodium channels from viral-vector transduced tsA201 cells were recorded and analyzed as described in Chapter II. Sodium currents from isolated ventricular myocytes were recorded at room temperature (22-23°C) using the whole-cell patch clamp technique. Electrodes were pulled from thin-wall borosilicate glass (OD: 1.2 mm, Warner Instrument Corp., Hamden, Connecticut, USA) on a P-97 multistage Flaming-Brown micropipette puller (Sutter Instruments, Novato, California, USA) and fire polished to a resistance between 0.8 and 1.2 MΩ. Data acquisition began 10 minutes after whole-cell configuration was established. Throughout the entirety of the experiment, a gravity-driven perfusion system (Perfusion Pencil system; AutoMate Scientific, Berkeley, California, USA) was used to superfuse positively transfected tsA201 cells with bath solution containing (in mM): 10 NaCl, 5 $CsCl_2$, 125 TEA-Cl, 1.8 $CaCl_2$, 1 $MgCl_2$, 10 HEPES; and 10 glucose, pH 7.4 (adjusted with CsOH). The pipette solution (intracellular solution) contained (in mM): 5 NaCl, 150 CsF, 5 EGTA, and 10

HEPES, pH 7.2 (adjusted with CsOH). Series resistance was compensated at 90%. Leak currents were subtracted by using an online P/4 procedure. Cells with voltage error greater than ±3 mV were excluded from analysis. Data acquisition was carried out using an Axopatch 200B patch clamp amplifier and pCLAMP 10.0 software (Molecular Devices, Sunnyvale, CA). All data were analyzed using pCLAMP 10.0 or Microsoft Excel 2007 and plotted using SigmaPlot 10.0 (Systat Software, Inc., San Jose, CA). Statistical analysis was performed using Student's t-Test.

Results

Animal model and culture

For this project, we chose to use adult guinea pig and rabbit cardiomyocytes because of their similarities to human ventricular action potentials compared to those of rats or mice (Figure 27). We optimized isolation protocols for both animals that yielded quiescent, rod-shaped, calcium-sensitive cardiomyocytes for experimentation. Proper myocyte function was verified through patch clamp and calcium imaging experiments (Figure 28). Because of the overall size of the cardiomyocyte, sodium current recordings in the native myocyte were very large, therefore, we decreased extracellular [Na^+] in order to control I_{Na} and maintain minimal voltage error.

Calcium imaging of isolated ventricular cardiomyocytes was performed using the ratiometric dye, Fura-2 AM. To elicit a calcium transient, myocytes were field stimulated at varying frequencies to determine the native calcium transient induced by excitation-contraction coupling (Figure 28C) Viable cells were capable of being stimulated to produce action potentials or calcium signals.

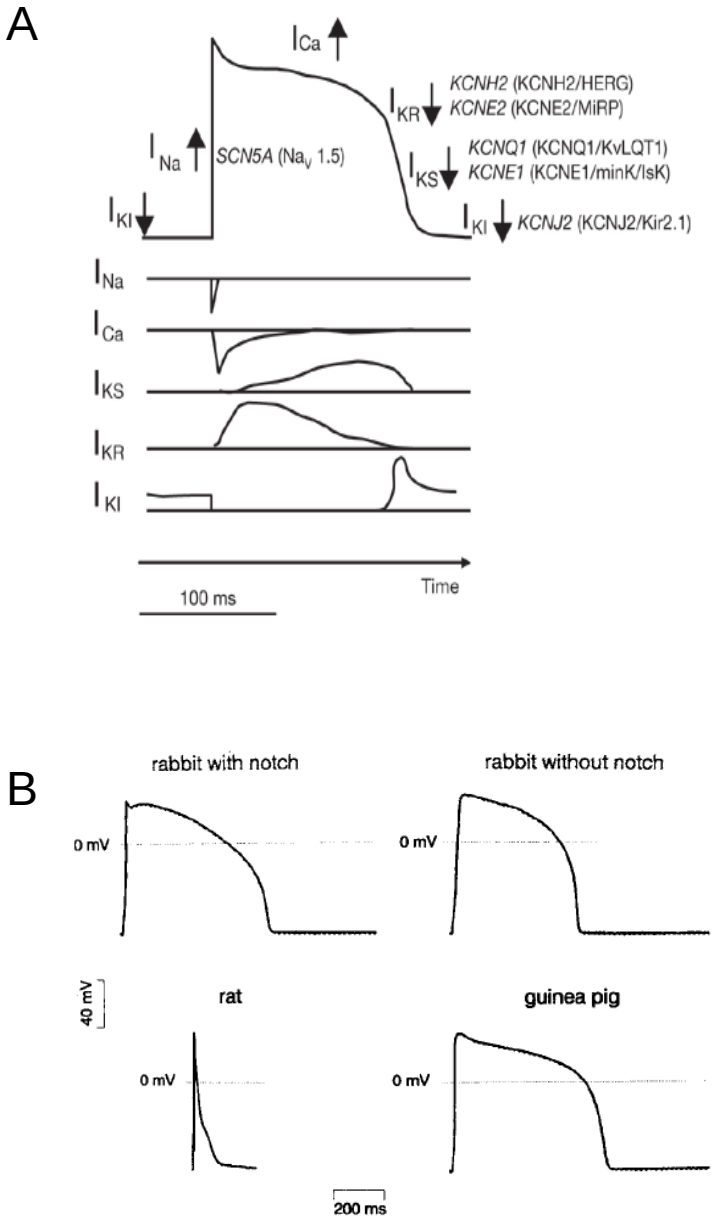

Figure 27. Action potential morphologies. (A) A representiation of the human cardiac action potential and the multiple currents responsible for the overall shape [64]. (B) Comparitive recordings of action potentials from animals commonly used for cardiac research [65].

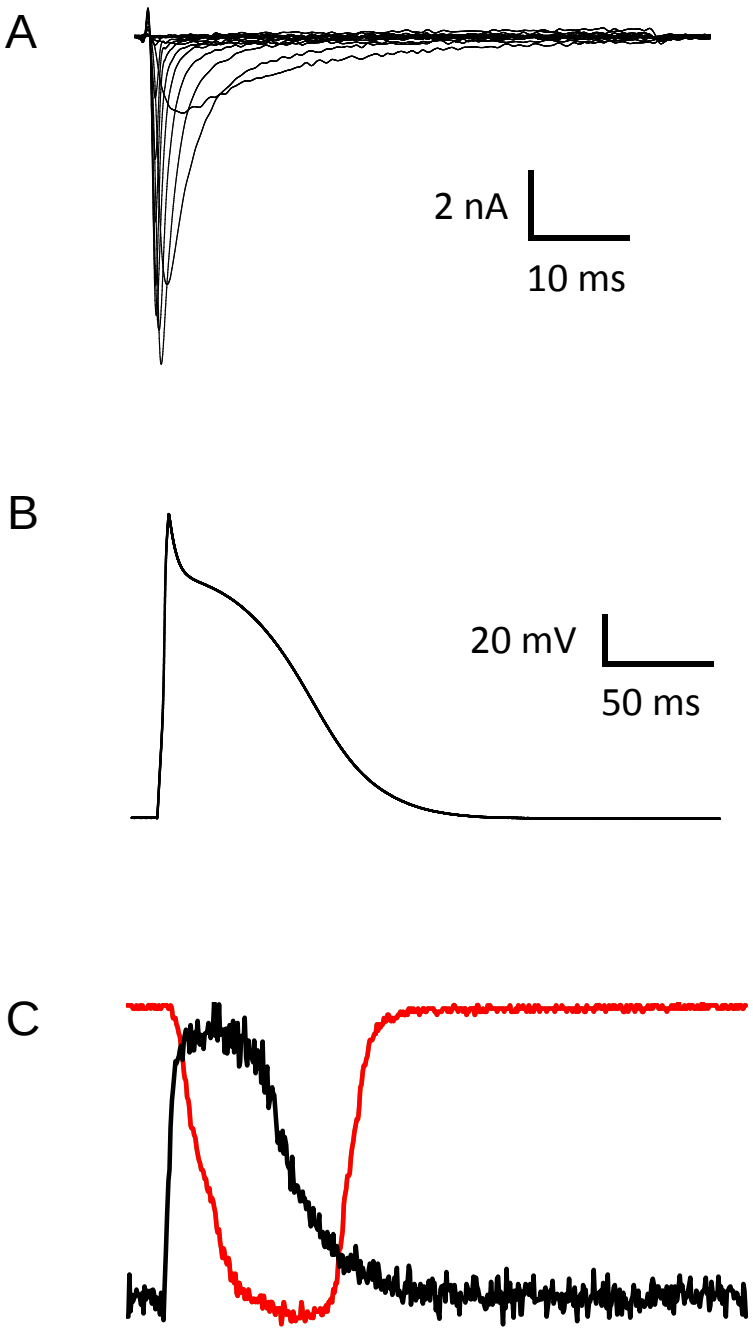

Figure 28. Properties of the isolated rabbit ventricular myocyte. A representative sodium current family (A) and a stimulated action potential (B), recorded from individual isolated rabbit ventricular myocytes. (C) Stimulated Fura-2 signal (ratio of F_{340}/F_{380}; background subtracted) recorded from an individual myocytes (black line) overlaid with concordant measurement of sarcomere length (red) showing myocyte contraction. Data extrapolated using IonWizard software and Microsoft Excel.

Lidocaine – resistant $Na_V1.5$

Our goal for this project was to express mutant cardiac sodium channels in native cells in order to determine adverse consequences of $Na_V1.5$ mutations R222Q, R814W, and delKPQ. Because the cardiac sodium channel, $Na_V1.5$, is abundantly expressed in native cardiomyocytes, it was desirable to use a pharmacological 'tag' to isolate exogenously-expressed channels. For this purpose, we engineered the mutation $Na_V1.5$-F1760A, which confers lidocaine-resistance upon the channel (Figure 29A).

At a concentration of 100 μM lidocaine, tonic block of wild type current is near 70% while the F1760A mutation is more resistant to drug and is only reduced by 30%. Similar results were seen in the background of mutation R814W (R814W: 73% tonic block; R814W-F1760A: 24% tonic block) (Figure 29B). Lidocaine also blocks the cardiac sodium channel in a use-dependent manner, resulting in a loss of about 30% of current for both wild type and R814W channels after 100 pulses (1 Hz). The F1760A mutation abolished the use-dependent effect of lidocaine for both WT and mutant channels (Figure 29C).

In both the WT and R814W – lidocaine-resistant mutants, the voltage dependence of activation was slightly hyperpolarized while the channel availability was right-shifted with a less-shallow slope. Because these changes affected both WT and R814W in a similar pattern, this resulted in a similar, slightly hyperpolarized shift in the window-current for both channels. The relationship between WT and R814W remained the same, with R814W presenting a larger, hyperpolarized window-current (Figure 30A).

Analysis of slow ramp currents (2s; 80mV/s) produced by F1760A and R814W-F1760A revealed that the F1760A mutation alone introduced a large, broad ramp current

into the WT channel and exaggerated the ramp current of R814W to very large peak values (Figure 30B). Because the F1760A mutation confers similar characteristics into the WT mutation as those that we suspect are responsible for the heart failure phenotype in R222Q and R814W, we chose not to continue with the lidocaine-resistant, F1760A channels.

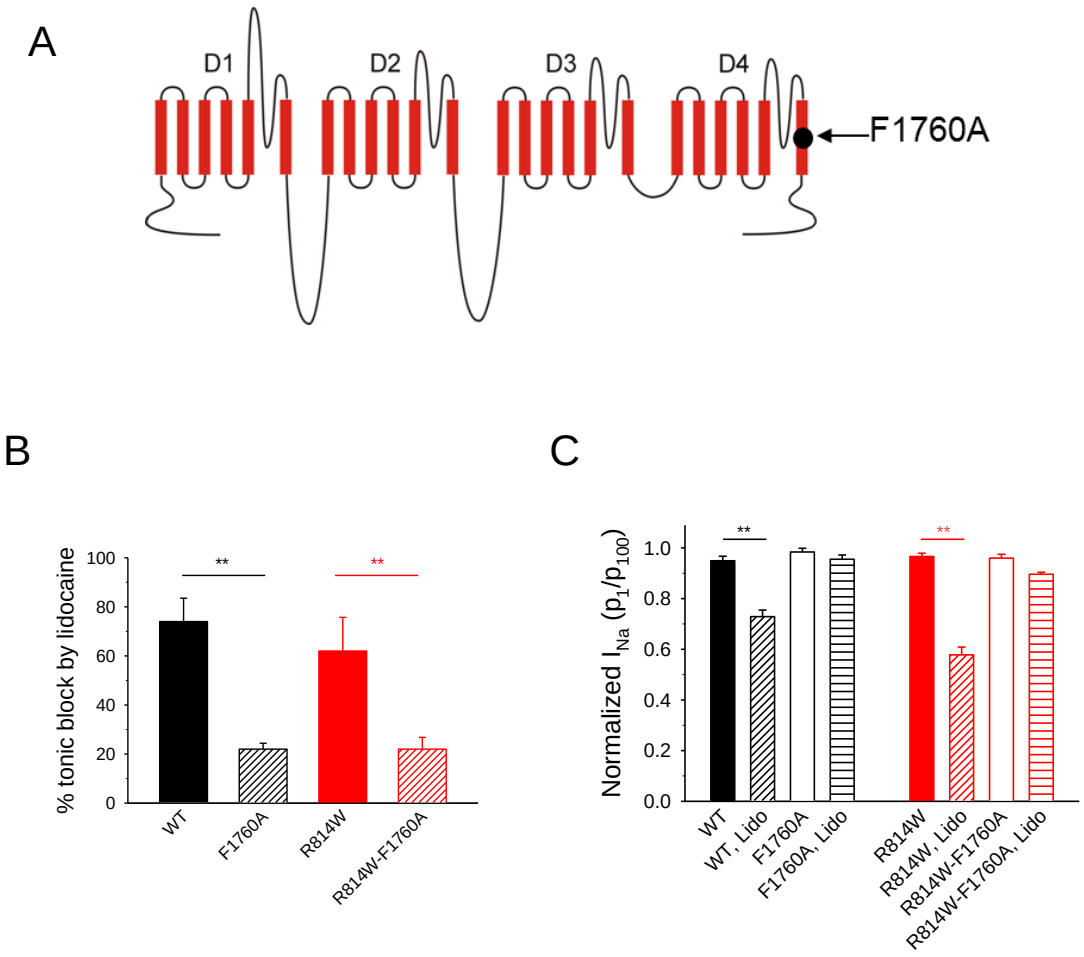

Figure 29. Lidocaine-resistance of $Na_V1.5$-F1760A. (A) Model of $Na_V1.5$ with the approximate location of the F1760A mutation marked (black circle). (B) Tonic block achieved by lidocaine on WT, R814W, and the lidocaine-resistant variants (F1760A, R814W-F1760A). (C) Pulse-train experiments (-20 mV; 1 Hz; 100 pulses) in the absence or presence of lidocaine. Normalized, 100th pulses are shown. Lidocaine concentration was 100 µM for all experiments. All data are represented as mean ± S.E.M for n = 5 – 7 cells.

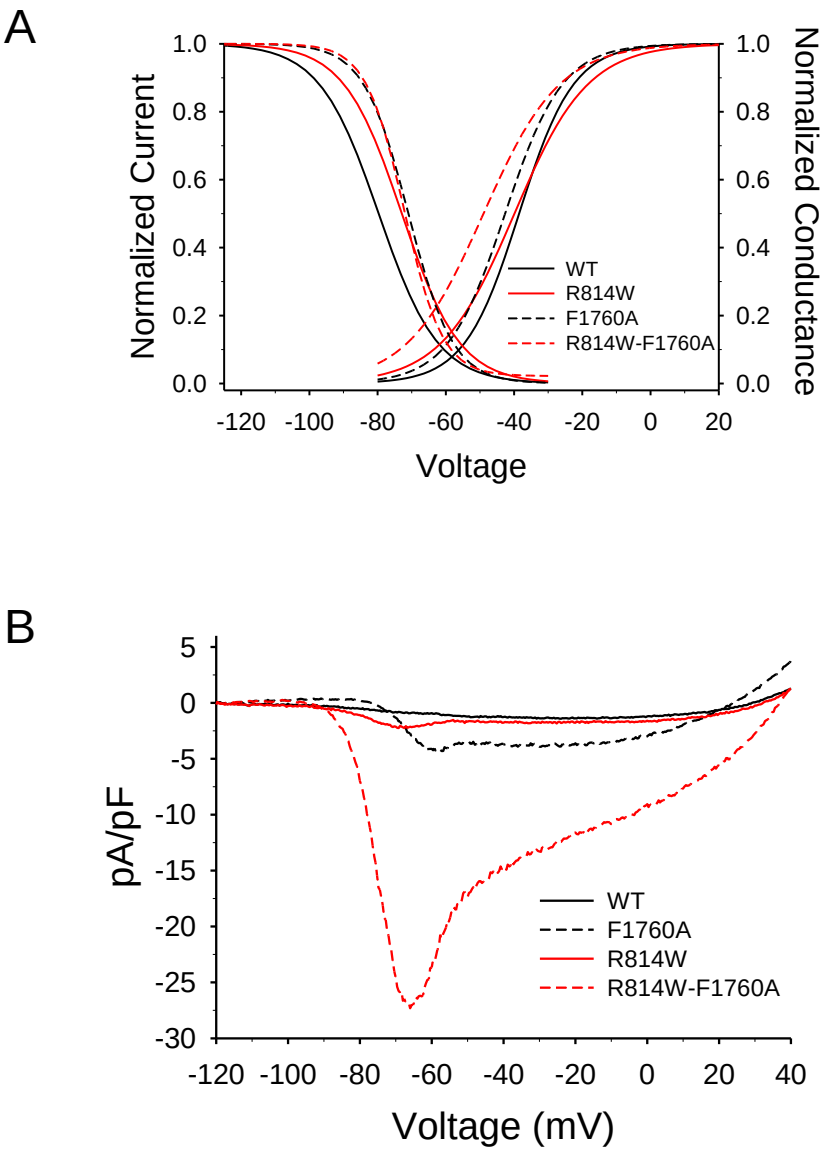

Figure 30. Properties of $Na_V1.5$-F1760A. (A) Overlay of Boltzman-fitted activation curves with Boltzmann-fitted channel availability properties. Window current can be seen as the area under where the curves intersect for each respectable channel. (B) Ramp-currents elicited by a two-second ramp current protocol from -120 mV to 40 mV (80mV/s). All data are represented as mean ± S.E.M for n = 11 – 15 cells.

Adenoviral vector production

Recombinant adenovirus produced using the AdenoVator system was capable of transducing guinea pig, rabbit, and neonatal rat ventricular myocytes, as demonstrated by fluorescence 48 hours post-infection. Multiple attempts were made to create adenoviral vectors containing WT or mutant cardiac sodium channels in the AdenoVator system; however, we were not successful as plaques did not form in cells transfected with the full adenoviral DNA containing *SCN5A* and variants.

We then contracted with the University of Iowa Gene Transfer Vector Core (GTVC) in order to produce adenoviral vectors containing WT or mutant cardiac sodium channels using the RAPAd method [42]. The GTVC kindly provided our lab with shuttle and backbone vectors necessary for virus production and, in concert, our lab and the GTVC attempted to produce adenoviral vectors.

We were capable of producing control adenovirus containing the gene encoding the marker mCherry that was able to transduce both guinea pig and rabbit ventricular cardiomyocytes, characterized by fluorescence emission at appropriate wave lengths. However, the RAPAd system was also unable to produce adenoviral vectors containing $Na_V1.5$ or the alternative channel mutations. This problem was mirrored at the GTVC, as they were also unable to produce the appropriate virus after multiple attempts, possibly due to insert size or overexpression of the gene of interest (personal communication with GTVC).

Lentiviral vectors containing $Na_V1.5$

Control and channel lentiviral vectors were successfully created, tested, and verified for function by infection of tsA201 cells (Figure 31). Attempts to infect isolated ventricular cardiomyocytes of both guinea pig and rabbit with lentivirus carrying CMV-*SCN5A*-IRES2-dsRed.MST were unsuccessful. Multiple infections with varying viral doses, infection times, and recovery times for expression (48-96 hours post infection) were examined without success. However, lentiviral vectors containing WT or mutant channel genes followed by the CD8 marker (CMV-*SCN5A**-IRES2-Leu2(CD8)) were capable of transducing NRVM, guinea pig, and rabbit isolated ventricular myocytes, verified by CD8 antibody conjugated bead attachment 48 – 72 hours post infection (Figure 32).

Calcium imaging by Fura-2 signal was performed on transduced rabbit ventricular myocytes to identify any changes of the calcium transient as a result of exogenous expression of the mutant cardiac sodium channels compared to WT channels (Figure 33-Figure 39). We expected to see an increase in baseline calcium levels, shorter time to peak, an increased peak calcium transient, and a slower, drawn out recovery of the calcium transient reported by the Fura-2 ratio. Of the parameters tested, only the recovery of the Fura-2 signal (time to 90% baseline; 1 Hz) for R814W was significantly different ($p < 0.05$) compared to myocytes transduced with WT channels (Figure 39). Overall, though, transduction of isolated rabbit ventricular myocytes with WT or mutant channels resulted in mostly no significant differences.

To examine the amount of channel expression we were achieving by lentiviral infection, we performed whole-cell patch clamp experiments on transduced

cardiomyocytes, examining current-density measurements of myocytes over-expressing WT or mutant cardiac sodium channel. Interestingly, in cells transduced with the lentiviral vectors, current-density did not increase, but rather decreased, contrary to what we had expected (Figure 40).

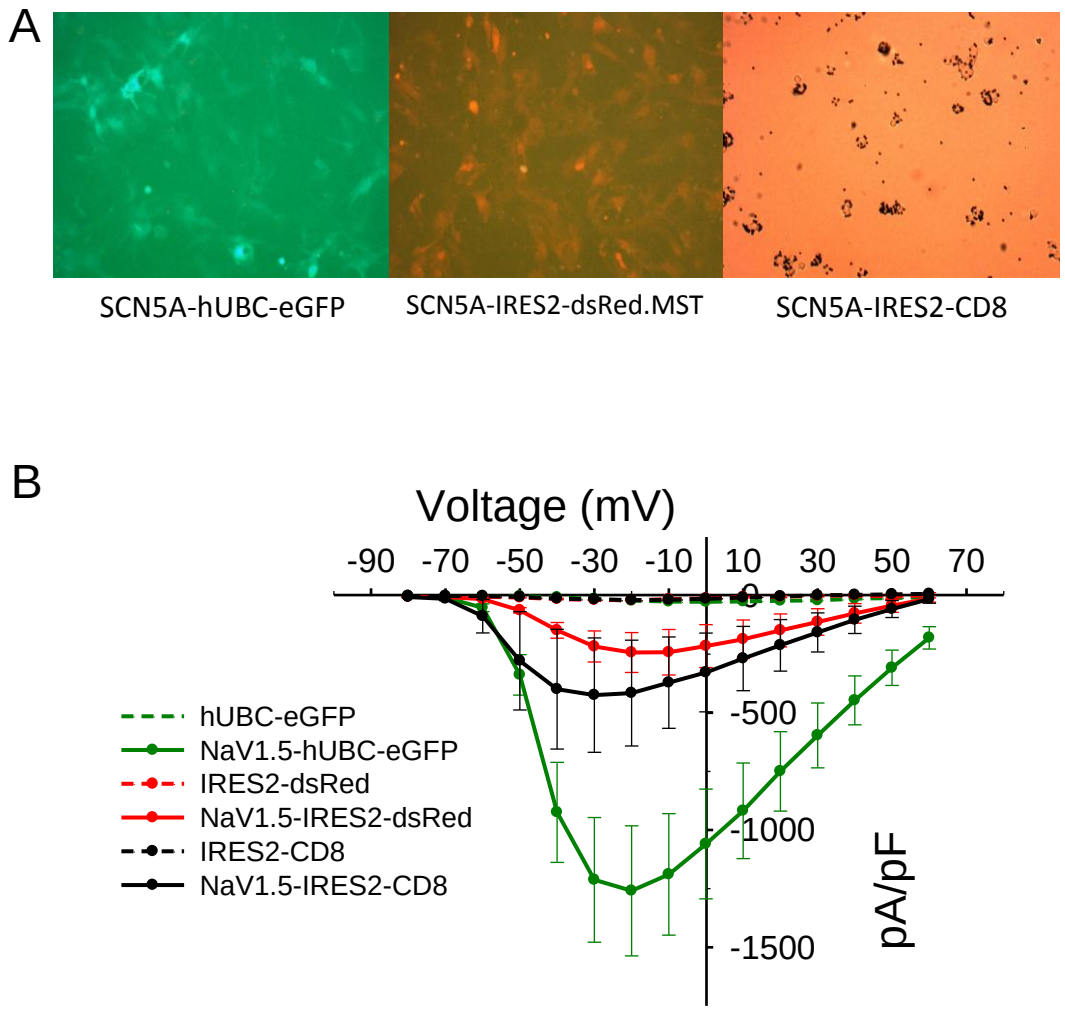

Figure 31. Lentiviral transduction of tsA201 cells. (A) Image verification of positive transduction of tsA201 cells with lentiviral vectors containing the sodium channel gene SCN5A and various marker proteins. (B) Current-density – Voltage plots of positively transduced tsA201 cells expressing the cardiac sodium channel $Na_V1.5$. All data are represented as mean ± S.E.M for n = 6 - 8 cells.

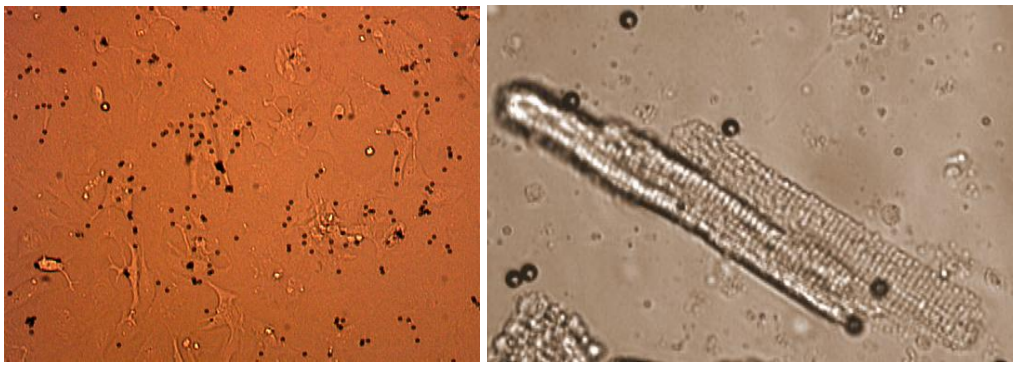

Figure 32. Lentiviral transduction of cardiomyocytes. Neonatal rat ventricular myocytes and Adult Rabbit ventricular myocyte transduced with lentivirus containing the expression construct CMV-NaV1.5-IRES2-CD8. Black circles are CD8 antibody conjugated beads attached to the cardiomyocyte.

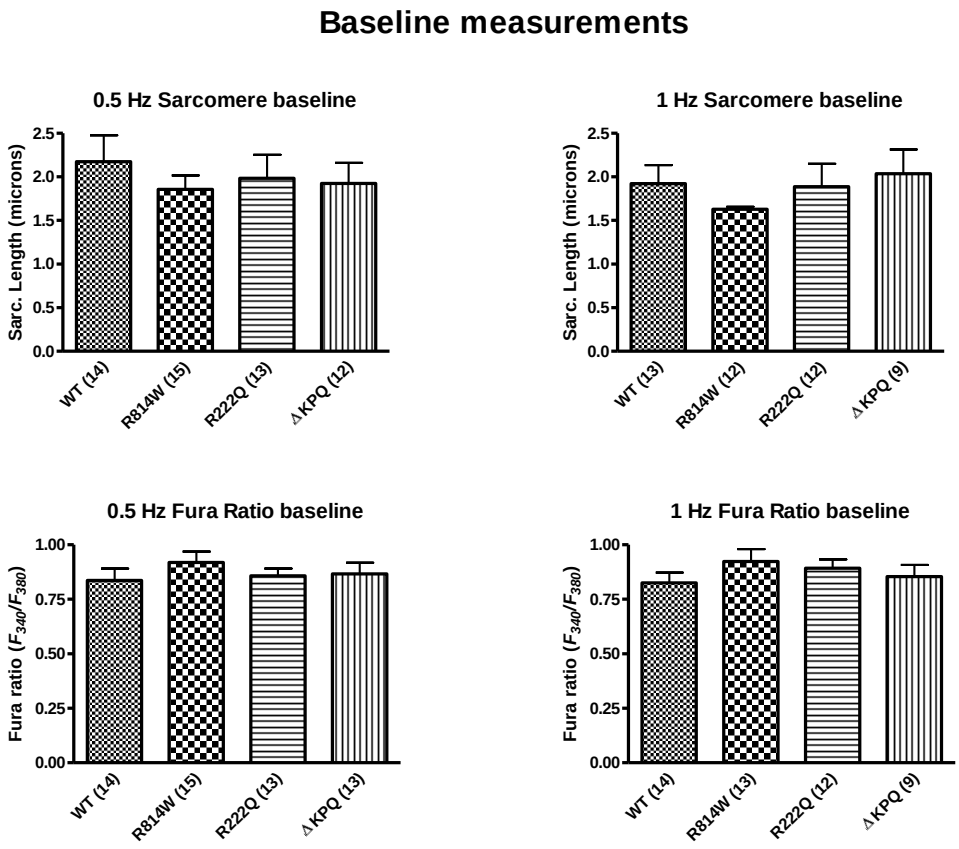

Figure 33. Baseline measurements of rabbit ventricular myocytes. (Top panels) Baseline sarcomere length measured in isolated myocytes during stimulation of 0.5 or 1.0 Hz. (Bottom panels) Baseline Fura ratio in cardiomyocytes loaded with Fura-2 during stimulation of 0.5 or 1.0 Hz. All data are represented as mean ± S.E.M. Number of cells measured (n) are listed along bottom of figures.

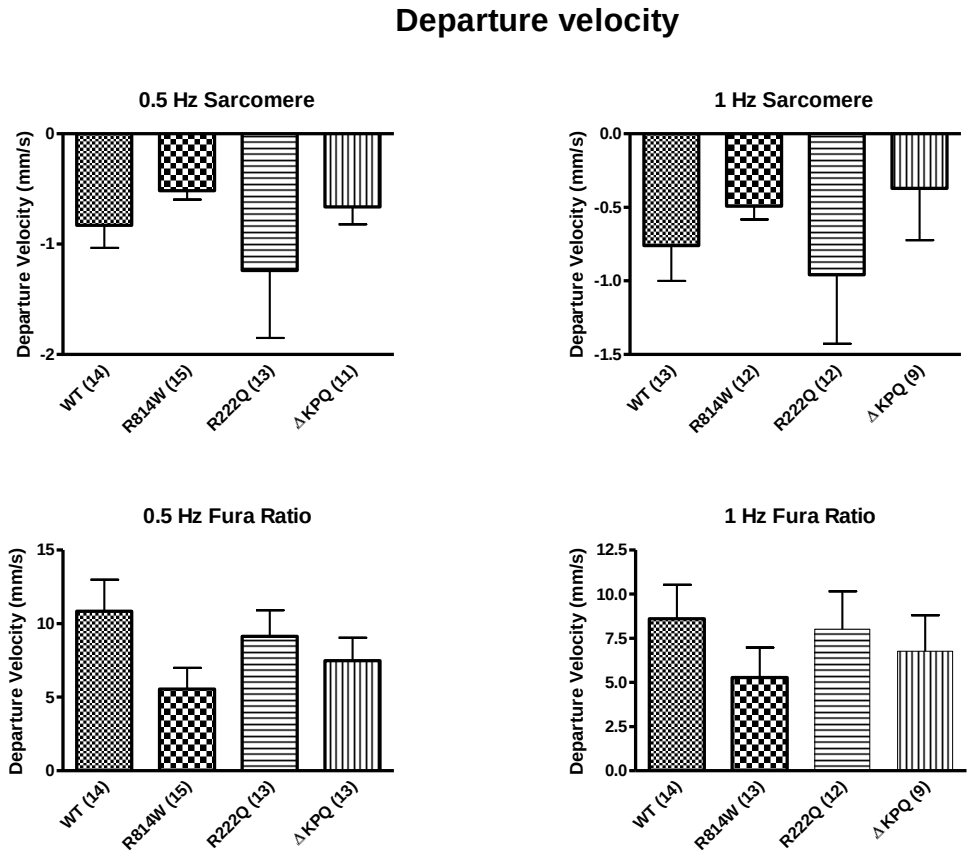

Figure 34. Departure velocity measurements of rabbit ventricular myocytes. Departure velocity measurements examine the rate of change of the respectable signal. (Top panels) Departure velocity of sarcomere length after stimulation at 0.5 or 1 Hz, indicating rate of contraction. (Bottom panels) Departure velocity of the Fura ratio after stimulation at 0.5 or 1 Hz in cardiomyocytes loaded with Fura-2 AM. All data are represented as mean ± S.E.M. Number of cells measured (n) are listed along bottom of figures.

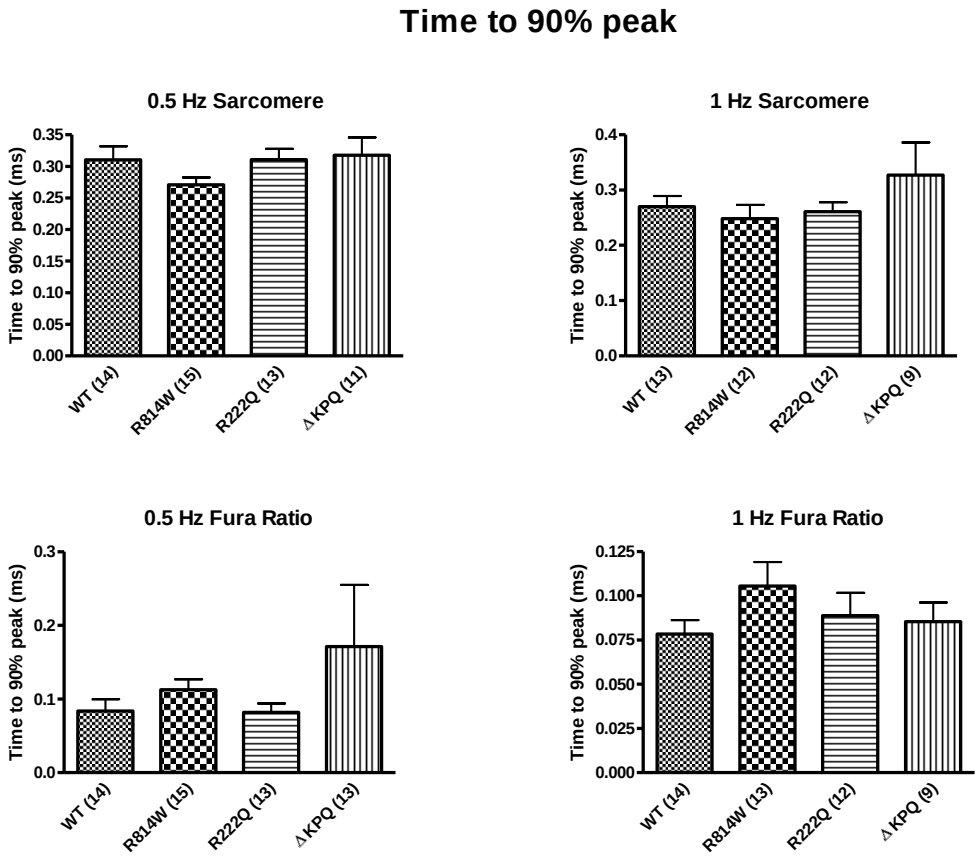

Figure 35. Time to peak measurements of rabbit ventricular myocytes. (Top panels) Time to peak (90%) measurements of sarcomere length during stimulation at 0.5 or 1 Hz. (Bottom panels) Time to peak (90%) of the Fura ratio during stimulation at 0.5 or 1 Hz in cardiomyocytes loaded with Fura-2 AM. All data are represented as mean ± S.E.M. Number of cells measured (n) are listed along bottom of figures.

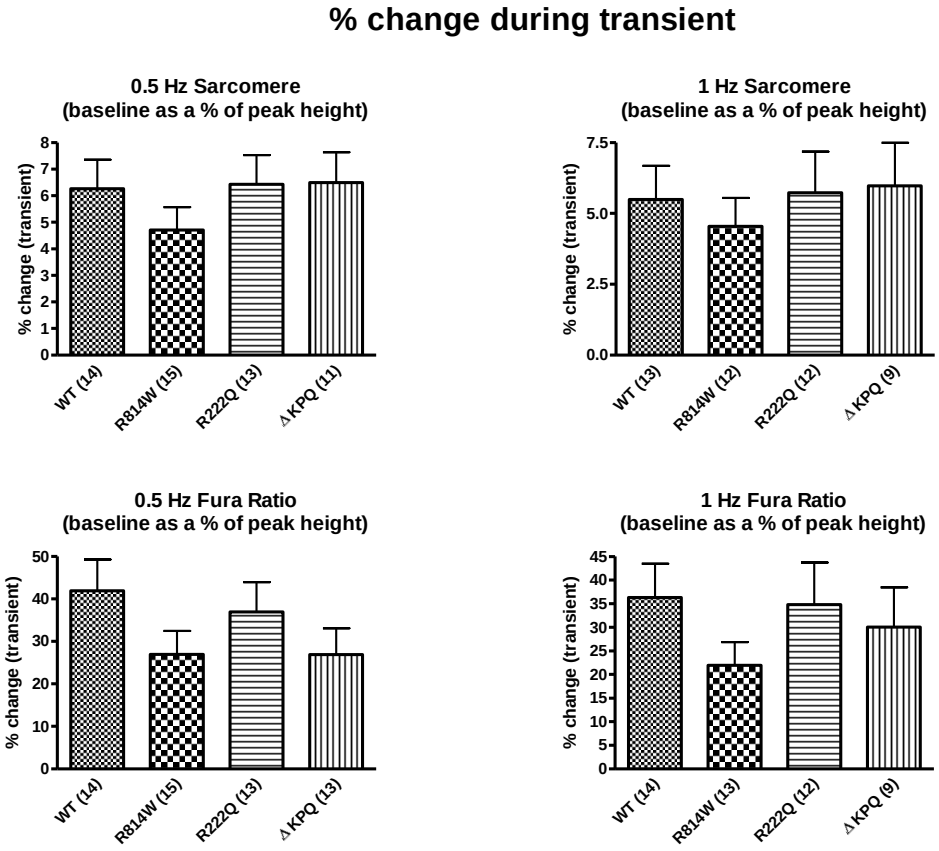

Figure 36. Measurement of peak height of rabbit ventricular myocytes. Peak height was measured as a percentage of baseline in order to account for differences in baseline measurements. (Top panels) Peak height in relation to baseline measurements of sarcomere length during stimulation at 0.5 or 1 Hz. (Bottom panels) Peak height of the Fura ratio during stimulation at 0.5 or 1 Hz in cardiomyocytes loaded with Fura-2 AM. All data are represented as mean ± S.E.M. Number of cells measured (n) are listed along bottom of figures.

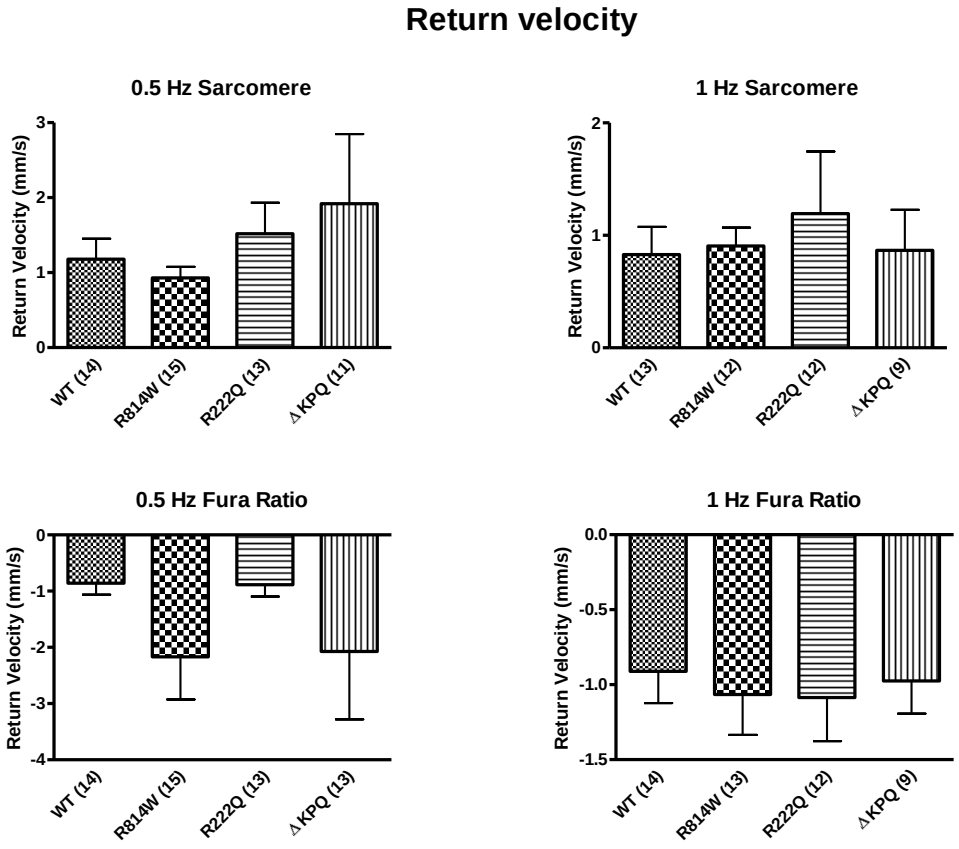

Figure 37. Measurement of rate of recovery of rabbit ventricular myocytes after stimulation. Return velocity measurements indicate the rate at which the respective peaks return to baseline. (Top panels) Return velocity of sarcomere length during stimulation at 0.5 or 1 Hz. (Bottom panels) Return velocity of the Fura ratio during stimulation at 0.5 or 1 Hz in cardiomyocytes loaded with Fura-2 AM. All data are represented as mean ± S.E.M. Number of cells measured (n) are listed along bottom of figures.

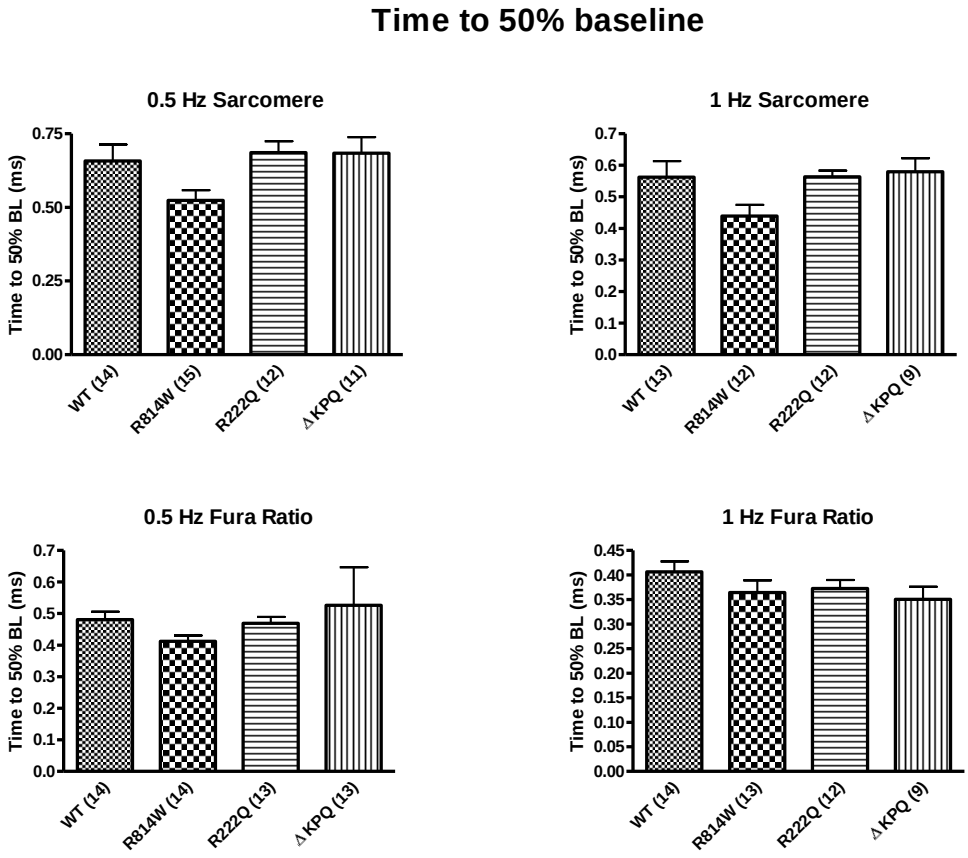

Figure 38. Time course of recovery of rabbit ventricular myocytes after stimulation. (Top panels) The time it takes to recover 50% of contracted sarcomere in relation to baseline during stimulation at 0.5 or 1 Hz. (Bottom panels) The time needed to recover 50% of peak Fura signal in relation to baseline during stimulation at 0.5 or 1 Hz in cardiomyocytes loaded with Fura-2 AM. All data are represented as mean ± S.E.M. Number of cells measured (n) are listed along bottom of figures.

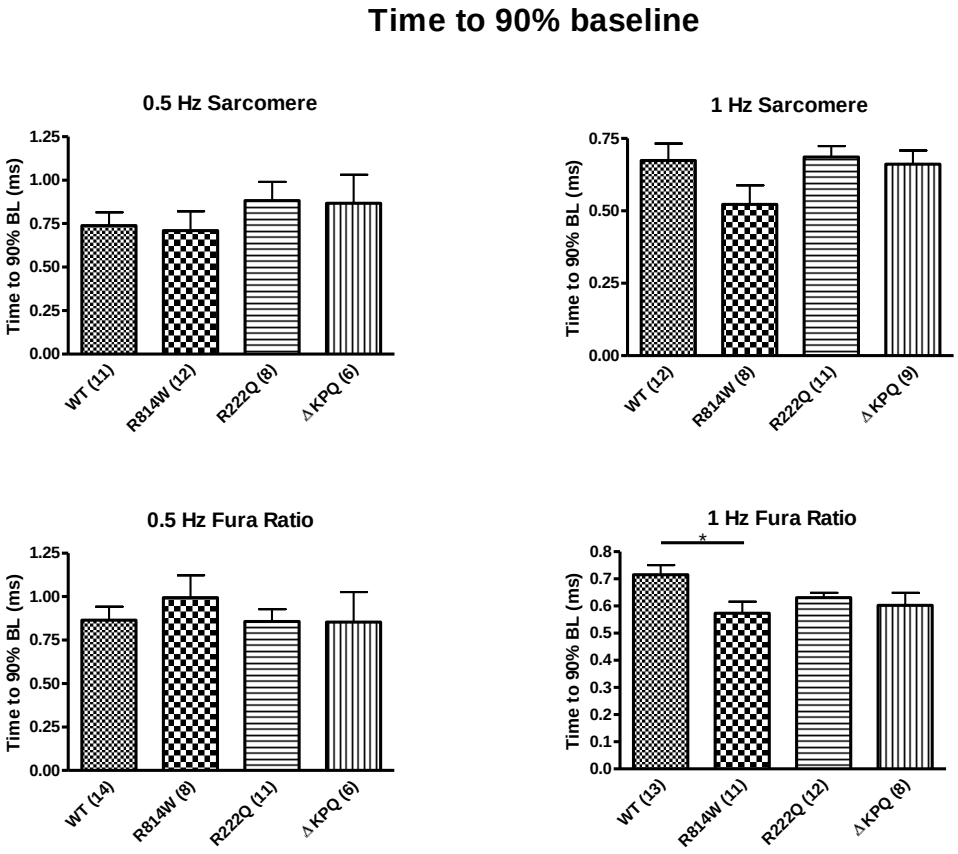

Figure 39. Time course of recovery of rabbit ventricular myocytes after stimulation. (Top panels) The time it takes to recover 90% of contracted sarcomere in relation to baseline during stimulation at 0.5 or 1 Hz. (Bottom panels) The time needed to recover 90% of peak Fura signal in relation to baseline during stimulation at 0.5 or 1 Hz in cardiomyocytes loaded with Fura-2 AM. All data are represented as mean ± S.E.M. Number of cells measured (n) are listed along bottom of figures.

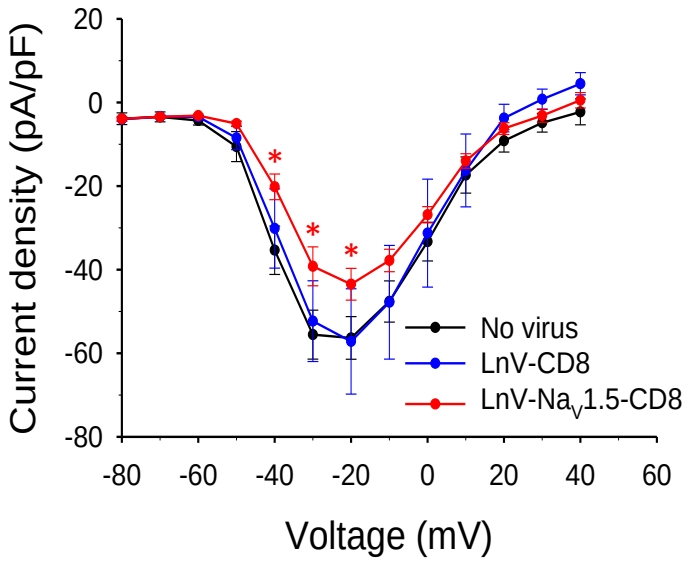

Figure 40. I_{Na} recorded from isolated rabbit ventricular myocytes. Sodium currents measured from native (black) myocytes or myocytes transduced with control lentivirus (blue) or lentivirus containing SCN5A (red). All data are represented as mean ± S.E.M. for n= 7 - 9 cells. * = $p<0.05$ compared to native sodium current density.

Discussion

Cardiac sodium channel mutations associated with heart failure expand the clinical spectrum of disease states associated with the protein $Na_V1.5$. Because of this unexpected correlation, we wanted to understand the mechanism of disease for the R222Q, R814W, and R225P mutations. We hypothesized that these mutations in the voltage sensing regions of their respective domains would result in an aberrant influx of sodium near membrane potentials typically associated with diastole, as identified by ramp current experiments. Proper myocyte function and cellular homeostasis relies on regulation of the sodium concentration gradient. Because of the direct relationship between sodium and calcium through the NCX, in this set of experiments, it was our aim to determine if the aberrant influx of sodium at hyperpolarized potentials produced by the mutations R222Q and R814W would disrupt calcium handling and potentially lead to myocardial insult. For sake of comparison, we chose to also characterize the LQTS mutation, delKPQ, which exhibits a larger ramp current then WT, however, peaks near the same membrane potential and should potentially result in a different calcium handling pattern, compared to R222Q and R814W. To test this, we chose to exogenously express WT or mutant cardiac sodium channels in guinea pig and rabbit isolated ventricular cardiomyocytes.

Transduction of isolated ventricular cardiomyocytes

Adenoviral vectors

Expression of exogenous genes and proteins in primary cells is a difficult task. Because cardiomyocytes are fully differentiated, gene transcription and translation is

decreased to a minimum, usually reserved for maintenance and house keeper gene regulation. Adenovirus and adenoviral vectors drive expression of their genomic payload as an extra chromosome and they do not rely upon insertion of genetic material into the host genome, compared to lentivirus. Thus, our initial efforts were placed on creating adenoviral vectors containing the human cardiac sodium channel gene, *SCN5A*.

We successfully produced control adenovirus capable of transducing guinea pig and rabbit cardiomyocytes with various marker proteins. Multiple attempts were made to produce adenovirus carrying the cardiac sodium channel gene and, ultimately, neither we nor the GTVC could create the necessary adenoviral constructs to transduce cardiomyocytes with human WT or mutant cardiac sodium channels.

We are unable to identify a direct reason for both the AdenoVator and RAPAd processes to be unsuccessful. Both methods used to create adenovirus are capable of accepting a genetic payload of ~8 kb. The promoter, gene, and marker construct (CMV-*SCN5A*-IRES2-mCherry) was roughly 8.5 kb, therefore, it is possible that our insert was excessive in length. However, attempts to create an adenoviral vector containing only promoter and channel (~6.5kb) were also unsuccessful in both vector producing systems.

Another concern is overexpression of our gene of interest in the HEK-293A adenoviral production line. Adenoviral plasmid DNA is directly transfected into the HEK cell line, where transcription and translation machinery have immediate access to the expression construct. Expression of $Na_V1.5$ driven by the CMV promoter over the time needed for viral production (10-14 days) could be excessive and cause changes to the cellular membrane, possibly affecting the budding of functional virus from the host cell (personal communication with GTVC).

Lentiviral vectors

Noting the success of previous work using a lentiviral vector to transduce myocytes with $Na_V1.5$ [48], we obtained lentiviral plasmid constructs and were able to produce lentiviral vectors containing the cardiac sodium channel gene with various expression markers. We tested the efficacy of the virus on tsA201 cells and verified function of the WT sodium channel by electrophysiological studies. We created lentiviral vectors containing the mutant channel R222Q, R814W, or delKPQ and successfully verified channel function. Transduction of both guinea pig and rabbit isolated ventricular myocytes was possible using lentiviral vectors containing sodium channel genes and the marker protein CD8.

Interestingly, attempts to infect myocytes with lentivirus containing *SCN5A* and a fluorescent marker were unsuccessful, possibly due to low expression of the exogenous construct. Because lentivirus is required to integrate into the host cell's genome and is limited to infection by one single virion, expression of lentiviral genes can be compromised by the location of insertion into the genome and the amount of transcription activity in those genetic regions. It is probable that both guinea pig and rabbit myocytes were successfully transduced by viruses containing fluorescent markers, however, reduced expression of exogenous marker genes may not have been enough to visually identify the small number of fluorescing proteins in the larger cardiomyocyte. By expressing a protein on the surface and using an unbiased, antibody interaction, as in the case with the Leu2 protein and CD8 antibody coated beads, the CD8 interaction provides a more sensitive means of identification of transduced cells.

Calcium imaging experiments were performed on healthy, isolated rabbit ventricular cardiomyocytes transduced by lentiviral vectors containing WT or mutant $Na_V1.5$ channels with the CD8 marker, using the ratiometric dye, Fura-2 AM. We had hypothesized that the large influx of sodium during diastole would result in blunting of the NCX, causing an increased baseline calcium level, a larger peak calcium transient, and an extended time course of the calcium signal as a result of higher sodium concentration affecting the function of the NCX. Compared to cells transduced with WT channels, there was no overall difference in the change of Fura-2 signal or contraction properties recorded from cells exogenously expressing R222Q, R814W, or delKPQ.

Because we were initially concerned about lower expression from our exogenous constructs, we measured sodium currents from transduced myocytes and noted a significant decrease in total sodium current in all cells that should be overexpressing sodium channels. This is contrary to what we expected; a larger number of channels should result in greater current. The decrease in current recorded from transduced myocytes may be a direct result of the cell down-regulating native cardiomyocyte expression as a result of over-expression of exogenous channels. This is only speculation, although, as without another reliable method to determine the amount of exogenous channel overexpression in the infected myocytes, it is impossible to identify the degree of influence the mutant cardiac channels are having on the function of the myocyte. Because of the inconclusive nature of the experiments and results, it is difficult to confirm or deny the hypothesis that these cardiac sodium channel mutations induce a heart failure phenotype by altering calcium handling in a ventricular cardiomyocyte.

CHAPTER IV

SUMMARY AND FUTURE DIRECTIONS

Summary

Voltage-gated sodium channels are a diverse group of proteins found throughout excitable tissues of the body. Activation of these channels stimulates pore openings and allows I_{Na} to conduct into the cell. This depolarization of the membrane potential produces the initial upstroke of the action potential in most cell types. In cardiac tissue, a multitude of currents shape and drive the cardiac action potential and, through the second messenger Ca^{2+}, contraction is stimulated by EC coupling. Mutations in the cardiac sodium channel, $Na_V1.5$, often result in altered action potential morphologies and can manifest as arrhythmias, such as long-QT and Brugada syndromes, identifiable on ECG recordings. Over the past 10 years, however, a number of mutations in $Na_V1.5$ have been discovered that manifest as cardiomyopathies and have encouraged researchers to thoroughly examine alternate routes of disease forming mechanisms.

In Chapter II, we studied a novel $Na_V1.5$ mutation, R225P, in a patient with amiodarone-responsive ventricular ectopy-associated cardiomyopathy. The mutation is located in one of the voltage-sensing regions of the channel and mutates one of the arginines critical for channel activation. Characterization of $Na_V1.5$-R225P revealed an altered activation, resulting in larger, hyperpolarized window- and ramp-currents compared to WT channels. The biophysical properties of R225P are similar to previously characterized mutations associated with cardiomyopathies (R222Q, R814W) that affect

the voltage-sensing regions of $Na_V1.5$. We propose that the hyperpolarized window- and ramp-currents are a potential biophysical fingerprint for mutations that could induce a heart failure phenotype.

Of particular interest, in addition to the activation defects, the mutation R225P also exhibits an enhanced slow inactivation resulting in a frequency-dependent decline of both peak- and ramp-current. We predict that this could affect the patient at periods of higher heart rates, resulting in a decrease of overall I_{Na} which negatively effects heart function. Examining this mutation in the presence of amiodarone, we showed that the R225P mutation is much more sensitive to amiodarone-induced frequency-dependent block than WT channels. We believe that amiodarone exacerbates an already enhanced slow inactivation and results in a decreased overall pool of mutant channels capable of disrupting ion homeostasis and inducing heart failure and this is the means of the therapeutic efficacy of the drug.

The association of $Na_V1.5$ mutations with cardiomyopathy invites further questions on the mechanism for this rare correlation. In Chapter III, we endeavored to determine if expression of R814W or R222Q could affect calcium regulation within cardiomyocytes expressing the mutant channels. To test this, we explored many options for expression of exogenous channels in an isolated ventricular myocyte. Though attempts to create an adenovirus carrying the cardiac sodium channel or mutations of interest were unsuccessful, we were successful in producing lentiviral vectors capable of transducing isolated rabbit ventricular myocytes.

Subsequent experiments examining calcium levels in myocytes transduced with exogenous $Na_V1.5$ or mutant channels by Fura-2 experiments revealed little to no

difference among all the parameters tested. Therefore, we conclude, that in these experiments overexpressing exogenous cardiac sodium channels through lentiviral transduction of isolated rabbit ventricular myocytes, there is no alteration of calcium handling resulting from overexpression of the mutations R222Q or R814W compared to WT channels. These experiments, however, are limited to the expression capabilities of the lentiviral vector's ability to transduce a primary cardiomyocyte and the results should be confirmed with another method of exogenous channel expression.

Future Directions

The complexity of diseases associated with mutations of the voltage-gated cardiac sodium channel, $Na_V1.5$, is expanding beyond arrhythmia and conduction disorders. The recent identification of $Na_V1.5$ mutations associated with cardiomyopathy phenotypes creates the necessity to examine the impact of these mutations in a more native cell line. The ability to analyze the biophysical properties of sodium channel mutations in a non-cardiomyocyte cell line, such as tsA201 cells, is critical for identifying functional discrepancies within the mutant channel compared to WT. However, in order to understand uncommon disease associations, such as cardiomyopathy, it is necessary to go beyond channel electrophysiology and examine the impact of mutations on processes of the cardiomyocyte, such as calcium signaling and pH regulation.

Heterozygous channel expression

The proband with $Na_V1.5$-R225P is heterozygous for the mutation, indicating that the wild type allele is also likely expressed. Interestingly, recent work from the lab of Isabelle Deschenes, Ph.D., (Case Western Reserve University, Cleveland, OH, USA) has indicated that, in co-expression studies designed to mimic the heterozygous setting in HEK293, co-expression of WT channels with functionally inactive sodium channel mutations associated with BrS can induce unexpected alterations of WT channel activity [49]. It has been proposed that α subunits of these channels may be interacting with one another and that the mutated channel is exerting a dominant-negative effect. Though the scope of these findings pertain to loss-of-function mutations, it would be intriguing to examine the resultant biophysical properties of the mutation R225P co-expressed with

WT channel in order to recapitulate the heterozygous state of the proband. Because the R225P mutation results in activation defects that promote a gain-of-function, we predict that the resultant current from co-expression studies would be a hybrid of biophysical characteristics already identified in WT and R225P channels. R225P activates at more hyperpolarized potentials compared to WT channel, therefore, we hypothesize that the ramp-current induced by R225P would still be a dominate feature and would skew the activation and combined peaks of the ramp-currents to more negative potentials while increasing charge movement. Because all of this is speculation, it would be valuable to examine the biophysical properties of R225P in a heterozygous setting.

Transgenic animal model

The three mutations, R222Q, R225P, and R814W, all were identified in patients with cardiomyopathies. In tsA201 cells, we identified a common defect in the activation of these channels that produced large, hyperpolarized ramp currents that we predict will introduce excess sodium into the myocyte during diastole and disrupt processes relying upon the sodium gradient and indirectly result in a heart failure phenotype. The ideal future direction of this work would be to analyze these mutations in a knock-in animal model.

The first option would be to create a knock-in model capable of expressing the respective mutations in an animal with action potential properties and contraction characteristics similar to that of human, such as the rabbit. Manipulating the rabbit genome in order to answer questions regarding human diseases is an interesting concept that has had success over the past decade [50]–[54]. The “knock-in” rabbit technology is

still in its infancy, however, advances using zinc finger nucleases to inactivate genes and mediate homologous recombination with vector DNA has had initial success in rabbits [54]. This opens up the possibilities of creating a rabbit expressing a mutant cardiac sodium channel targeted to the locus of an original *SCN5A* gene copy that would allow appropriate biological expression patterns and regulation that is difficult to achieve in a transgenic model. Because the rabbit action potential and calcium handling more closely mimics that of human, it may yield results that correlate better to what is seen in the human disease in terms of the cardiomyopathy-associated sodium channel mutations.

Another option would be to make a mouse "knock-in" model expressing the mutant channels of interest. Though the action potential morphology of the mouse is different compared to human or other animals such as rabbit, many successful studies have exhibited the validity of the mouse model in relationship to $Na_V1.5$ mutations [55]–[58]. We predict the cardiomyopathy-associated mutations conduct aberrant I_{Na} during diastole, resulting in higher $[Na^+]_i$ and altered ion regulation. Regardless of action potential properties in the murine system, the myocyte would still need to regulate $[Na^+]_i$ in order to maintain proper function. This could result in blunting of the NCX and lead to alterations in Ca^{2+} transients, as predicted. However, it is important to note that, in mouse and rat, Ca^{2+} removal through NCX is lower and uptake of Ca^{2+} into the SR is greater compared to other animal models [59]. Because this mimics what we predict is the disease progenitor in human disease, critical analysis of the data would be essential in order to determine specific factors related to heart failure.

Overall, having a transgenic model, mouse or rabbit, would give access to cardiomyocytes stably expressing mutant channels and would remove some of the

variables from the experimental limitations, such as viral production and transduction efficiency. We believe this would yield more consistent results and allow for better interpretation of the data in regards to our working hypothesis. Using isolated transgenic ventricular myocytes, it would be valuable to perform the Fura-2 experiments again, in order to verify the data presented here. It would also be interesting to examine pH regulation within myocytes expressing the mutant channels. These experiments would be done with the ratiometric dye, BCECF, similar to how the experiments for Fura-2 were performed.

Having an animal model expressing these mutations would also be valuable for analysis of therapeutic treatments using animals that may be able to mimic the cardiomyopathy identified in human patients. In the case of R225P, the heart failure symptoms of the patient are successfully controlled with amiodarone; however, the side effects of amiodarone are detrimental and can have lasting consequences. Quinidine has also been shown to have efficacy in treating similar cardiomyopathy phenotypes [24]. Though we can speculate a potential therapeutic mechanism for these drugs, it would be beneficial to analyze whole heart and cardiomyocyte function in the absence or presence of these drugs. Because of the non-specific effects of amiodarone and the deleterious side effects associated with the drug, confirming the direct mechanism of action could allow the identification of potential pharmaceutical agents with better overall health outcomes.

Induced pluripotent stem cells

Induced pluripotent stem cell-derived cardiomyocytes (iPSC-CM) also could serve as a valuable tool in examining $Na_V1.5$ mutations associated with heart failure. This

relatively novel approach allows the researcher to create an iPSC-CM line derived from the patient with the disease phenotype, allowing for a personalized approach to identify direct disease mechanisms within the context of an individual's own genetic framework. Direct examination of disease-specific iPSC-CMs has already been shown to be of value in multiple instances, including further examination of *SCN5A* mutations associated with long-QT and overlap syndromes [60], [61]. In the case of $Na_V1.5$ heart failure mutations, we speculate that the disease is the result of an influx of sodium during diastole that disrupts ion homeostasis and results from a continuous insult to individual myocytes. Using iPSC-CMs to examine this hypothesis would be ideal, as they have a longer usability time in culture compared to isolated ventricular myocytes, which allows the cells to be paced for an extended period to recapitulate the probability that these diseases develop over time. However, if the mechanism for $Na_V1.5$-induced cardiomyopathy is a result of conduction issues, IPSC-CMs may not mimic the complete disease state. Before IPSC-CMs become fully reliable as a model system, advances need to be made in differentiation techniques, identification methods, and data interpretation [62].

Clinical implications

In Chapter II, we identified another $Na_V1.5$ mutation, R225P, associated with a heart failure phenotype. The patient's condition was able to be controlled with a combination of amiodarone and a beta-blocking drug (propranolol or nadolol). Both Laurent *et al* and Mann *et al* noted in their reports on the cardiomyopathy-associated mutation R222Q that patients treated with amiodarone also responded favorably [24], [25]. We presented data here on the effect of amiodarone for both WT and R225P,

identifying an enhanced inactivation resulting in frequency-dependent block in the presence of the drug and identifying a potential mechanism for the therapeutic effect of amiodarone. Interestingly, a group of patients with R222Q responded well to treatment with quinidine, a drug that has been noted to affect the sodium channel in a use-dependent manner [24], [63]. Together, the data suggest that both amiodarone and quinidine may affect the cardiac sodium channel in the same way and potentially yield similar therapeutic benefits. Therefore, we believe that amiodarone treatment or a similar drug that blocks frequency-dependent current may be beneficial for patients with a cardiac sodium channel-associated cardiomyopathy.

REFERENCES

[1] A. L. George, “Inherited disorders of voltage-gated sodium channels.,” *J. Clin. Invest.*, vol. 115, no. 8, pp. 1990–9, Aug. 2005.

[2] W. A. Catterall, A. L. Goldin, and S. G. Waxman, “International Union of Pharmacology. XLVII. Nomenclature and structure-function relationships of voltage-gated sodium channels.,” *Pharmacol. Rev.*, vol. 57, no. 4, pp. 397–409, Dec. 2005.

[3] E. Savio-Galimberti, M. H. Gollob, and D. Darbar, “Voltage-gated sodium channels: biophysics, pharmacology, and related channelopathies.,” *Front. Pharmacol.*, vol. 3, p. 124, Jan. 2012.

[4] M. B. Rook, M. M. Evers, M. A. Vos, and M. F. A. Bierhuizen, “Biology of cardiac sodium channel $Na_V1.5$ expression.,” *Cardiovasc. Res.*, vol. 93, no. 1, pp. 12–23, Jan. 2012.

[5] A. O. Grant, “Cardiac ion channels.,” *Circ. Arrhythm. Electrophysiol.*, vol. 2, no. 2, pp. 185–94, Apr. 2009.

[6] D. M. Bers, “Cardiac excitation-contraction coupling.,” *Nature*, vol. 415, no. 6868, pp. 198–205, Jan. 2002.

[7] S. Despa and D. M. Bers, “Na^+ transport in the normal and failing heart - remember the balance.,” *J. Mol. Cell. Cardiol.*, vol. 61, pp. 2–10, Aug. 2013.

[8] B. Pieske and S. R. Houser, “$[Na^+]_i$ handling in the failing human heart.,” *Cardiovasc. Res.*, vol. 57, no. 4, pp. 874–86, Mar. 2003.

[9] D. A. Eisner and K. R. Sipido, “Sodium calcium exchange in the heart: necessity or luxury?,” *Circ. Res.*, vol. 95, no. 6, pp. 549–51, Sep. 2004.

[10] D. M. Bers, W. H. Barry, and S. Despa, “Intracellular Na^+ regulation in cardiac myocytes.,” *Cardiovasc. Res.*, vol. 57, no. 4, pp. 897–912, Mar. 2003.

[11] J. C. Fantinelli, A. Orlowski, E. A. Aiello, and S. M. Mosca, “The electrogenic cardiac sodium bicarbonate co-transporter (NBCe1) contributes to the reperfusion injury.,” *Cardiovasc. Pathol.*, pp. 1–7, Mar. 2014.

[12] A. Baartscheer, M. Hardziyenka, C. A. Schumacher, C. N. W. Belterman, M. M. G. J. van Borren, A. O. Verkerk, R. Coronel, and J. W. T. Fiolet, "Chronic inhibition of the Na^+/H^+ - exchanger causes regression of hypertrophy, heart failure, and ionic and electrophysiological remodelling.," *Br. J. Pharmacol.*, vol. 154, no. 6, pp. 1266–75, Jul. 2008.

[13] N. V. Munshi, "Gene regulatory networks in cardiac conduction system development.," *Circ. Res.*, vol. 110, no. 11, pp. 1525–37, May 2012.

[14] G. Salama and B. London, "Mouse models of long QT syndrome.," *J. Physiol.*, vol. 578, no. Pt 1, pp. 43–53, Jan. 2007.

[15] W. M. Smith and J. J. Gallagher, "'Les torsades de pointes': an unusual ventricular arrhythmia.," *Ann. Intern. Med.*, vol. 93, no. 4, pp. 578–84, Oct. 1980.

[16] M. Horie and S. Ohno, "Genetic basis of Brugada syndrome," *J. Arrhythmia*, vol. 29, no. 2, pp. 71–76, Apr. 2013.

[17] A. L. George, "Molecular and genetic basis of sudden cardiac death.," *J. Clin. Invest.*, vol. 123, no. 1, pp. 75–83, Jan. 2013.

[18] P. G. Meregalli, A. a M. Wilde, and H. L. Tan, "Pathophysiological mechanisms of Brugada syndrome: depolarization disorder, repolarization disorder, or more?," *Cardiovasc. Res.*, vol. 67, no. 3, pp. 367–78, Aug. 2005.

[19] J. P. P. Smits, M. W. Veldkamp, and A. a M. Wilde, "Mechanisms of inherited cardiac conduction disease.," *Europace*, vol. 7, no. 2, pp. 122–37, Mar. 2005.

[20] W. P. McNair, L. Ku, M. R. G. Taylor, P. R. Fain, D. Dao, E. Wolfel, and L. Mestroni, "SCN5A mutation associated with dilated cardiomyopathy, conduction disorder, and arrhythmia.," *Circulation*, vol. 110, no. 15, pp. 2163–7, Oct. 2004.

[21] T. M. Olson, V. V Michels, J. D. Ballew, S. P. Reyna, M. L. Karst, K. J. Herron, S. C. Horton, R. J. Rodeheffer, and J. L. Anderson, "Sodium channel mutations and susceptibility to heart failure and atrial fibrillation.," *JAMA*, vol. 293, no. 4, pp. 447–54, Jan. 2005.

[22] W. P. McNair, G. Sinagra, M. R. G. Taylor, A. Di Lenarda, D. A. Ferguson, E. E. Salcedo, D. Slavov, X. Zhu, J. H. Caldwell, and L. Mestroni, "SCN5A mutations associate with arrhythmic dilated cardiomyopathy and commonly localize to the voltage-sensing mechanism.," *J. Am. Coll. Cardiol.*, vol. 57, no. 21, pp. 2160–8, May 2011.

[23] T. P. Nguyen, D. W. Wang, T. H. Rhodes, and A. L. George, "Divergent biophysical defects caused by mutant sodium channels in dilated cardiomyopathy with arrhythmia.," *Circ. Res.*, vol. 102, no. 3, pp. 364–71, Feb. 2008.

[24] G. Laurent, S. Saal, M. Y. Amarouch, D. M. Béziau, R. F. J. Marsman, L. Faivre, J. Barc, C. Dina, G. Bertaux, O. Barthez, C. Thauvin-Robinet, P. Charron, V. Fressart, A. Maltret, E. Villain, E. Baron, J. Mérot, R. Turpault, Y. Coudière, F. Charpentier, J.-J. Schott, G. Loussouarn, A. A. M. Wilde, J.-E. Wolf, I. Baró, F. Kyndt, and V. Probst, "Multifocal ectopic Purkinje-related premature contractions: a new SCN5A-related cardiac channelopathy.," *J. Am. Coll. Cardiol.*, vol. 60, no. 2, pp. 144–56, Jul. 2012.

[25] S. A. Mann, M. L. Castro, M. Ohanian, G. Guo, P. Zodgekar, A. Sheu, K. Stockhammer, T. Thompson, D. Playford, R. Subbiah, D. Kuchar, A. Aggarwal, J. I. Vandenberg, and D. Fatkin, "R222Q SCN5A mutation is associated with reversible ventricular ectopy and dilated cardiomyopathy.," *J. Am. Coll. Cardiol.*, vol. 60, no. 16, pp. 1566–73, Oct. 2012.

[26] A. Morales, T. Painter, R. Li, J. D. Siegfried, D. Li, N. Norton, and R. E. Hershberger, "Rare variant mutations in pregnancy-associated or peripartum cardiomyopathy.," *Circulation*, vol. 121, no. 20, pp. 2176–82, May 2010.

[27] J. Cheng, A. Morales, J. D. Siegfried, D. Li, N. Norton, J. Song, J. Gonzalez-Quintana, J. C. Makielski, and R. E. Hershberger, "SCN5A rare variants in familial dilated cardiomyopathy decrease peak sodium current depending on the common polymorphism H558R and common splice variant Q1077del.," *Clin. Transl. Sci.*, vol. 3, no. 6, pp. 287–94, Dec. 2010.

[28] K. Nair, R. Pekhletski, L. Harris, M. Care, C. Morel, T. Farid, P. H. Backx, E. Szabo, and K. Nanthakumar, "Escape capture bigeminy: Phenotypic marker of cardiac sodium channel voltage sensor mutation R222Q," *Hear. Rhythm*, vol. 9, no. 10, pp. 1681–1688.e1, 2012.

[29] A. L. George, "Mechanisms in Heritable Sodium Channel Diseases," in *Cardiac Electrophysiology: from Cell to Bedside*, 6th ed., D. P. Zipes and J. Jalife, Eds. Philadelphia, Pennsylvania: Elsevier - Health Sciences Division, 2013, pp. 491–500.

[30] P. Gosselin-Badaroudine, D. I. Keller, H. Huang, V. Pouliot, A. Chatelier, S. Osswald, M. Brink, and M. Chahine, "A proton leak current through the cardiac sodium channel is linked to mixed arrhythmia and the dilated cardiomyopathy phenotype.," *PLoS One*, vol. 7, no. 5, p. e38331, Jan. 2012.

[31] P. B. Bennett, K. Yazawa, N. Makita, and A. L. George, "Molecular mechanism for an inherited cardiac arrhythmia.," *Nature*, vol. 376, no. 6542, pp. 683–5, Aug. 1995.

[32] G. Millat, P. Chevalier, L. Restier-Miron, A. Da Costa, P. Bouvagnet, B. Kugener, L. Fayol, C. Gonzàlez Armengod, B. Oddou, V. Chanavat, E. Froidefond, R. Perraudin, R. Rousson, and C. Rodriguez-Lafrasse, "Spectrum of pathogenic mutations and associated polymorphisms in a cohort of 44 unrelated patients with long QT syndrome.," *Clin. Genet.*, vol. 70, no. 3, pp. 214–27, Sep. 2006.

[33] C. R. Bezzina, M. B. Rook, W. A. Groenewegen, L. J. Herfst, A. C. van der Wal, J. Lam, H. J. Jongsma, A. A. M. Wilde, and M. M. A. M. Mannens, "Compound heterozygosity for mutations (W156X and R225W) in SCN5A associated with severe cardiac conduction disturbances and degenerative changes in the conduction system.," *Circ. Res.*, vol. 92, no. 2, pp. 159–68, Feb. 2003.

[34] H. Lerche, N. Mitrovic, V. Dubowitz, and F. Lehmann-Horn, "Paramyotonia congenita: the R1448P Na^+ channel mutation in adult human skeletal muscle.," *Ann. Neurol.*, vol. 39, no. 5, pp. 599–608, May 1996.

[35] N. G. Kambouris, H. B. Nuss, D. C. Johns, G. F. Tomaselli, E. Marban, and J. R. Balser, "Phenotypic Characterization of a Novel Long-QT Syndrome Mutation (R1623Q) in the Cardiac Sodium Channel," *Circulation*, vol. 97, no. 7, pp. 640–644, Feb. 1998.

[36] N. Makita, N. Shirai, M. Nagashima, R. Matsuoka, Y. Yamada, N. Tohse, and a Kitabatake, "A de novo missense mutation of human cardiac Na^+ channel exhibiting novel molecular mechanisms of long QT syndrome.," *FEBS Lett.*, vol. 423, no. 1, pp. 5–9, Feb. 1998.

[37] D. W. Wang, K. Yazawa, A. L. George, and P. B. Bennett, "Characterization of human cardiac Na^+ channel mutations in the congenital long QT syndrome.," *Proc. Natl. Acad. Sci. U. S. A.*, vol. 93, no. 23, pp. 13200–5, Nov. 1996.

[38] A. Cha, P. C. Ruben, A. L. George, E. Fujimoto, and F. Bezanilla, "Voltage sensors in domains III and IV, but not I and II, are immobilized by Na^+ channel fast inactivation.," *Neuron*, vol. 22, no. 1, pp. 73–87, Jan. 1999.

[39] C. Maack, S. Cortassa, M. A. Aon, A. N. Ganesan, T. Liu, and B. O'Rourke, "Elevated cytosolic Na^+ decreases mitochondrial Ca^{2+} uptake during excitation-contraction coupling and impairs energetic adaptation in cardiac myocytes.," *Circ. Res.*, vol. 99, no. 2, pp. 172–82, Jul. 2006.

[40] M. Kohlhaas, T. Liu, A. Knopp, T. Zeller, M. F. Ong, M. Bohm, B. O'Rourke, C. Maack, and M. Böhm, "Elevated cytosolic Na^+ increases mitochondrial formation of reactive oxygen species in failing cardiac myocytes," *Circulation*, vol. 121, no. 14, pp. 1606–1613, Apr. 2010.

[41] M. Estacion and S. G. Waxman, "The response of Na(V)1.3 sodium channels to ramp stimuli: multiple components and mechanisms.," *J. Neurophysiol.*, vol. 109, no. 2, pp. 306–14, Jan. 2013.

[42] R. D. Anderson, R. E. Haskell, H. Xia, B. J. Roessler, and B. L. Davidson, "A simple method for the rapid generation of recombinant adenovirus vectors.," *Gene Ther.*, vol. 7, no. 12, pp. 1034–8, Jun. 2000.

[43] D. Finkelshtein, A. Werman, D. Novick, S. Barak, and M. Rubinstein, "LDL receptor and its family members serve as the cellular receptors for vesicular stomatitis virus.," *Proc. Natl. Acad. Sci. U. S. A.*, vol. 110, no. 18, pp. 7306–11, Apr. 2013.

[44] J. Sadoshima, L. Jahn, T. Takahashi, T. J. Kulik, and S. Izumo, "Molecular characterization of the stretch-induced adaptation of cultured cardiac cells. An in vitro model of load-induced cardiac hypertrophy.," *J. Biol. Chem.*, vol. 267, no. 15, pp. 10551–60, May 1992.

[45] A. Calderone, C. M. Thaik, N. Takahashi, D. L. Chang, and W. S. Colucci, "Nitric oxide, atrial natriuretic peptide, and cyclic GMP inhibit the growth-promoting effects of norepinephrine in cardiac myocytes and fibroblasts.," *J. Clin. Invest.*, vol. 101, no. 4, pp. 812–8, Feb. 1998.

[46] L. M. Oleksa, L. C. Hool, and R. D. Harvey, "Alpha 1-adrenergic inhibition of the beta-adrenergically activated Cl^- current in guinea pig ventricular myocytes.," *Circ. Res.*, vol. 78, no. 6, pp. 1090–9, Jun. 1996.

[47] C. M. Campbell, J. D. Campbell, C. H. Thompson, E. S. Galimberti, D. Darbar, C. G. Vanoye, and A. L. George, "Selective targeting of gain-of-function KCNQ1 mutations predisposing to atrial fibrillation.," *Circ. Arrhythm. Electrophysiol.*, vol. 6, no. 5, pp. 960–6, Oct. 2013.

[48] P. J. Mohler, I. Rivolta, C. Napolitano, G. LeMaillet, S. Lambert, S. G. Priori, and V. Bennett, "$Na_V1.5$ E1053K mutation causing Brugada syndrome blocks binding to ankyrin-G and expression of $Na_V1.5$ on the surface of cardiomyocytes.," *Proc. Natl. Acad. Sci. U. S. A.*, vol. 101, no. 50, pp. 17533–8, Dec. 2004.

[49] J. Clatot, A. Ziyadeh-Isleem, S. Maugenre, I. Denjoy, H. Liu, G. Dilanian, S. N. Hatem, I. Deschênes, A. Coulombe, P. Guicheney, and N. Neyroud, "Dominant-negative effect of SCN5A N-terminal mutations through the interaction of Na(v)1.5 α-subunits.," *Cardiovasc. Res.*, vol. 96, no. 1, pp. 53–63, Oct. 2012.

[50] V. Duranthon, N. Beaujean, M. Brunner, K. E. Odening, A. N. Santos, I. Kacskovics, L. Hiripi, E. J. Weinstein, and Z. Bosze, "On the emerging role of rabbit as human disease model and the instrumental role of novel transgenic tools.," *Transgenic Res.*, vol. 21, no. 4, pp. 699–713, Aug. 2012.

[51] K. E. Odening, B. A. Jung, C. N. Lang, R. Cabrera Lozoya, D. Ziupa, M. Menza, J. Relan, G. Franke, S. Perez Feliz, G. Koren, M. Zehender, C. Bode, M. Brunner, M. Sermesant, and D. Föll, "Spatial correlation of action potential duration and diastolic dysfunction in transgenic and drug-induced LQT2 rabbits.," *Heart Rhythm*, vol. 10, no. 10, pp. 1533–41, Oct. 2013.

[52] Z. Ivics, L. Hiripi, O. I. Hoffmann, L. Mátés, T. Y. Yau, S. Bashir, V. Zidek, V. Landa, A. Geurts, M. Pravenec, T. Rülicke, Z. Bösze, and Z. Izsvák, "Germline transgenesis in rabbits by pronuclear microinjection of Sleeping Beauty transposons.," *Nat. Protoc.*, vol. 9, no. 4, pp. 794–809, Apr. 2014.

[53] L. Hiripi, D. Negre, F.-L. Cosset, K. Kvell, T. Czömpöly, M. Baranyi, E. Gócza, O. Hoffmann, B. Bender, and Z. Bosze, "Transgenic rabbit production with simian immunodeficiency virus-derived lentiviral vector.," *Transgenic Res.*, vol. 19, no. 5, pp. 799–808, Oct. 2010.

[54] T. Flisikowska, I. S. Thorey, S. Offner, F. Ros, V. Lifke, B. Zeitler, O. Rottmann, A. Vincent, L. Zhang, S. Jenkins, H. Niersbach, A. J. Kind, P. D. Gregory, A. E. Schnieke, and J. Platzer, "Efficient immunoglobulin gene disruption and targeted replacement in rabbit using zinc finger nucleases.," *PLoS One*, vol. 6, no. 6, p. e21045, Jan. 2011.

[55] C. A. Remme, A. O. Verkerk, D. Nuyens, A. C. G. van Ginneken, S. van Brunschot, C. N. W. Belterman, R. Wilders, M. a van Roon, H. L. Tan, A. a M. Wilde, P. Carmeliet, J. M. T. de Bakker, M. W. Veldkamp, and C. R. Bezzina, "Overlap syndrome of cardiac sodium channel disease in mice carrying the equivalent mutation of human SCN5A-1795insD.," *Circulation*, vol. 114, no. 24, pp. 2584–94, Dec. 2006.

[56] D. Nuyens, M. Stengl, S. Dugarmaa, T. Rossenbacker, V. Compernolle, Y. Rudy, J. F. Smits, W. Flameng, C. E. Clancy, L. Moons, M. A. Vos, M. Dewerchin, K. Benndorf, D. Collen, E. Carmeliet, and P. Carmeliet, "Abrupt rate accelerations or premature beats cause life-threatening arrhythmias in mice with long-QT3 syndrome.," *Nat. Med.*, vol. 7, no. 9, pp. 1021–7, Sep. 2001.

[57] S. L. Yong, Y. Ni, T. Zhang, D. J. Tester, M. J. Ackerman, and Q. K. Wang, "Characterization of the cardiac sodium channel SCN5A mutation, N1325S, in single murine ventricular myocytes.," *Biochem. Biophys. Res. Commun.*, vol. 352, no. 2, pp. 378–83, Jan. 2007.

[58] H. Watanabe, T. Yang, D. M. Stroud, J. S. Lowe, L. Harris, T. C. Atack, D. W. Wang, S. B. Hipkens, B. Leake, L. Hall, S. Kupershmidt, N. Chopra, M. a Magnuson, N. Tanabe, B. C. Knollmann, A. L. George, and D. M. Roden, "Striking In vivo phenotype of a disease-associated human SCN5A mutation producing minimal changes in vitro.," *Circulation*, vol. 124, no. 9, pp. 1001–11, Aug. 2011.

[59] D. M. Bers, *Excitation-Contraction Coupling and Cardiac Contractile Force*, Second., vol. 237. Dordrecht: Springer Netherlands, 2001.

[60] D. Malan, S. Friedrichs, B. K. Fleischmann, and P. Sasse, "Cardiomyocytes obtained from induced pluripotent stem cells with long-QT syndrome 3 recapitulate typical disease-specific features in vitro.," *Circ. Res.*, vol. 109, no. 8, pp. 841–7, Sep. 2011.

[61] R. P. Davis, S. Casini, C. W. van den Berg, M. Hoekstra, C. A. Remme, C. Dambrot, D. Salvatori, D. W. Oostwaard, A. A. M. Wilde, C. R. Bezzina, A. O. Verkerk, C. Freund, and C. L. Mummery, "Cardiomyocytes derived from pluripotent stem cells recapitulate electrophysiological characteristics of an overlap syndrome of cardiac sodium channel disease.," *Circulation*, vol. 125, no. 25, pp. 3079–91, Jun. 2012.

[62] B. C. Knollmann, "Induced pluripotent stem cell-derived cardiomyocytes: boutique science or valuable arrhythmia model?," *Circ. Res.*, vol. 112, no. 6, pp. 969–76; discussion 976, Mar. 2013.

[63] D. J. Snyders and L. M. Hondeghem, "Effects of quinidine on the sodium current of guinea pig ventricular myocytes. Evidence for a drug-associated rested state with altered kinetics.," *Circ. Res.*, vol. 66, no. 2, pp. 565–79, Mar. 1990.

[64] T. J. Jentsch, C. A. Hübner, and J. C. Fuhrmann, "Ion channels: function unravelled by dysfunction.," *Nat. Cell Biol.*, vol. 6, no. 11, pp. 1039–47, Nov. 2004.

[65] A. Varró, D. A. Lathrop, S. B. Hester, P. P. Nánási, and J. G. Papp, "Ionic currents and action potentials in rabbit, rat, and guinea pig ventricular myocytes.," *Basic Res. Cardiol.*, vol. 88, no. 2, pp. 93–102.